SORPTION ENHANCED ETHANOL REFORMING OVER COBALT, NICKEL INCORPORATED MCM-41 FOR HYDROGEN PRODUCTION

A THESIS SUBMITTED TO
THE GRADUATE SCHOOL OF NATURAL AND APPLIED SCIENCES
OF
MIDDLE EAST TECHNICAL UNIVERSITY

BY

SEVAL GÜNDÜZ

IN PARTIAL FULFILLMENT OF THE REQUIREMENTS
FOR
THE DEGREE OF MASTER OF SCIENCE
IN
CHEMICAL ENGINEERING

FEBRUARY 2011

Approval of the thesis:

SORPTION ENHANCED ETHANOL REFORMING OVER COBALT, NICKEL INCORPORATED MCM-41 FOR HYDROGEN PRODUCTION

submitted by **SEVAL GÜNDÜZ** in partial fulfillment of the requirements fort he degree of **Master of Science in Chemical Engineering Depertment, Middle East Technical University** by,

Prof. Dr. Canan ÖZGEN ----------
Dean, Graduate School of **Natural and Applied Sciences**

Prof. Dr. Deniz ÜNER ----------
Head of Department, **Chemical Engineering**

Prof. Dr. Timur DOĞU
Supervisor, **Chemical Engineering Dept., METU** ----------

Examining Committee Members:

Prof. Dr. H. Önder ÖZBELGE ----------
Chemical Engineering Dept., METU

Prof. Dr. Timur DOĞU ----------
Chemical Engineering Dept., METU

Prof. Dr. Gürkan KARAKAŞ ----------
Chemical Engineering Dept., METU

Doc. Dr. Naime A. SEZGİ ----------
Chemical Engineering Dept., METU

Doc. Dr. Sena YAŞYERLİ ----------
Chemical Engineering Dept., Gazi University

Date: 08.02.2011

I hereby declare that all information in this document has been obtained and presented in accordance with academic rules and ethical conduct. I also declare that, as required by these rules and conduct, I have fully cited and referenced all material and results that are not original to this work.

Name, Last Name: Seval GÜNDÜZ

Signature:

ABSTRACT

SORPTION ENHANCED ETHANOL REFORMING OVER COBALT, NICKEL INCORPORATED MCM-41 FOR HYDROGEN PRODUCTION

Gündüz, Seval
M.Sc., Depertment of Chemical Engineering
Supervisor: Prof. Dr. Timur DOĞU

February, 2011, 139 pages

The interest in hydrogen as a clean energy source has increased due to depletion of limited fossil resources and environmental impact related to CO_2 emissions. Hydrogen production from bio-ethanol, which already contains large amount of water, by steam reforming reaction, has shown excellent potential with CO_2 neutrality. However, steam reforming of ethanol reaction is a highly complex process including many side reactions which decrease hydrogen yield and have a negative effect on process economy. Also, thermodynamic limitations cause decrease in hydrogen yield. In the present study, a new reaction process called sorption enhanced steam reforming has been investigated to improve hydrogen yield in ethanol reforming over Ni and Co impregnated MCM-41 type mesoporous catalysts. In this process in-situ removal of CO_2 by CaO was used to improve hydrogen yield significantly.

Catalysts play a crucial role in both steam reforming of ethanol and sorption enhanced steam reforming of ethanol reactions. Discovery of mesoporous catalyst supports, like MCM-41, started a new pathway in catalysis research. In this study, Co and Ni incorporated MCM-41 type materials having metal/Si molar ratio of 0.1 were synthesized by impregnation method, characterized and tested in both steam

reforming of ethanol and sorption enhanced steam reforming of ethanol reactions at 500^{o}C, 550^{o}C and 600^{o}C. EDS and XRD results of the synthesized catalysts showed that Co and Ni were successfully incorporated and well dispersed in the MCM-41 support. The characteristic ordered pore structure of MCM-41 was partially conserved. Synthesized Co-MCM-41 and Ni-MCM-41 had surface area and pore diameter values of 303.6 m^2/g – 1.98 nm and 449 m^2/g – 2.2 nm, respectively.

Catalytic test results obtained with both catalysts proved that hydrogen yield values were significantly enhanced in the presence of CaO during in situ capture of CO_2. Catalytic performance of Ni-MCM-41 was much better than Co-MCM-41 in ethanol reforming reaction. The highest hydrogen yield obtained with Co-MCM-41 catalyst was achieved at 550^{o}C as 3.1 with in situ capture of CO_2. This value is not high enough for practical use of this catalyst. At the same temperature, the corresponding hydrogen yield value was only 1.62 in the absence of CaO. The catalytic test results obtained with Ni-MCM-41 at 600^{o}C, gave a hydrogen yield value of 5.6 in the sorption enhanced reforming run, which is about 94% of the maximum possible hydrogen yield of six.

Keywords: Co-MCM-41, Ni-MCM-41, steam reforming, sorption enhanced steam reforming, hydrogen

ÖZ

KOBALT, NİKEL EKLENMİŞ MCM-41 ÜZERİNDE HİDROJEN ÜRETİMİ AMACIYLA ADSORPSİYON DESTEKLİ ETANOL REFORMLAMA

Gündüz, Seval
Yüksek Lisans, Kimya Mühendisliği
Tez Danışmanı: Prof. Dr. Timur DOĞU

Şubat 2011, 139 sayfa

Kısıtlı miktardaki fosil kaynakların tükenmeye yüz tutması ve CO_2 emisyonuna bağlı çevresel etki nedeniyle temiz enerji kaynağı olan hidrojene ilgi artmaktadır. Yüksek miktarda su içeren biyo-etanolden buharlı reformlama reaksiyonu ile hidrojen üretimi, CO_2 nötrlüğü nedeniyle yüksek potansiyel taşımaktadır. Fakat etanol buharlı reformlama reaksiyonu, hidrojen verimini azaltan ve proses ekonomisine negatif etki yapan birçok yan reaksiyona sahip kompleks bir prosestir. Ayrıca termodinamik limitasyonlar hidrojen veriminde azalmaya yol açar. Bu çalışmada, Ni ve Co impregne edilmiş MCM-41 tipi mezogözenekli katalizörler üzerinde denenen etanol buharlı reformlama reaksiyonunun hidrojen verimini arttırmak için adsorpsiyon destekli buharlı reformlama adı verilen yeni bir proses incelenmiştir. Bu proseste hidrojen verimini arttırmak amacıyla CO_2'nin CaO aracılığıyla uzaklaştırılması yöntemi kullanılmıştır.

Katalizörler, hem etanol buharlı reformlama reaksiyonu hem de adsorpsiyon destekli buharlı reformlama reaksiyonu üzerinde önemli rol oynamaktadırlar. MCM-41 tipi mezogözenekli katalizörlerin keşfi, kataliz çalışmalarında yeni bir dönem başlatmıştır. Bu çalışmada, metal/Si mol oranı 0.1 olan, Co ve Ni içeren MCM-41 tipi malzemeler impregnasyon yöntemi ile sentezlenmiş, karakterize edilmiş ve 500^oC, 550^oC ve 600^oC'lerde hem etanol buharlı reformlama hem de adsorpsiyon

destekli etanol buharlı reformlama reaksiyonlarında test edilmiştir. Sentezlenen katalizörlerin EDS ve XRD sonuçları, Co ve Ni'in MCM-41 yapısına başarıyla katıldığını göstermektedir. MCM-41'in karakteristik gözenek yapısı kısmen korunmuştur. Sentezlenen Co-MCM-41 ve Ni-MCM-41 katalizörlerinin yüzey alanı ve gözenek çapı değerleri sırasıyla; 303.6 m^2/g – 1.98 nm ve 449 m^2/g – 2.2 nm'dir.

Her iki katalizörle elde edilen katalitik test sonuçları, hidrojen veriminin CaO varlığında önemli ölçüde arttığını kanıtlamıştır. Ni-MCM-41 katalizörünün katalitik performansı Co-MCM-41 katalizörüne göre daha fazladır. Co-MCM-41 katalizörü ile elde edilen en yüksek hidrojen verimi CO_2 adsorpsiyonu sırasında 550^oC'de 3.1 olarak elde edilmiştir. Bu değer katalizörün pratik kullanımı için uygun değildir. Aynı sıcaklıkta CaO kullanılmadığında hidrojen verimi sadece 1.62'dir. 600^oC'de Ni-MCM-41 katalizörünün adsorsiyon destekli reformlama reaksiyonunda hidrojen verimi 5.6'dır ve bu değer elde edilebilecek en yüksek hidrojen verimi olan 6'nın %94'ününe tekabül eder.

Anahtar Kelimeler: Co-MCM-41, Ni-MCM-41, buharlı reformlama, adsorpsiyon destekli buharlı reformlama, hidrojen

To My Family

ACKNOWLEDGEMENTS

First and foremost acknowledgements go to my supervisor Prof. Dr. Timur DOĞU for his support and guidance throughout my studies. Without his support and suggestions, this work would not be possible. I would also like to present my gratefulness to Prof. Dr. Gülşen DOĞU for her kindness.

I would like to thank my lab-mates Canan Şener, Zeynep Obalı, Cem Tokay, Ayça Arınan, Sultan Orman, Caner Hocaoğlu and Gökhan Çelik.

Finally I would like to thank my family who support me throughout my life and did not sleep when I studied in laboratory at nights.

I am grateful to all my friends who helped me to put this work together.

TABLE OF CONTENTS

LIST OF TABLES

LIST OF FIGURES

CHAPTER 1

INTRODUCTION

Nowadays fuel consumption increases due to the growing population, economy and improvement in human life style. It is expected that energy consumption will rise from 412 quadrillion British Thermal Unit (Btu) in 2002 to 553 quadrillion Btu in 2015 and then to 645 quadrillion Btu in 2025 **[1]**. At this point the questions of "how can such amount of energy be provided" and "what are the resources available" must be answered. According to Song **[2]**, use of today's dominant energy sources such as petroleum, natural gas and coal will continue as the primary energy sources in the 21st century, as well. However, increasing use of these fossil fuels creates two main problems. These are; they are limited and concentrated in some regions of the world and they add environmental pollutants such as SO_2 and greenhouse gases such as CO_2 to the atmosphere. Therefore, finding ways to satisfy the energy demand of the future with less environmental impact have been a major research area.

Unlike fossil fuels, hydrogen burns cleanly without emitting any environmental pollutants. Hydrogen can be produced from a wide range of primary fuels such as natural gas, coal, biomass, water, solar, wind and nuclear which reduces the dependence on limited fossil fuels. Therefore, hydrogen is considered to be an energy carrier of the future. Hydrogen production techniques can be classified into three main categories, which are thermochemical, electrochemical and biological techniques. This study focused on the hydrogen production using steam reforming process which is a member of thermochemical technique. As mentioned before, many feedstocks can be used in hydrogen production by reforming reaction. Among all the alternatives, bio-ethanol seems to be a good candidate, because ethanol steam reforming reaction provides closed carbon loop (generated CO_2 in steam reforming reaction is used in photosynthesis process) and could be easily reformed into hydrogen rich gas in the presence of steam at lower temperatures of other resources,

like natural gas. Presence of water in bio-ethanol may be used in the reforming process. Other advantages are; safety and ease handling, storage and transportation of ethanol. Additionally, it is non-toxic to human health.

In practice, it is not easy to achieve ethanol steam reforming reaction alone due to reaction reversibility, coke formation and undesired reaction pathways. Possible side reactions that can occur during steam reforming of ethanol process are dehydration to form ethylene, dehydrogenation and decomposition of ethanol to methane and other hydrocarbons. These side reactions decrease hydrogen yield as expected. Also, equilibrium limitations in water gas shift reaction cause presence of high concentration of CO in the product stream, which also cause a decrease in hydrogen yield. Hydrogen yield can be improved by separating one of the products during reaction. Since H_2 separation process is expensive and difficult to achieve, in this study, CO_2 was separated from product gas mixture to enhance hydrogen yield, which is called as sorption enhanced steam reforming process.

Catalyst plays significant role in both steam reforming of ethanol and sorption enhanced steam reforming of ethanol reactions. Recent researches have focused on the mesoporous catalysts especially MCM-41 type material which is a member of M41S family discovered by Mobil researchers in 1992. These materials have large internal surface area above 1000 m^2/g and uniform pore size distribution. Catalytic activity of MCM-41 type materials can be enhanced by integration of active metals onto this material.

In this study, cobalt and nickel impregnated MCM-41 catalysts, having Co/Si and Ni/Si molar ratios of 0.1, were synthesized, characterized and tested in both steam reforming of ethanol and sorption enhanced steam reforming of ethanol reactions.

In Chapter 2, steam reforming of ethanol reaction is investigated in detail. In sub-sections, review of hydrogen production processes, general aspects of steam reforming of ethanol reaction, thermodynamics of the reaction and catalysts used in steam reforming of ethanol reaction are given.

In Chapter 3, sorption enhanced steam reforming of ethanol process is introduced.

In Chapter 4, mesoporous materials especially M41S family members are summarized and literature survey on modification of MCM-41 type materials for catalytic purposes is given.

In Chapter 5, experimental studies including catalyst preparation, characterization and reaction set-up are described.

In Chapter 6, characterization results of catalysts and catalytic test results are given. Steam reforming of ethanol and sorption enhanced steam reforming of ethanol reactions are compared according to ethanol conversion, hydrogen yield and product selectivity at the same conditions. Finally, conclusions and recommendations are displayed in Chapter 7.

CHAPTER 2

STEAM REFORMING OF ETHANOL FOR HYDROGEN PRODUCTION

The increase in global population with increasing quality of life, has drastically increased world energy demand and therefore increased the fuel consumptions **[3]**. The fact is that fossil fuel resources will not be sufficient to supply future energy demand. Fast depletion of fossil based fuels also pollutes the world and causes global warming by the emission of greenhouse gases. Therefore, the demand for clean and renewable energy alternative has increased tremendously in recent years **[3]**.

Unlike fossil fuels, hydrogen burns cleanly with no emission of environmental pollutants and possesses the highest energy content per unit of weight, namely 120.7 kj/g **[4]**. Hydrogen is considered to be a potential energy carrier of the future and could gain an important role in reducing environmental emissions.

Besides its advantages, hydrogen has also some disadvantages, like storage and transportation. However, these problems can be solved by on-board production of hydrogen.

2.1. Review of Hydrogen Production Processes

Hydrogen production techniques can be investigated under four groups; these are thermochemical technique, electrochemical technique, photobiological technique and photoelectrochemical technique.

2.1.1. Thermochemical Technique

Steam reforming is the most widely used thermochemical process to produce hydrogen from various feedstocks such as natural gas, coal, gasoline, methane, propane, light diesel, dry biomass and biomass-derived liquid fuels. Gasification and pyrolysis processes are the other members of thermochemical technology **[4]**.

2.1.2 Electrochemical Technique

Electrolysis of water to produce hydrogen can be studied under electrochemical technique **[4]**. This technology would be competitive only if low-cost electricity is available.

2.1.3 Photobiological Technique

In photobiological technique, natural photosynthetic activity of bacteria and green algae is used to produce hydrogen. The major problem of this technology is its very slow production rates **[5]**. This technique is still immature and in the early stage of investigation.

2.1.4 Photoelectrochemical Technique

In this process, hydrogen is produced by splitting water by illuminating a water-immersed semiconductor, such as titania, with sunlight **[6]**. Photoelectrochemical technique is also in the early stages of development.

Steam reforming technology is the most energy-efficient technology currently available. Although hydrogen rich gas production by steam reforming reaction is limited by thermodynamic balance, the reaction is relatively fast. In addition, catalytic steam reforming of hydrocarbons is the most cost effective process when compared to other technologies.

Table 2.1: Cost and energy efficiency from selected technologies to produce hydrogen **[4]**

Technology	Cost ($/kg H_2)	Energy Efficiency %
Coal Gasification	2.17	60
Biomass Gasification	7.07	45-50
Water Electrolysis	7.36	27
Methane Steam Reforming	3.94	70

By steam reforming reaction, hydrogen can be produced from many feedstocks, like methane, gasoline, coal, natural gas, propane, light diesel, dry biomass, biomass-derived liquid fuels (methanol, ethanol, biodiesel …). Among all the alternatives, alcohols are good candidates since they can easily decompose into hydrogen rich mixture in the presence of steam. Methanol is the most studied alcohol for hydrogen production; however it is highly toxic and obtained from non-renewable fossil-based fuels. Ethanol is a better alternative, because;

- It is renewable and becoming increasingly available
- It can be produced from biomass (cellulose)
- It already contains significant amount of water, when produced by fermentation
- It is easy to transport and store
- It is low in toxicity and biodegradable
- It could be easily decomposed in the presence of steam to form hydrogen rich mixture
- One liter ethanol contains 103 g hydrogen, which is higher than hydrogen mass in one liter of liquid hydrogen (70.8 g/l)
- It is free from catalyst poisons such as sulfur. **[4]**

2.2. General Aspects of Steam Reforming of Ethanol Reaction

The overall steam reforming of ethanol can be represented as **[7]**;

$$C_2H_5OH+3H_2O\rightarrow 2CO_2+6H_2 \qquad (2.1)$$

However, there are several side reactions that occur during steam reforming of ethanol. Some possible reactions that may occur during ethanol steam reforming process are summarized in Table 2.2.

Table 2.2: Possible reaction paths that may occur in steam reforming of ethanol process

Reaction	Equation	Remarks
Sufficient Steam Supply	$C_2H_5OH+3H_2O\rightarrow 2CO_2+6H_2$	Ideal pathway, the highest hydrogen production
Insufficient Steam Supply	$C_2H_5OH+H_2O\rightarrow 2CO+4H_2$ $C_2H_5OH+2H_2\rightarrow 2CH_4+H_2O$	Undesirable products, lower hydrogen production
Dehydrogenation Acetaldehyde decomposition Acetaldehyde steam reforming	$C_2H_5OH\rightarrow C_2H_4O+H_2$ $C_2H_4O\rightarrow CH_4+CO$ $C_2H_4O+H_2O\rightarrow 3H_2+2CO$	Reaction pathways for hydrogen production in practice
Dehydration Coke formation	$C_2H_5OH\rightarrow C_2H_4+H_2O$ $C_2H_4\rightarrow$polymeric deposits (coke)	Undesired pathway in the presence of acidic catalysts, main source of coke formation
Decomposition	$C_2H_5OH\rightarrow CO+CH_4+H_2$ $2C_2H_5OH\rightarrow C_3H_6O+CO+3H_2$ $C_2H_5OH\rightarrow 0.5CO_2+1.5CH_4$ $C_2H_5OH\rightarrow CH_2O+ CH_4$	Coke formation, low hydrogen production
Methanation Methane decomposition Boudouard reaction	$CO+3H_2\rightarrow CH_4+H_2O$ $CO_2+4H_2\rightarrow CH_4+2H_2O$ $CH_4\rightarrow 2H_2+C$ $2CO\rightarrow CO_2+C$	Reaction network of decomposition products
Water gas shift reaction (WGSR)	$CO+H_2O\rightarrow CO_2+H_2$	Reduce coke formation, enhance hydrogen production

As it can be seen from Table 2.2, hydrogen production may take place through different reaction pathways. In order to maximize hydrogen production, it is

vital to ensure sufficient supply of steam and minimize dehydration, dehydrogenation and decomposition reactions.

The possible reaction pathways and thermodynamics of ethanol steam reforming are reviewed in Section 2.3.

2.3. Thermodynamics of Ethanol Steam Reforming Reaction

Steam reforming of ethanol process involves multiple reaction pathways which affect the hydrogen purity. The selectivity of the reactions depends strongly on the process variables and the type of catalyst used. In order to investigate the effect of the variables on the product composition, the main step is to perform a thermodynamic analysis of the process.

According to the studies conducted by Garcia et. al. **[8]** and Vasudeva et. al. **[9]**, H_2 and CO concentrations in the product stream increase and CH_4 concentration decrease with increasing temperature. In order to achieve the highest hydrogen production, high temperature and high water-to-ethanol ratios are needed. They concluded that temperature higher than 650 K, atmospheric pressure and water-to-ethanol molar ratio of up to 10 in the feed is required to get the highest H_2 production, to minimize the concentrations of side products in the product stream and to avoid the coke deposition on the catalyst.

Another thermodynamic analysis of steam reforming of ethanol reaction was performed by Fishtik et. al **[10]**. They claimed that from a thermodynamic point of view, ethanol is unstable with respect to a mixture of H_2O, H_2, CO, CO_2 and CH_4. At low water concentrations and low temperature, ethanol decomposes according to the reaction;

$$2C_2H_5OH \rightarrow 3CH_4 + CO_2 \qquad (2.2)$$

In the case of low water concentration and high temperature, the reaction given below is dominant.

$$C_2H_5OH \rightarrow CH_4 + H_2 + CO \qquad (2.3)$$

To dominate the steam reforming reaction, temperature range of 700 – 800 K and above and high amount of water are needed. High temperature and high water

amount increase the extents of water gas shift reaction and methane steam reforming reactions which reduce the amounts of undesired side products CO and CH_4.

Wang et. al. **[11]** studied the thermodynamics of steam reforming of ethanol reaction from a different point of view. According to Wang et. al., in addition to effect of temperature, and water/ethanol ratio, the effect of inert gases should also be considered in the thermodynamic analysis of steam reforming of ethanol. They concluded that the coke-formation temperatures decrease with increasing water/ethanol ratio and high inert gas-to-ethanol ratio favors the hydrogen yield.

Different from the previous studies, Ionnides **[12]** performed his analysis with respect to solid polymer fuel cell applications and concluded that water-to-ethanol feed ratio should not be much higher than stoichiometric value in order to make the process feasible because high amounts of water in feed stream needs high heat energy to be evaporated.

The common outcomes of the studies mentioned above are;

- High temperature favors hydrogen production in steam reforming of ethanol reaction.
- Atmospheric pressure is sufficient for the process.
- High water-to-ethanol ratio enhances the steam reforming of ethanol reaction, water gas shift reaction and methane steam reforming reactions.
- Steam reforming of ethanol is a thermodynamically feasible process.

2.4. Catalysts Used for Ethanol Steam Reforming Reaction

Steam reforming of ethanol (SRE) is a very complicated process due to the possibility of many undesired pathways which have a negative effect on ethanol conversion and hydrogen yield. Therefore, catalyst plays significant role in this process, since each catalyst induces different reaction paths.

The oldest studies about steam reforming of ethanol reaction focused on the oxide catalysts such as alumina (Al_2O_3), vanadia (V_2O_5), zinc oxide (ZnO) and ceria (CeO_2). The study conducted by Llorca et. al **[13]** showed that alumina and vanadia exhibited high activity towards ethanol conversion. Complete conversion of ethanol

was achieved with alumina and vanadia catalysts at 623 K. However, only small amounts of H_2 were produced with these catalysts since undesired reactions dominated the reaction pathway. High amounts of C_2H_4 and C_2H_4O were observed in the product stream. They also studied ZnO catalyst for steam reforming of ethanol reaction at 723 K, atmospheric pressure and with a steam/ethanol ratio of 13 and concluded that ZnO is the best oxide catalyst among the others. Complete conversion of ethanol was achieved with a relatively high yield of hydrogen. They claimed that the product gas contained 97.7% H_2. However no information was available about the durability of the catalyst.

Oxide-supported metal catalysts were also studied for steam reforming of ethanol reaction. The most studied oxide supported metal catalysts were Co/Al_2O_3, Ni/Al_2O_3 and Co/ZnO. Haga et. al. **[14]** studied steam reforming of ethanol reaction over Co/Al_2O_3 catalyst and compared the results with the Co/SiO_2, Co/MgO, Co/ZrO_2 and Co/C catalysts and concluded that Co/Al_2O_3 was a promising catalyst among the others. Comas et. al. **[15]** investigated Ni/Al_2O_3 catalyst via steam reforming of ethanol reaction at high temperatures above 773 K and steam-to-ethanol molar ratio of 6. This study showed that 91% H_2 can be achieved via steam reforming of ethanol reaction over Ni/Al_2O_3 catalyst at given conditions.

Noble metals were also studied in steam reforming of ethanol reaction. Rh, Pt, Ru and Pd are the most studied noble metals for reforming process. Although they showed good performance towards ethanol steam reforming reaction, they are very expensive and it is not economically feasible to use these metals as catalyst.

With the discovery of mesoporous materials, researchers' attention has focused on the metal incorporated novel mesoporous materials. Detailed literature survey study was done on this topic and given in Chapter 4.

CHAPTER 3

SORPTION ENHANCED STEAM REFORMING OF ETHANOL

As mentioned in the previous chapter, due to depletion of fossil fuel resources and environmental impact, the interest in hydrogen as a clean and renewable energy source has increased recently. As a result, efficient H_2 production techniques are of great importance. In this context, hydrogen production from bio-renewable sources such as ethanol by steam reforming reaction has shown a great potential with the advantage of CO_2 neutrality of bio-ethanol **[16]**. The ideal pathway of complete steam reforming of ethanol is given below.

$$C_2H_5OH + 3H_2O \longleftrightarrow 2CO_2 + 6H_2 \qquad \Delta H^o_{25\,^oC} = 173\ kj/mol \quad (3.1)$$

However, in practice, it is not easy to achieve the reaction given above alone due to reaction reversibility, coke formation and undesired reaction pathways **[16]**. Possible side reactions that can occur during steam reforming of ethanol are given below.

Dehydrogenation of Ethanol

$$C_2H_5OH \longleftrightarrow C_2H_4O + H_2 \qquad \Delta H^o_{25\,^oC} = 68\ kj/mol \quad (3.2)$$

Dehydration of Ethanol

$$C_2H_5OH \longleftrightarrow C_2H_4 + H_2O \qquad \Delta H^o_{25\,^oC} = 44\ kj/mol \quad (3.3)$$

Decomposition of Ethanol

$$C_2H_5OH \longleftrightarrow CO + CH_4 + H_2 \quad (3.4)$$

Methane Decomposition

$$CH_4 \longrightarrow H_2 + C \quad (3.5)$$

Boudouard Reaction

$$2CO \longrightarrow CO_2 + C \quad (3.6)$$

Due to these side reactions, product gas has low hydrogen purity. The hydrogen yield in the product gas can be improved by using membrane reactor, which can separate hydrogen from product gas mixture **[17, 18]**. Particular membranes for steam reforming reaction for H_2 rich gas production are Hydrogen Transport Membrane (HTM), Ion Transport Membrane (ITM), Palladium Membrane (PM) and Inorganic Membranes for High Temperature Hydrogen Separation (IMTL) **[17]**. However, in addition to the complexity of steam reforming of ethanol reaction, the operation of membrane technology has its own difficulties. Membrane pore blockage, thermal and mechanical stability problems and the dilution caused by the need for sweep (permeate purge) gases are some limitations of the membrane reactor system **[16]**.

Nowadays, a new reaction process has been proposed to improve hydrogen production by steam reforming. This process is called sorption-enhanced steam reforming and it is based on Le Chatelier's principle in which the reaction equilibrium will be shifted to favor increase of the reactant conversion upon in situ removal of hydrogen or carbon dioxide **[16]**. Since removal of hydrogen in a single reformer unit is very difficult and expensive to achieve, byproduct CO_2 is selected for capturing from the product gas mixture. If CO_2 generated from the steam reforming process is separated from product gas phase by using a solid adsorbent such as CaO or hydrotalcites, H_2 production can be enhanced toward completion **[16]**. The CO_2 capture with sorbent CaO and overall sorption enhanced steam reforming of ethanol (SESRE) reactions are illustrated in Equation 3.7 and Equation 3.8, respectively.

$$CaO_{(s)} + CO_2 \leftrightarrow CaCO_{3(s)} \tag{3.7}$$

$$C_2H_5OH + 3H_2O + 2CaO \leftrightarrow 2CaCO_{3(s)} + 6H_2 \tag{3.8}$$

In addition to high H_2 production capacity, the other advantages, such as less coke formation, easy CO_2 sequestration or recovery and achieving a product gas having CO and CO_2 concentrations below 100 ppm are expected in sorption enhanced steam reforming process. Very low CO concentration in the product gas is needed in fuel cell applications.

The sorption enhanced steam reforming technology studies conducted up to now have been focused on CH_4 as feedstock. Wang et. al. **[19]** studied steam methane reforming reaction coupled with in situ CO_2 capture. They concluded that, to achieve the objective of hydrogen production with low CO content, the appropriate choice of operation parameters is required. According to the study, the bed residence time has a significant effect on the sorption enhancement behavior. The longer bed residence time is needed for promoting H_2 purity and controlling CO concentration. Another study was conducted by Yi et. al. **[20]** in which Ni-based catalyst and dolomite as sorbent was used with a steam-to-methane ratio of 3 and at pressures between 1 and 3 bars. It was claimed that, at 460^oC and 1 bar, a product gas containing 96 mol % H_2 with CO concentration being near 50 ppm was obtained. At 440 ^oC and 3 bar, the product gas contained 92 mol % H_2 and CO concentration was reduced to 11 ppm. Under the light of this study, it was concluded that low temperature and high pressure are effective in reducing the CO concentration, but with a sacrifice in H_2 concentration.

Wang et. al. **[21]** studied the thermodynamic features of hydrogen production by sorption enhanced steam reforming of propane with the method of Gibbs free energy minimization to investigate the effect of pressure (1-5 atm), temperature (700-1100 K), water-to-propane ratio (1-18) on equilibrium composition and carbon formation. The results showed that atmospheric pressure and water-to-propane ratio of 12 are suitable for both steam reforming of propane and sorption enhanced steam reforming of propane. The optimum temperature for sorption enhanced reforming of propane was 825 K. Stoichiometric value which is 10 moles of H_2 per mole of propane was achieved with no CO or CO_2 production with only impurity being CH_4.

Glycerol was studied as a feedstock for sorption enhanced steam reforming process by Dupont et. al. **[22],** in a continuous flow fixed-bed reactor. Experiments were conducted under atmospheric pressure within a temperature range of 400-700^oC. Commercial Ni-based catalyst and dolomite sorbent were used in the reactions. The results showed that H_2 production increased with the increasing temperature and the formation of by-product methane became negligible above 500 ^oC. Dupont et. al. concluded that the longest CO_2 breakthrough time and the highest

H_2 yield can be achieved at or above 500 ^oC for the glycerol steam reforming with in situ removal of CO_2 using calcined dolomite as the sorbent.

The advantages of in situ CO_2 sorption have been studied both experimentally and conceptually mostly with methane and some experiments conducted with propane and glycerol as mentioned above. However little study has been done with ethanol. The distinct chemical properties of ethanol and the complicated reaction mechanism of ethanol reforming require further investigation on sorption enhanced steam reforming of ethanol (SESRE) for application of H_2 production **[16]**.

Lysikov et. al. **[23]** studied H_2 production via sorption enhanced steam reforming process with various feedstocks on $CaCO_3$-calcined acceptor and commercial Ni catalyst. They concluded that ethanol exhibited advantage over the other studied fuels (methane, propane-butane mixture and methanol) by yielding high quality H_2. Iwasaki et. al. **[24]** conducted experimental study via sorption enhanced steam reforming of ethanol process on 1 wt % Rh/CeO_2 catalyst and Li_4SiO_4 as sorbent and concluded that the highest hydrogen concentration in product stream was 96% at 550 ^oC. Essaki et. al. **[25]** claimed that product gas containing 99% H_2 concentration could be achieved via sorption enhanced steam reforming of ethanol reaction with CO being below 0.12%, on commercial 58 wt % Ni/Al_2O_3 catalyst and Li_4SiO_4 as sorbent operated at 850-900^oC, 1 atm and steam-to-ethanol ratio of 3.

Since sorption enhanced steam reforming of ethanol reaction is a hybrid process of CO_2 capture and complicated steam reforming of ethanol, catalyst used in the process plays an important role in ethanol conversion and product gas concentration profile. Commercial Ni-based catalysts with different support materials such as Al_2O_3, hydrotalcite-like materials etc are tested in SESRE process.

The reported results mentioned above have encouraged scientists to investigate the sorption enhanced steam reforming concept. Under the light of these studies, our aim in this work is to perform both steam reforming of ethanol (SRE) and sorption enhanced steam reforming of ethanol (SESRE) reactions under the same conditions to investigate the effects of CO_2 removal on ethanol conversion, hydrogen yield and product distribution over novel mesoporous catalysts.

CHAPTER 4

MESOPOROUS CATALYSTS

In this study, MCM-41 which is a member of M41S family was chosen as the host material. Due to its large internal surface area and narrow pore size distribution **[26]**, MCM-41 attracted significant attention in recent years, as a support material. To enhance the catalytic activity of MCM-41 towards reforming reaction, active metals cobalt and nickel were incorporated into MCM-41 structure. In this chapter, properties of M41S family mesoporous materials and especially MCM-41, characterization techniques for MCM-41 type materials, modification of MCM-41 for catalytic purposes, and the literature survey on the Co and Ni incorporated MCM-41 catalysts are given.

4.1. Porous Materials

Porous materials can be classified according to IUPAC definition into three groups; microporous, mesoporous and macroporous materials **[27]**. Microporous materials have pore diameter less than 2 nm, mesoporous materials have pore diameter between 2nm and 50 nm and macroporous materials have pore diameter larger than 50 nm.

Microporous materials, especially zeolites, take great attention within industrial areas such as oil refining, petrochemistry and chemical synthesis and they are also very important as adsorbents. Their success in catalytic applications is based on **[28]**:

- High surface area and adsorption capacity,
- Controlled adsorption properties (vary from hydrophobic to hydrophilic type materials),
- Generation of active sites in the framework,

- Their channel structure, which allows zeolites to present different types of shape selectivity such as product, reactant and transition state, which
- can be used to direct a given catalytic reaction towards the desired product, avoiding the side reactions.

Despite the advantages listed above, zeolites have a vital limitation that they are not able to process molecules that are larger than their pore diameters (1-1.2 nm). Because of that, attention of researchers is focused on increasing the pore diameter to bring them into mesoporous region without damaging the porous structure of the material. For this purpose, many researches were conducted. Researchers at Union Carbide discovered $AlPO_4$ structures having a pore size range of 1.3-1.5 nm. Soon after, related materials such as SAPO's (silicoaluminophosphates) and MeAPOs (metal aluminophosphates) were synthesized **[27]**. The common problems of these materials are their lack of thermal and hydrothermal stability.

In 1992, Mobil scientists discovered a new family of nanostructured mesoporous materials, named as M41S family **[29]**. This discovery was the solution of zeolite pore diameter limitation and opened a new avenue in the porous material research and catalysis.

4.2. M41S Family

The main groups of M41S family, which was discovered by Mobil scientists in 1992, are MCM-41 with one-dimensional, hexagonally-ordered pore structure, MCM-48 with three-dimensional, cubic-ordered pore structure and MCM-50 with unstable lamellar structure. Possible structures of MCM-41, MCM-48 and MCM-50 are given in Figure 4.1.

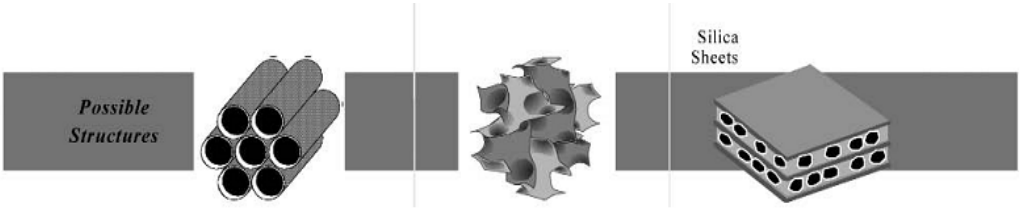

Figure 4.1: The M41S family of materials including MCM-41, MCM-48 and MCM-50 **[29]**

M41S family materials have unique physical and chemical properties. Generally, these ordered mesoporous materials have large surface area, approximately 1200 m^2/g and have uniform channels ranging from 2 to 50 nm.

From the atomic level, this family of mesoporous materials is disordered and amorphous, however, the pores in the materials are uniformly arranged and pore diameters are narrowly distributed in size **[30]]**.

Main components of M41S synthesis are structure-directing surfactant, a source of silica, a solvent and a catalyst (an acid or a base). Materials' structure depends on the behavior of surfactant molecules in solvent. In water-surfactant binary systems, surfactant molecules display various structures with increasing surfactant concentration. These structures are schematically shown in Figure 4.2.

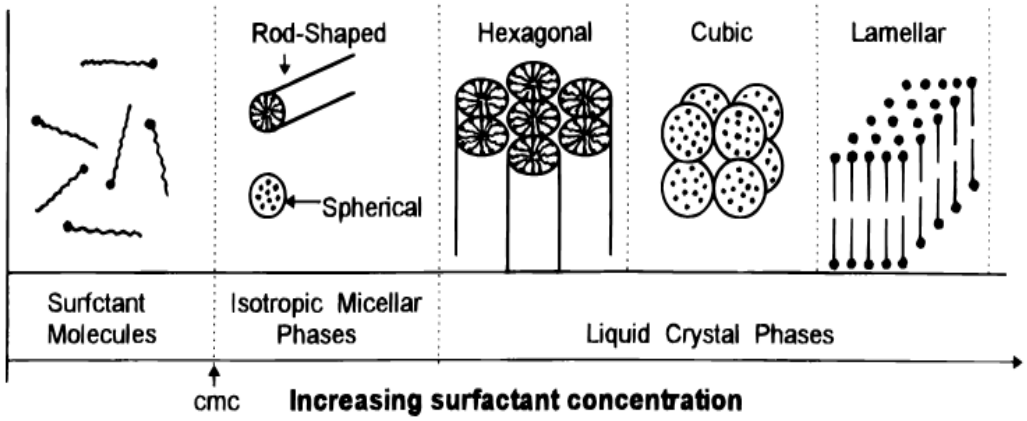

Figure 4.2: Surfactant behavior in water-surfactant binary system **[31]**

As shown in Fig. 4.2, at low concentrations, surfactants exist as monomolecules. Surfactant molecules aggregate together to form micelles with increasing surfactant concentration to decrease the system entropy **[31]**. The lowest concentration at which monomolecules aggregate to form micelles is called cmc (critical micellization concentration). As the surfactant concentration increases further, hexagonal phases appear. Further concentration increase leads to lamellar phase formation. In some cases, between hexagonal and lamellar phases, cubic forms can form.

The detailed explanation of M41S family members is presented in the following sections.

4.2.1. MCM-41

MCM-41 has been studied widely because the other members of M41S family are either thermally unstable or difficult to obtain.

MCM-41 type mesoporous materials have unique unidirectional, honeycomb-like structure as shown in Figure 4.3. They have large internal surface area approximately 1000 m^2/g, good thermal and hydrothermal stability, and hexagonally arranged channels with diameters varying from 1.5 to 10 nm **[32]**.

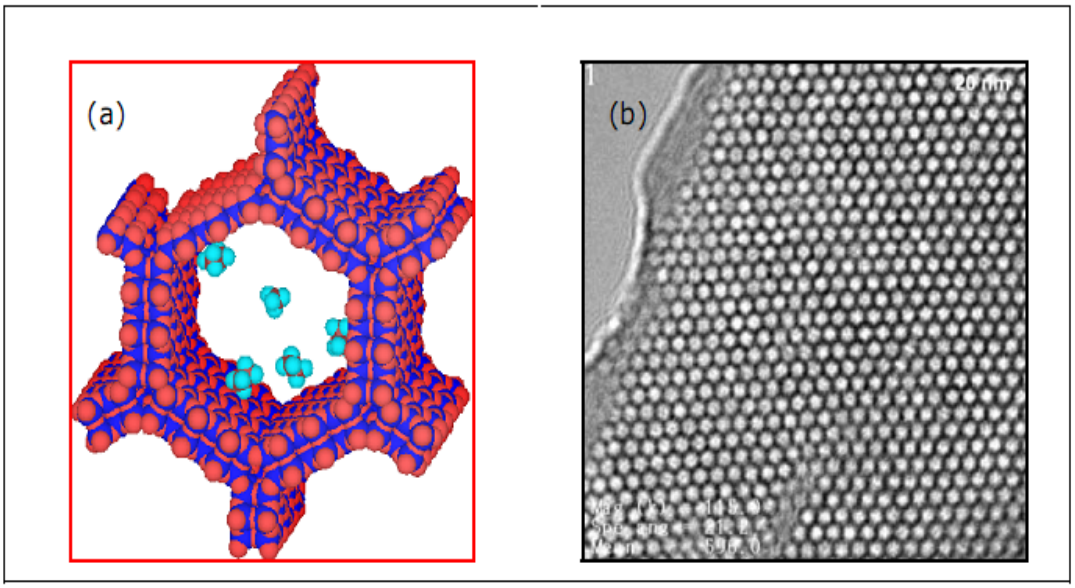

Figure 4.3: (a) Schematical representation of MCM-41 (b) TEM image of MCM-41 **[33]**

The mechanisms responsible for the formation of MCM-41 have attracted much attention. Two typical mechanisms have been proposed so far by Beck et al **[34]** and Stucky et al. **[35]**. The mechanism proposed by Beck et al is called liquid crystal templating (LCT) mechanism and the mechanism proposed by Stucky et al is called transformation mechanism from lamellar to hexagonal phase **[31]**.

Liquid Crystal Templating (LCT) Mechanism

According to the liquid crystal templating (LCT) mechanism proposed by Beck et al **[34]**, structure is defined by the organization of surfactant molecules into liquid crystals which serve as templates for the formation of MCM-41 structure **[36]**. The first step in the formation of MCM-41 structure according to LCT mechanism is formation of rod-shaped micelles. Then hexagonal liquid crystal mesophases form prior to the addition of silicate species and with the addition of silicate species, hexagonal array with silicate layer structure appears. Finally, after calcination, MCM-41 with cylindrical pores is obtained. Beck et al also proposed a second pathway for the formation of MCM-41. In this second pathway; randomly ordered rod-shaped micelles interact with silicate species and silicate encapsulated micelles form. These randomly ordered composite species spontaneously pack into highly ordered mesoporous phase with hexagonal arrangement and after calcination, MCM-41 structure can form **[31]**. The schematic model of LCT mechanism via two possible pathways is shown in Figure 4.4.

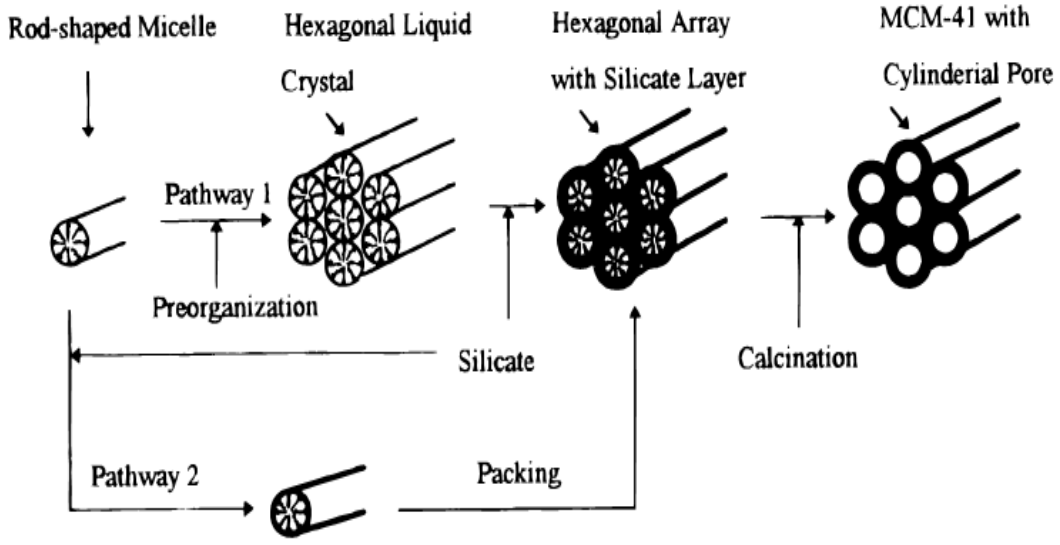

Figure 4.4: The schematic model of LCT mechanism via two possible pathways **[31]**

In 1993, Chen et al **[37]** investigated that no hexagonal liquid crystalline mesophases present either in the synthesized gel or in the surfactant solution. Therefore, it was concluded that pathway 2 is responsible for the formation of MCM-41 structure.

Transformation Mechanism from Lamellar to Hexagonal Phase

According to transformation mechanism proposed by Stucky et al. **[35]**, in early stage of the formation mechanism, ion exchange occurs between silicate oligomers and surfactant in the precursor solution and surfactant-silica complex is formed. This complex then forms a silicatropic liquid crystal (SLC) phase. Before the condensation of silicate species, a low-curvature lamellar phase is formed. The condensation of silicate causes a rearrangement of surfactant and causes mesophase transformation from low-curvature lamellar phase to high-curvature hexagonal one **[36]**. The schematic representation of transformation mechanism is given in Figure 4.5.

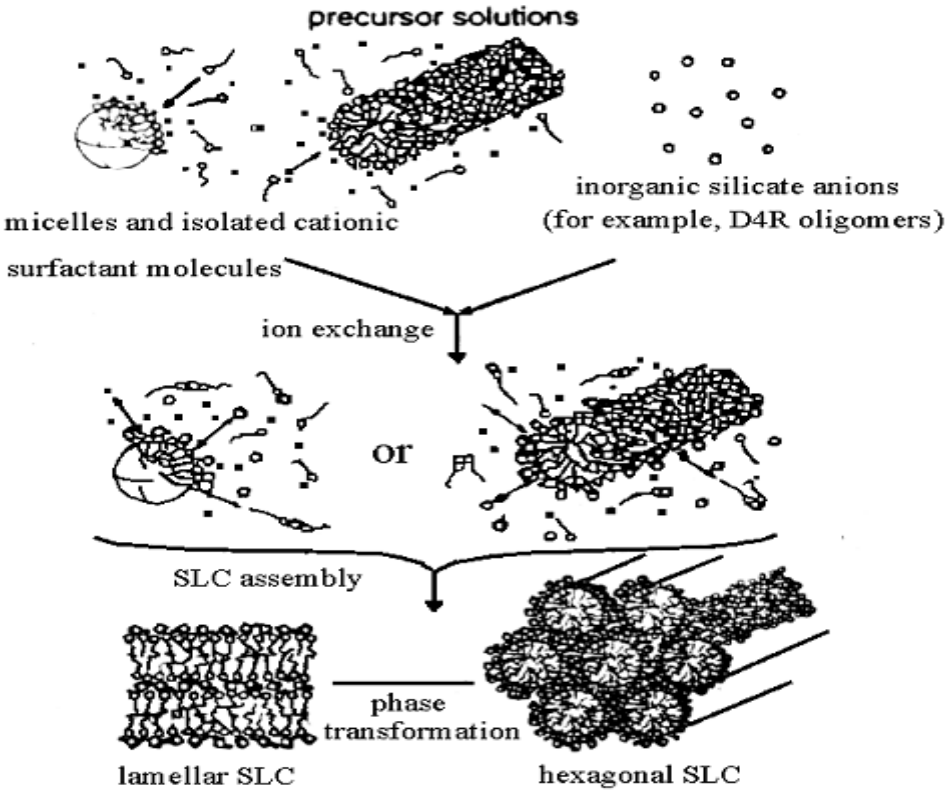

Figure 4.5: Schematic model for transformation mechanism from lamellar to hexagonal phase **[36]**

4.2.2. MCM-48

MCM-48 has a 3-dimensional cubic structure as shown in Figure 4.6. The unique physical features of MCM-48 are its high specific surface area up to 1600 m^2/g, specific pore volume up to 1.2 cm^3/g and high thermal stability. MCM-48 material has an interwoven and branched pore structure which provides favorable mass transfer kinetics in catalytic and separation applications **[38]**. Besides its interesting properties, difficult, expensive and not reproducible synthesis methods used for MCM-48 formation makes this M41S family member's large-scale synthesis impractical.

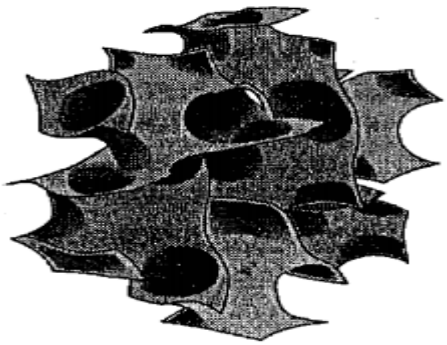

Figure 4.6: 3-dimensional cubic structure of MCM-48 **[39]**

4.2.3. MCM-50

MCM-50 possesses a lamellar arrangement of surfactant and silica layers. This structure collapses upon calcinations and does not give a mesoporous compound **[40]**. The schematic representation of MCM-50 structure is shown in Figure 4.7.

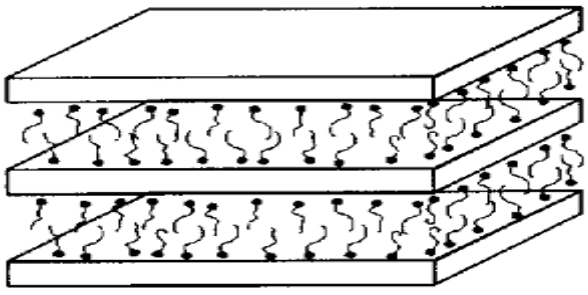

Figure 4.7: MCM-50 lamellar structure **[40]**

4.3. Characterization Techniques for MCM-41 Type Materials

4.3.1. X-Ray Diffraction (XRD)

X-ray diffraction is a method for determining the crystal structure of a material. This method is very convenient for analyzing the structure of ordered porous materials. The XRD pattern of a material is unique like a fingerprint. In the case of MCM-41, the XRD peaks do not result from crystal structure in the atomic range but from the well ordered pores. A well-ordered, hexagonal, honeycomb-like structured MCM-41 gives a sharp (100) plane diffraction main peak and three reflection peaks of higher Miller Index planes, (110), (200) and (210) **[41]**.

4.3.2. Nitrogen Physisorption (BET)

Low-temperature (77 K) nitrogen adsorption (physisorption) is accepted as a standard procedure for the determination of the surface area and pore size distribution of a wide range of porous materials **[42]**. MCM-41 materials having uniform pores ranging from 1.5 to 10 nm have been characterized extensively by nitrogen physisorption. The resulting isotherm obtained from nitrogen physisorption technique gives pore structure information of MCM-41, including pore size, surface area and pore size distribution.

The characteristic nitrogen physisorption (adsorption) isotherm of MCM-41 shows a sharp step in the mesoporous range of P/P_o= 0.2 to 0.5 which indicates the liquid condensation of N_2 at 77 K in the uniform mesopores of MCM-41.

4.3.3. Energy Dispersive Spectroscopy (EDS)

Energy dispersive spectroscopy (EDS) is an analytical technique used for the elemental analysis or chemical characterization of a sample **[43]**. In this technique, material is bombarded with electrons in an electron beam instrument to produce characteristic X-rays. Produced X-rays are detected by an energy dispersive spectrometer. Each element has a unique atomic structure allowing X-rays that are

characteristic of the element's atomic structure. By analyzing the X-ray data detected by energy dispersive spectrometer, elements present in the material can be investigated.

4.3.4. Scanning Electron Microscopy (SEM)

Scanning electron microscope (SEM) is a type of electron microscope that images the sample surface by scanning it with a high energy beam of electrons in a raster scan pattern. The electrons interact with the atoms that make up the sample producing signals that contain information about the sample's surface topography, composition and other properties such as electrical conductivity **[44]**.

4.4. Literature Survey on Modification of MCM-41 for Catalytic Purposes

MCM-41 type mesoporous materials have taken significant attention due to their unique physical properties, such as high internal surface area, large pore size and narrow pore size distribution, which are very important features of a good catalyst. However, in terms of catalytic activity, MCM-41 itself is not considered as an active catalyst. Catalytic functions can be introduced to MCM-41 by incorporation of active sites into its structure. Mesoporous structures are good supports for acids, bases, metals or metal oxides **[27]**. Incorporation can be achieved by several methods; common ones are impregnation and direct synthesis methods. In the extent of this study, cobalt and nickel incorporated MCM-41 type catalysts were investigated.

Cobalt-based catalysts have been widely applied for hydrogenation reactions and reforming reactions **[45]**. To obtain a high metal dispersion, Co is generally incorporated into a high surface area support. Various supports have been used for Co incorporation, such as MgO **[46, 47]**, ZrO_2 **[46, 48]**, Al_2O_3 **[46, 47, 49]**, CeO_2 **[47, 48, 50]**, TiO_2 **[47]** and SiO_2 **[46, 47]**. Recent researches have focused on Co incorporated novel mesoporous material MCM-41 due to its high surface area and superior dispersion of Co metal **[51, 52]**. Different researchers applied different procedures for the synthesis of Co incorporated MCM-41 and used these catalysts in

different reactions. Haller et al **[51]** synthesized Co-MCM-41 type catalyst having Co/Si ratio of 0.01 by direct synthesis method. The aim of this study was to investigate the pH effect on the dispersion of Co in the MCM-41 framework. They concluded that higher pH values enhance the metal dispersion and improve the structural order of MCM-41 resulting in a more porous and stable catalyst. Yang et al **[52]** studied methane dry reforming reaction over Co incorporated MCM-41 catalyst, synthesized by direct synthesis method and modified with Pt which was introduced by impregnation method. It was concluded that there was a strong interaction between Pt and Co which improved the catalytic performance of the material.

Supported Ni catalysts have been widely studied due to their high activity towards hydrogenation, hydrotreating and steam-reforming reactions **[53]**. In the study conducted by Bettahar et al **[53]**, Ni containing MCM-41 mesoporous catalysts were synthesized by both ion exchange and wet impregnation methods and tested in hydrogenation of benzene reaction. Another example can be given from the study of Haller et al **[54],** that they prepared Ni-MCM-41 catalysts containing 1-3 wt% Ni and the methanation of carbon dioxide reaction was carried out over those synthesized catalysts. It was concluded that higher selectivity and yield were achieved with higher Ni loaded catalysts (3% Ni). Ni incorporated catalysts are very popular in reforming reactions. Yang et al **[55]** studied carbon dioxide reforming of methane reaction over Ni-MCM-41 and Zr modified Ni-MCM-41 catalyst. They proposed that addition of Zr enhanced the structural stability of the catalyst and provided a better dispersion of active Ni sites. Zr modified Ni-MCM-41 catalysts also showed comparable or enhanced initial catalytic activities.

4.5. Objectives of the Study

Hydrogen is considered as the energy carrier of the future since it burns cleanly without emitting any environmental pollutants and possesses the highest energy content per unit mass. Among the feedstocks used in hydrogen production processes, ethanol is a good candidate due to its low toxicity, low price, easy transportation and storage and easy decomposition in the presence of steam.

Ethanol steam reforming reaction is a very complex process due to the possibility of many undesired reaction pathways and thermodynamic limitations have

a negative effect on ethanol conversion and hydrogen purity of the product gas. To overcome the thermodynamic limitations, sorption enhanced concept has been proposed. In the studies conducted via sorption enhanced steam reforming process up to now, usually methane was used as feedstock. However, the complex nature of ethanol steam reforming coupled with in situ capture of CO_2 needs more studies to be understood.

For this reason, in this study two different catalysts; Co impregnated and Ni impregnated MCM-41, were synthesized and tested in both steam reforming of ethanol and sorption enhanced steam reforming of ethanol reactions to observe the effect of in situ capture of CO_2 on ethanol conversion, hydrogen yield and product distributions. Additionally, reactions were repeated at different temperatures to see the temperature effect on steam reforming reaction.

CHAPTER 5

EXPERIMENTAL

In this study, a Co-MCM-41 type mesoporous catalyst with a Co/Si ratio of 0.1 and a Ni-MCM-41 type mesoporous catalyst, again containing a Ni/Si molar ratio of 0.1 were synthesized by impregnation method and tested in both steam reforming of ethanol reaction and sorption enhanced steam reforming of ethanol reaction at 500^{o}C, 550^{o}C and 600^{o}C.

5.1. Synthesis of Catalysts

5.1.1. MCM-41 Synthesis

5.1.1.i. Chemicals

- Silica Source: Sodium silicate solution (SiO_2.NaOH) – MERCK
- Surfactant Source: N-Cetyl-N,N,N-trimethylammonium bromide ($C_{19}H_{42}BrN$) – MERCK
- Solvent: Deionized water
- Acid Source: Sulfuric acid (H_2SO_4) – MERCK

5.1.1.ii. Synthesis Procedure

There are 4 main steps for MCM-41 synthesis. These steps are; preparation of synthesis solution, hydrothermal synthesis, filtering/washing and calcination. Detailed information for each step is given below.

- **Preparation of Synthesis Solution**

13.2 gr surfactant (CTMABr) was dissolved in 87 ml deionized water. Solution was continuously stirred at 500 rpm at 30^{o}C until clear solution was

obtained. The pH of the obtained clear solution was nearly 6. 11.3 ml sodium silicate solution was added to clear surfactant solution. The pH of the solution increased to 11.7 – 12.1. By the addition of 4N sulfuric acid, the pH of the solution was adjusted to 11. The final gel was stirred for 1 h at 30°C.

- **Hydrothermal Synthesis**

Final gel was put into a Teflon bottle placed into a stainless-steel autoclave. Hydrothermal synthesis was performed in an oven at 120°C, for 96 h.

- **Filtering/Washing**

The resultant solid product was washed with deionized water and filtered several times until the pH of the wash water remained constant. After washing, solid product was dried at 40°C under vacuum.

- **Calcination**

Solid product was placed into a quartz tube equipped with a membrane filter. Calcination was performed in a tubular furnace with a heating rate of 1°C/min from ambient temperature to 600°C and kept at 600°C for 6 hours under the flow of dry air.

At the end of calcinations, solid material inside the quartz tube was cooled down to ambient temperature under the flow of dry air. Finally, MCM-41 material was obtained.

Steps of MCM-41 synthesis are shown in Figure 5.1.

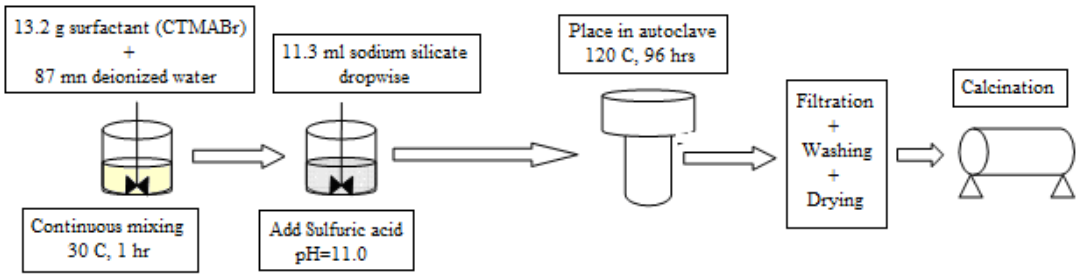

Figure 5.1: Steps of MCM-41 synthesis

5.1.2. Catalyst Preparation

5.1.2.i. Preparation of Co-MCM-41 Catalyst

2.005 g calcined MCM-41 support material was put into 30 ml deionized water and stirred for 2 hours. At the same time, 0.9732 g $Co(NO_3)_2.6H_2O$ was dissolved in deionized water and stirred until metal salt was dissolved completely in deionized water. After 2 hours, $Co(NO_3)_2.6H_2O$ solution was added drop-wise to MCM-41 suspension. Resulting solution was stirred for 24 hours. Obtained solution was dried at room temperature and then at 40^oC for 2 days. Solid product was then calcined at 600^oC for 6 hours under dry air flow and reduced at 550^oC for 4 hours under H_2 flow. Finally, obtained catalyst was named as Co-MCM-41.

5.1.2.ii. Preparation of Ni-MCM-41 Catalyst

Synthesis procedure of Ni-MCM-41 catalyst was similar to Co-MCM-41 synthesis procedure. 2.0276 g MCM-41 material was suspended in 30 ml deionized water and stirred for 2 hours. 0.9900 g $Ni(NO_3)_2.6H_2O$ was dissolved in deionized water and added drop-wise to MCM-41 suspension. Resulting solution was stirred for 1 day and then dried at room temperature and after that at 40 ^oC for 1-2 days. Solid product was calcined at 600^oC for 6 hours under dry air flow and reduced at 550^oC for 4 hours under H_2 flow. Finally, obtained catalyst was named as Ni-MCM-41.

5.2. Characterization of Catalysts

X-ray diffraction (XRD), energy dispersive spectroscopy (EDS), nitrogen physisorption (BET) and scanning electron microscopy (SEM) techniques were used to characterize synthesized catalysts. Additionally, thermal gravimetric analysis (TGA) method was employed for used catalysts after reaction.

5.2.1. X-ray Diffraction (XRD)

The XRD data of the synthesized catalysts were obtained by Rigaku D/MAX2200 diffractometer in Metallurgical and Material Engineering in METU. XRD pattern of support material MCM-41 was obtained by Rigaku Ultima IV diffractometer in Central Laboratory in METU.

5.2.2. Energy Dispersive Spectroscopy (EDS)

The compositional information about the synthesized catalysts was determined by JSM-6400 Electron Microscope (JEOL) in Metallurgical and Material Engineering in METU.

5.2.3. Nitrogen Physisorption (BET)

Adsorption and desorption isotherms, surface area, pore size distribution, average pore size and average pore volume data of the catalysts were obtained by Quantachrome Corpotarion, Autosorb-6 device in Central Laboratory in METU.

5.2.4. Scanning Electron Microscopy (SEM)

The topographical and compositional information about the synthesized catalysts and spent catalysts in the reaction were obtained by JSM-6400 Electron Microscope (JEOL) equipped with NORAN System 6 X-ray Microanalysis System & Semafore Digitizer in Metallurgical and Material Engineering in METU.

5.2.5. Thermal Gravimetric Analysis (TGA)

Thermal gravimetric analysis of the spent catalysts in the reaction was obtained by a thermal analysis system (TGA, DTA, DSC, TMA) in Chemical Engineering Department in METU.

5.3. Reaction Set-up

The catalyst was placed in a quartz tube which was put into a tubular furnace. The reaction temperature was adjusted by the help of temperature controller inside the tubular furnace. The liquid feed was prepared with a H_2O/C_2H_5OH molar ratio of 3.2 (50 liq. vol. %) and the prepared liquid feed was introduced to the system by a Cole Parmer liquid injection pump, with a volumetric flow rate of 0.9 ml/hr. Liquid feed was then evaporated in the preheater (130 ^oC-150 ^oC) and the water-ethanol vapor was mixed with carrier gas Argon (20 ml/min water-ethanol vapor, 30 ml/min Ar). Ar gas flow rate was adjusted by a gas mass flow controller placed at the entrance of the preheater. The total flow rate of the gas stream, which was introduced to the reactor inlet was 50 ml/min. A condenser was placed between the reactor and the gas chromatograph. The liquified products were collected in condenser and the product gas was analyzed by Agilent Technologies 6850 Gas Chromatograph. Thermal conductivity detector and Porapak S column were used in the chromatograph and Ar was selected as reference gas for the chromatograph. The schematic representation of the reaction set-up is given in Figure 5.2.

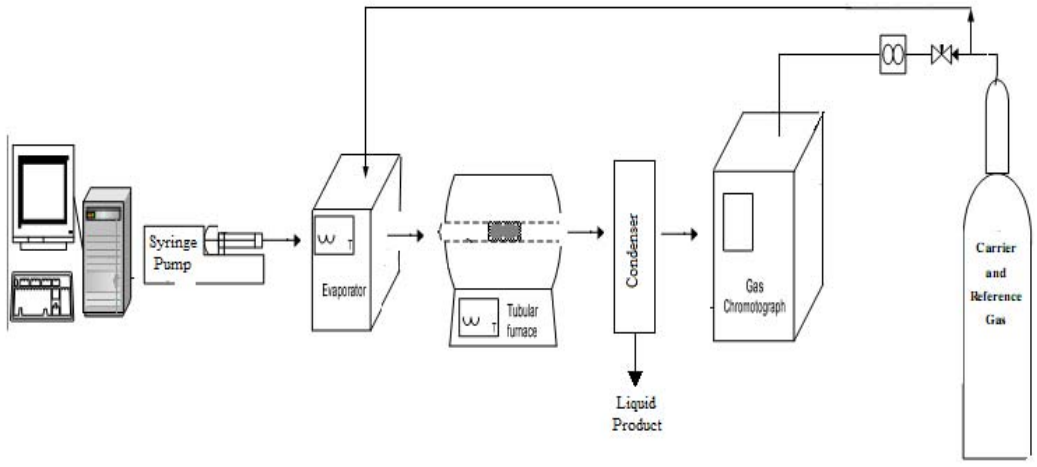

Figure 5.2: Schematic representation of the reaction set-up

CHAPTER 6

RESULTS AND DISCUSSIONS

In this study, Co-MCM-41 and Ni-MCM-41 type catalytic materials having Co/Si and Ni/Si molar ratios of 0.1 were synthesized. Synthesized materials were characterized by X-Ray Diffraction (XRD), Nitrogen Physisorption (BET), Scanning Electron Microscopy (SEM) and Energy Dispersive Spectroscopy (EDS) methods and tested in steam reforming and sorption enhanced steam reforming of ethanol reactions at 500^{o}C, 550^{o}C and 600^{o}C. The results were compared to investigate the effect of CO_2 capture during the reaction on the ethanol conversion and hydrogen yield.

6.1. Characterization of Catalysts

The synthesized materials were analyzed by XRD, EDS, SEM and BET characterization techniques.

6.1.1. Characterization of MCM-41

The support material MCM-41 used for catalyst synthesis was characterized by XRD and Nitrogen physisorption techniques.

6.1.1.i. X-Ray Diffraction (XRD) Results of MCM-41

XRD provides direct information of the pore architecture of the material. In the case of mesoporous materials, the diffraction patterns only have reflection peaks in the low angle range (2θ less than 10). No reflection seen at higher angles which means that the pore walls were mainly amorphous. The ordering lies in the pore

structure and the low-angle diffraction peaks can be indexed according to different lattices **[41]**

The structure of MCM-41 is presented schematically in Figure 6.1.

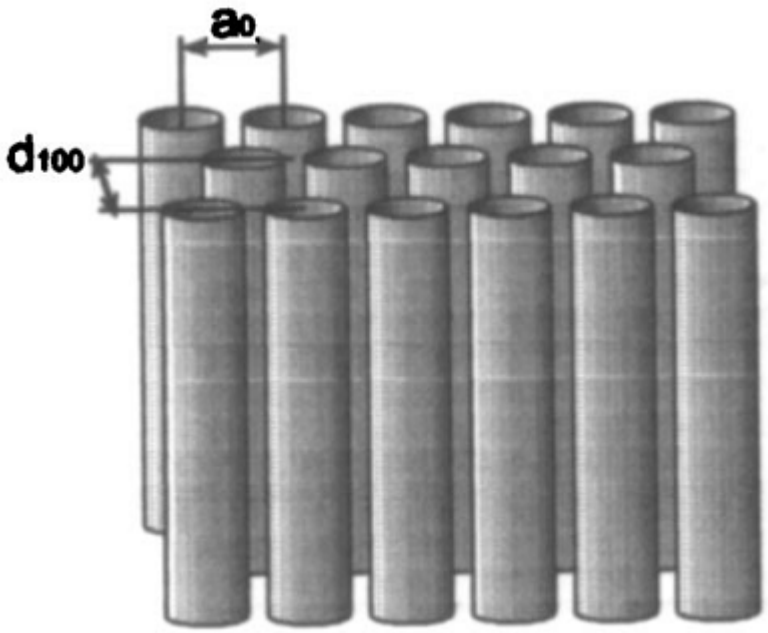

Figure 6.1: Schematic representation of the structure of hexagonal MCM-41 **[56]**.

From the XRD pattern of MCM-41, the value of d_{100} can be obtained and hexagonal unit cell parameter a_0 (the distance between the nearest centers of cylindrical mesopores) can be calculated. From d_{100} value obtained from XRD pattern, lattice parameter a_0 can be calculated by the formula given below **[56]**.

$$a_0 = 2\frac{d_{100}}{\sqrt{3}} \qquad (6.1)$$

The XRD pattern of MCM-41 synthesized for the scope of this study is shown in Figure 6.2. XRD spectrum of the MCM-41 sample showed a sharp (100) peak and three reflection peaks corresponding to (110), (200) and (210), which meant that the sample had an ordered pore structure.

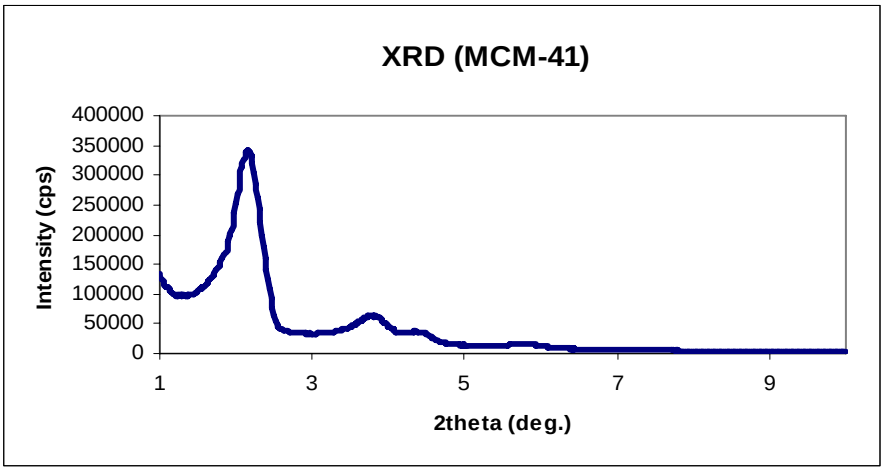

Figure 6.2: XRD pattern of synthesized MCM-41

XRD pattern of synthesized MCM-41 has a major peak at 2.2° and three reflection peaks at 3.8°, 4.4° and 5.8°. Sharp and noise-free peaks of MCM-41 material indicated that the desired structure of MCM-41 was successfully synthesized.

Reflection angles, corresponding d-spacing values and calculated lattice parameter a_0 value for MCM-41 sample are summarized in Table 6.1.

Table 6.1: Reflection angles, corresponding d-spacing values and calculated lattice parameter a_0 value for MCM-41 sample

Sample	d-value (nm)		2theta (deg.)	a_0
MCM-41	d_{100}	4.061	2.173	4.689
	d_{110}	2.309	3.820	
	d_{200}	2.010	4.400	
	d_{210}	1.513	5.836	

6.1.1.ii. N_2 Physisorption (BET) Results of MCM-41

Surface area, average pore diameter and pore volume and pore size distribution data of synthesized MCM-41 were obtained by using its nitrogen

adsorption-desorption isotherm. The nitrogen adsorption-desorption isotherm of MCM-41 sample is given in Figure 6.3.

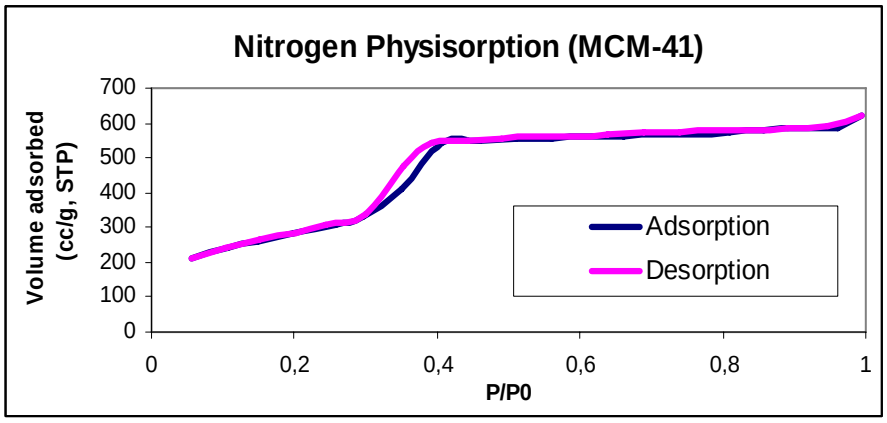

Figure 6.3: Nitrogen physisorption isotherm of MCM-41 sample

Figure 6.3 shows that synthesized MCM-41 material had a typical Type IV isotherm indicating mesoporous structure. BET and BJH surface area values, pore size and pore volume data are listed in Table 6.2.

Table 6.2: BET and BJH surface area, pore size and pore volume data of MCM-41

Sample	**BET Surface Area (m^2/g)**	**BJH Surface Area (m^2/g)**	**BJH Pore Volume (cc/g)**	**BJH Desorption Pore Diameter (nm)**
MCM-41	1040	1334	1.027	2.75

It is clearly seen from Table 6.2 that high surface area MCM-41 material having pore size in the mesoporous range was synthesized. Synthesized MCM-41 material can be a good catalyst support due to its high surface area (1040 m^2/g), large pore volume (1.027 cc/g) and large pore size (2.75 nm). Pore size distribution curve for MCM-41 is given in Figure 6.4. As shown in Figure 6.4, pore size distribution of MCM-41 is very narrow indicating a very ordered structure.

By using lattice parameter calculating with the data obtained from XRD pattern and pore diameter value obtained from nitrogen physisorption isotherm, pore wall thickness (δ) can be calculated with the relation given below **[56]**.

$$\delta = a_0 - d_p \qquad (6.2)$$

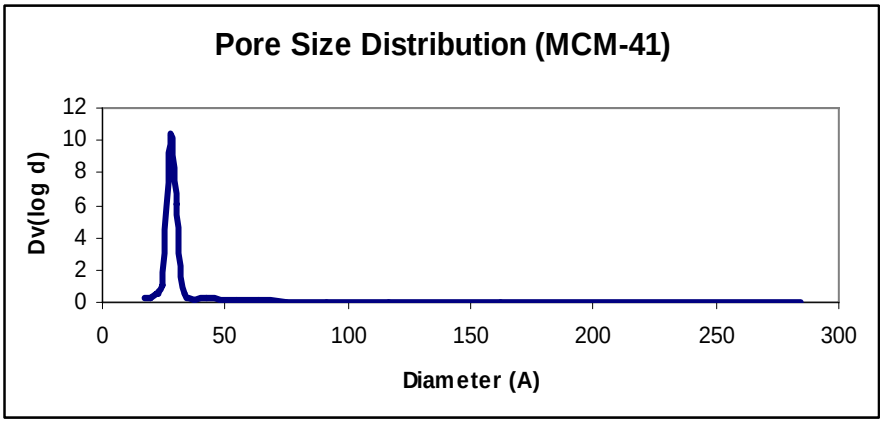

Figure 6.4: Pore size distribution of MCM-41

The d_{100} value, lattice parameter, pore diameter and pore wall thickness data of synthesized MCM-41 are tabulated in Table 6.3.

Table 6.3: d_{100}, lattice parameter, pore diameter and pore wall thickness of MCM-41

Sample	**d_{100} (nm)**	**a_0 (nm)**	**Pore Diameter (nm)**	**Pore Wall Thickness (δ) (nm)**
MCM-41	4.061	4.689	2.75	1.939

6.1.2. Characterization of Co-MCM-41 Catalyst

Co-MCM-41 material used as catalyst was characterized by XRD, Nitrogen physisorption (BET), EDS and SEM techniques.

6.1.2.i. X-ray Diffraction (XRD) Results of Co-MCM-41

The XRD pattern of Co-MCM-41 catalyst synthesized by impregnation method with Co/Si molar ratio of 0.10 is given in Figure 6.5.

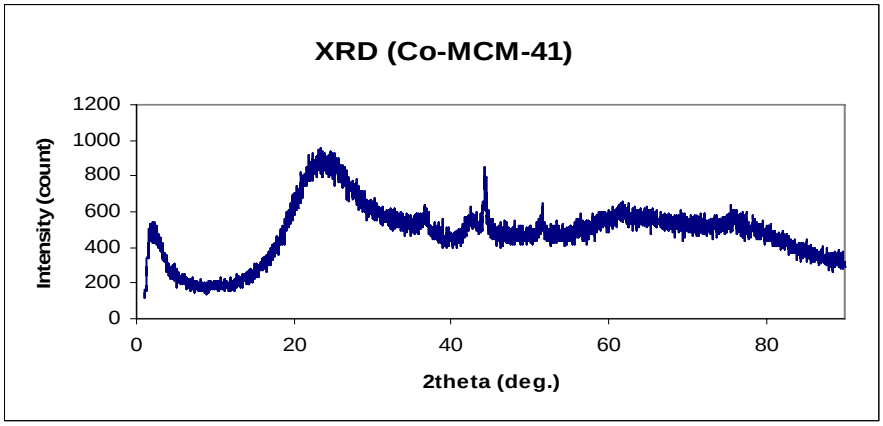

Figure 6.5: XRD pattern of Co-MCM-41 catalyst

As shown in Figure 6.5, at smaller angle range (2theta values between 1 and 10) only the main peak at 2theta value of 1.86° is sharp enough to observe. The reflection peaks disappeared after Co impregnation into the MCM-41 structure. The main peak indicated that MCM-41 structure was partially conserved after the impregnation step and the loss of the reflection peaks showed that some deterioration occurred in the well ordered structure of MCM-41. Sharp peaks at wider angle range between 2theta values of 35 and 60 indicate the presence of Co and/or CoO clusters. Peak at 42.4 corresponds to CoO peak and peaks at 44.32° and 51.52° correspond to metallic Co peaks. Particle size of Co and CoO clusters ($t_{particle}$) can be estimated by using Scherrer's equation **[57]** given below.

$$t_{particle} = \frac{C \times \lambda}{B \times \cos(\frac{2\theta}{2})} \qquad (6.3)$$

where;

$t_{particle}$: particle size of metal cluster

C: Crystal shape factor (0.89)

λ: Wavelength (1.54 Å)

B: FWHM; full width at half max (radians)

θ: Bragg Angle

Particle size of Co and CoO clusters present in the structure of Co-MCM-41 catalyst was calculated as 11.6 nm and 4.9 nm, respectively by Equation 6.2. Calculation of particle sizes of clusters is given in Appendix A1.

6.1.2.ii. Energy Dispersive Spectroscopy (EDS) Results of Co-MCM-41

Elemental composition of synthesized catalyst Co-MCM-41 was identified with Energy Dispersive Spectroscopy (EDS) method. The results of EDS analysis of Co-MCM-41 is summarized in Table 6.4.

Table 6.4: EDS analysis result of Co-MCM-41

Sample	Element	Weight Conc. %	Atomic Conc. %	Co/Si	
				Weight	Atomic
Co-MCM-41	Si	79.26	88.91	0.26	0.12
	Co	20.74	11.09		

As mentioned earlier, Co-MCM-41 catalyst was prepared with a Co/Si molar ratio of 0.10 which is very close to the EDS result 0.12 which indicates that Co was successfully impregnated in the structure of MCM-41.

6.1.2.iii. Scanning Electron Microscopy (SEM) Results of Co-MCM-41

The SEM images of synthesized Co-MCM-41 catalyst are given in Figure 6.6.

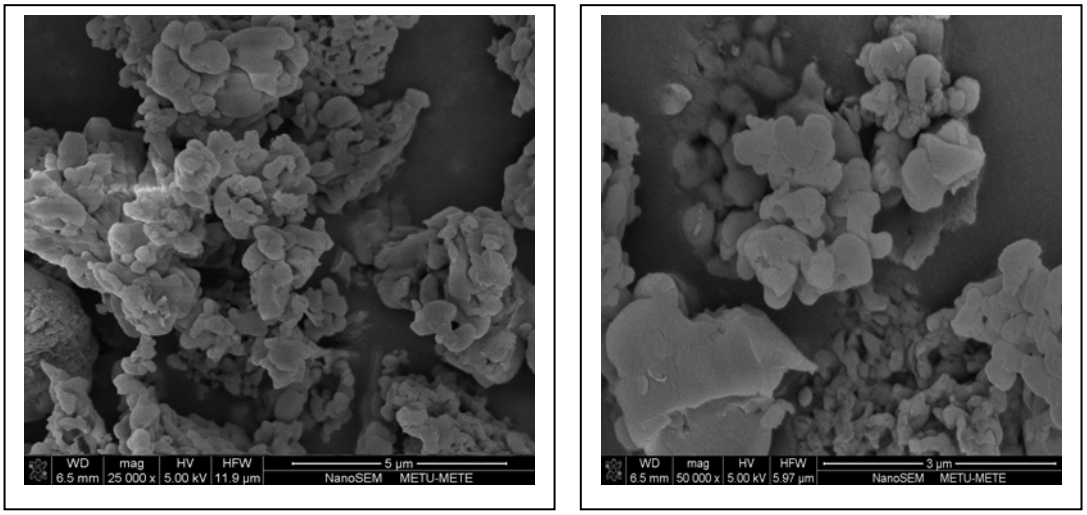

Figure 6.6: SEM images of Co-MCM-41 catalyst

SEM images of catalysts are given in Appendix B1.

6.1.2.iv. Nitrogen Physisorption (BET) Results of Co-MCM-41

Nitrogen physisorption isotherms of Co-MCM-41 catalyst are shown in Figure 6.7.

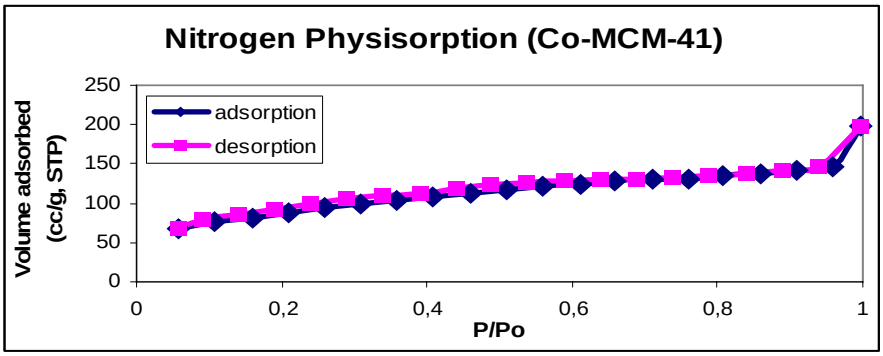

Figure 6.7: Nitrogen physisorption isotherms of Co-MCM-41

As shown in Figure 6.7, the typical shape of type IV isotherm is not as clear as it is for the pure MCM-41. This phenomenon concluded that some deterioration was occurred in the mesoporous structure of MCM-41 during impregnation step.

BET and BJH surface area values, pore size and pore volume data of Co-MCM-41 catalyst are listed in Table 6.5.

Table 6.5: BET and BJH surface area, pore size and pore volume data of Co-MCM-41

Sample	BET Surface Area (m^2/g)	BJH Surface Area (m^2/g)	BJH Desorption Pore Volume (cc/g)	BJH Desorption Pore Diameter (nm)
Co-MCM-41	303.6	271.6	0.259	1.891

BET surface area of Co-MCM-41 catalyst was lower than the surface area of pure MCM-41 which indicated that some of the smaller pores present in the structure of MCM-41 were plugged by large Co clusters.

Pore size distribution curve for Co-MCM-41 is given in Figure 6.8. These plots are based on the BJH desorption data points.

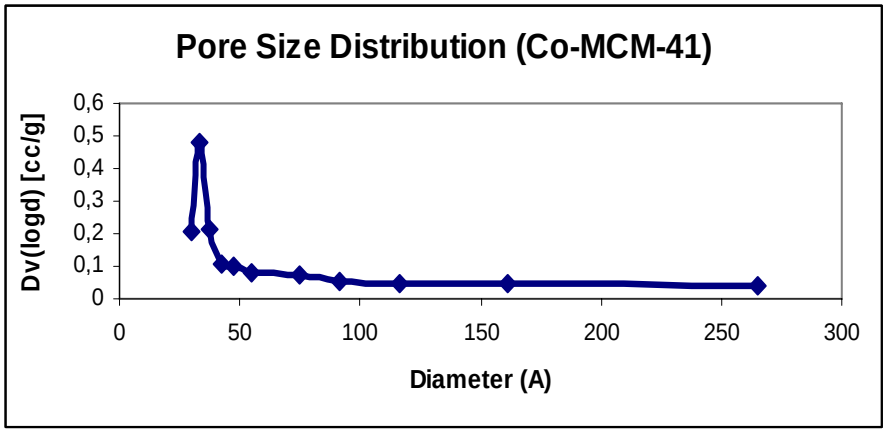

Figure 6.8: Pore size distribution curve of Co-MCM-41

6.1.3. Characterization Results of Ni-MCM-41

Ni-MCM-41 catalytic material prepared in this study was also characterized by XRD, nitrogen physisorption (BET), EDS and SEM techniques.

6.1.3.i. X-ray Diffraction (XRD) Results of Ni-MCM-41

The XRD pattern of Ni-MCM-41 catalyst synthesized by impregnation method with Ni/Si molar ratio of 0.10 is given in Figure 6.9.

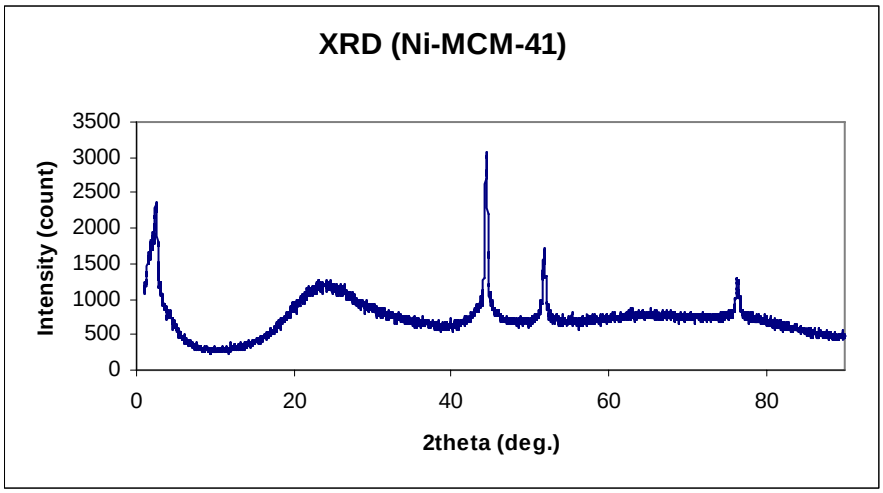

Figure 6.9: XRD pattern of Ni-MCM-41 catalyst

As shown in Figure 6.9, the main peak at 2theta value of 2.50^{o} is sharp enough to observe, which means that MCM-41 structure was partially conserved after the impregnation step. The reflection peaks disappeared during Ni impregnation into the MCM-41 structure. The loss of the reflection peaks showed that some deterioration occurred in the well ordered structure of MCM-41. Sharp peaks at wider angle range between 2theta values of 40^{o} and 80^{o} indicated the presence of Ni and NiO clusters. Peaks at 44.48^{o} and 51.82^{o} correspond to metallic Ni peaks and peak at 76.38^{o} corresponds to NiO. The particle size of Ni and NiO clusters were calculated as 21.2 nm and 25.0 nm, respectively by Equation 6.2.

6.1.3.ii. Energy Dispersive Spectroscopy (EDS) Results of Ni-MCM-41

Elemental composition of synthesized catalyst Ni-MCM-41 was identified with Energy Dispersive Spectroscopy (EDS) method. The results of EDS analysis of Ni-MCM-41 is summarized in Table 6.6.

Table 6.6: EDS analysis result of Ni-MCM-41

Sample	Element	Weight Conc. %	Atomic Conc. %	Ni/Si	
				Weight	Atomic
Ni-MCM-41	Si	79.38	88.95	0.26	0.12
	Ni	20.62	11.05		

EDS result showed that impregnation of Ni in the structure of MCM-41 structure was successfully achieved.

6.1.3.iii. Scanning Electron Microscopy (SEM) Results of Ni-MCM-41

The SEM images of synthesized Ni-MCM-41 catalyst are given in Figure 6.10.

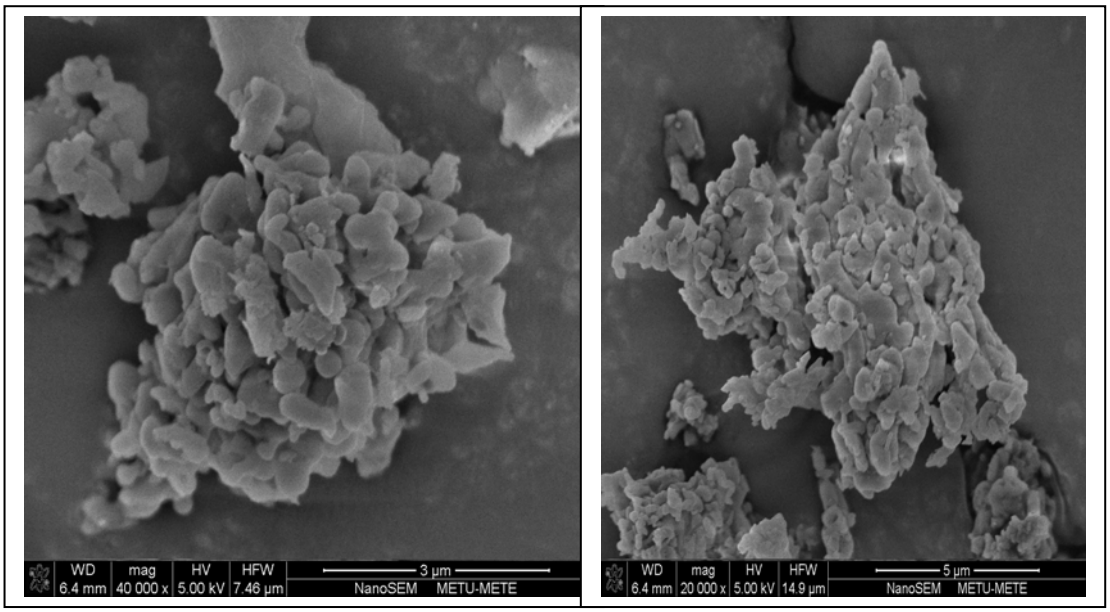

Figure 6.10: SEM images of Ni-MCM-41 catalyst

6.1.3.iv. Nitrogen Physisorption (BET) Results of Ni-MCM-41

Nitrogen physisorption isotherm graph of Ni-MCM-41 catalyst is illustrated in Figure 6.11.

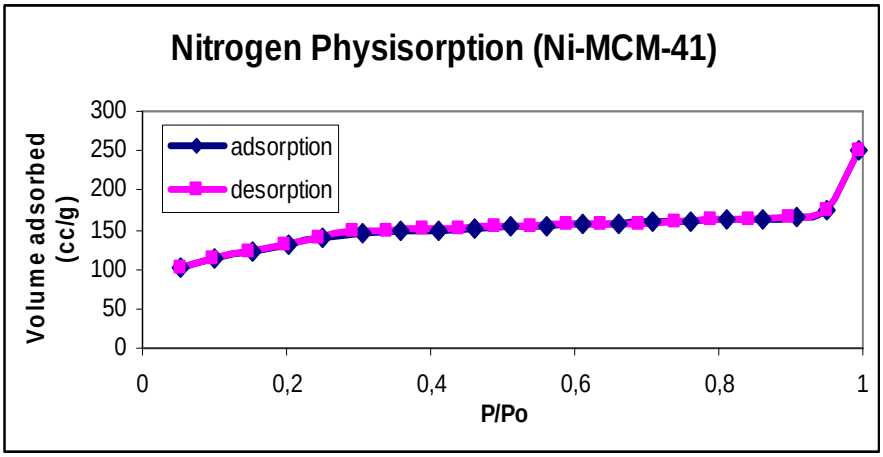

Figure 6.11: Nitrogen physisorption isotherm of Ni-MCM-41

As in the case of Co impregnated catalyst's nitrogen physisorption isotherm, the typical shape of type IV isotherm of Ni-MCM-41 catalyst is not as clear as it is for the pure MCM-41, which showed that some deterioration occurred in the mesoporous structure of MCM-41 during the impregnation step.

BET and BJH surface area values, pore size and pore volume data of Ni-MCM-41 catalyst are listed in Table 6.7.

Table 6.7: BET and BJH surface area, pore size and pore volume data of Ni-MCM-41

Sample	**BET Surface Area (m^2/g)**	**BJH Surface Area (m^2/g)**	**BJH Desorption Pore Volume (cc/g)**	**BJH Desorption Pore Diameter (nm)**
Ni-MCM-41	449.0	351.3	0.293	2.172

BET surface area of Ni-MCM-41 catalyst was lower than the surface area of pure MCM-41 which indicated that some of the smaller pores present in the structure of MCM-41 were plugged by large Ni clusters.

The pore size distribution curve belonging to Ni-MCM-41 catalyst is shown in Figure 6.12.

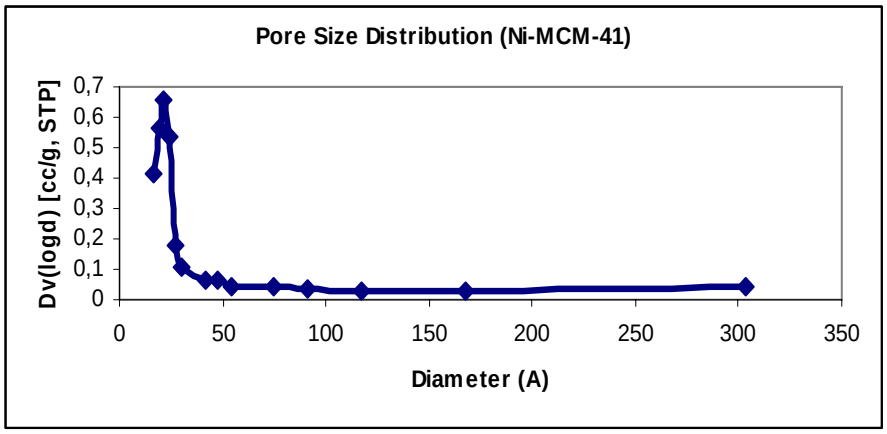

Figure 6.12: Pore size distribution curve of Ni-MCM-41 catalyst

6.2. Catalytic Test Results of Catalysts

The synthesized materials Co-MCM-41 (Co/Si molar ratio: 0.1) and Ni-MCM-41 (Ni/Si molar ratio: 0.1) were tested for steam reforming and sorption enhanced steam reforming of ethanol reactions and the results are given and discussed in this section. Catalytic tests were performed at atmospheric pressure at 500^{o}C, 550^{o}C and 600^{o}C and the reaction conditions were same for Co and Ni incorporated catalysts. In each experiment, Ar was used as carrier gas and reference gas for the GC. Calibration factors for elements in GC are given in Appendix D1. H_2O/EtOH molar ratio was 3.2 and the same for all experiments. Feed gas (H_2O/EtOH) and carrier gas Ar volumetric flow rates were kept constant at 20 ml/min and 30 ml/min respectively in each experiment. Catalyst amount packed to the reactor was 0.15 g and the amount was constant for each experiment. In sorption enhanced steam reforming of ethanol reactions, 1.5 g CaO was used for CO_2 capture. CaO used in sorption enhanced reactions was obtained by the calcination of $CaCO_3$ at 900^{o}C which was taken from a limestone quarry in Dikmen-ANKARA for the study conducted by Doğu in 1979 **[58]**. Chemical composition of used limestone is given as %52.7 CaO, %43.8 CO_2, %1.2 SiO_2, %1.8 MgO and %0.5 other oxides **[59]**. The density of uncalcined limestone was 2.66 g/ml and it was non-porous. Pore

radius and surface area of calcined limestone (CaO) was 600 nm and 0.99 m^2/g, respectively **[58]**.

The catalytic activities of the synthesized catalysts were evaluated according to their ethanol conversion, hydrogen yield and product selectivities.

Ethanol conversion was defined as follows;

$$X_{EtOH} = \frac{Moles\ of\ \ EtOH\ converted}{Moles\ of\ \ EtOH\ \ fed\ to\ the\ reactor} * 100 \qquad (6.3)$$

Hydrogen yield was defined as follows;

$$Y_{H_2} = \frac{Moles\ of\ \ hydrogen\ produced}{Moles\ of\ \ EtOH\ \ fed\ to\ the\ reactor} \qquad (6.4)$$

The selectivity of any product (CO, CO_2, CH_4, C_2H_4, CH_2O, C_2H_4O) was defined as follows;

$$S_i = \frac{(\#\ of\ C\ atoms\ in\ \ product\ i)x(Moles\ of\ \ \ product\ i\ \ formed)}{2x(Moles\ of\ \ EtOH\ converted)} * 100 \qquad (6.5)$$

The catalytic results of Co-MCM-41 and Ni-MCM-41 will be compared in the following sections to understand the effect of temperature and especially to understand the effect of CO_2 capture (sorption enhanced reforming) on product distribution. Raw reaction data over both catalysts for steam reforming and sorption enhanced steam reforming of ethanol reactions are given in Appendix C1 and Appendix C2, respectively.

6.2.1. Co-MCM-41 Test Results

Three steam reforming of ethanol reaction experiments and three sorption enhanced steam reforming of ethanol reaction experiments were performed over Co-MCM-41 catalyst at 500°C, 550°C and 600°C.

6.2.1.i. 500 °C Results with Co-MCM-41

Reactions mentioned in this section were performed at atmospheric pressure at 500°C. In section 6.2.1.i.a, catalytic activity of Co-MCM-41 catalyst towards steam reforming of ethanol reaction will be evaluated according to ethanol conversion, hydrogen yield and product selectivity. In section 6.2.1.i.b, catalytic activity of Co-MCM-41 catalyst towards sorption enhanced steam reforming of ethanol reaction will be evaluated. In section 6.2.1.i.c, steam reforming and sorption enhanced steam reforming of ethanol processes will be compared according to ethanol conversion and hydrogen yield. Sample calculation of kinetic parameters for steam reforming reaction is given in Appendix E1 and sample calculation for sorption enhanced steam reforming of ethanol reaction is given in Appendix E2.

6.2.1.i.a. Steam Reforming of Ethanol Reaction (500°C)

Ethanol conversion was calculated according to Equation 6.3. Conversion of ethanol with respect to time for Co-MCM-41 catalyst at 500°C for steam reforming of ethanol reaction was plotted in Figure 6.13.

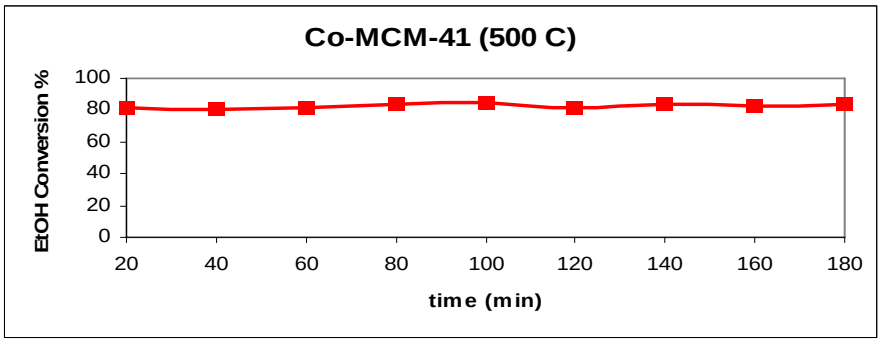

Figure 6.13: Ethanol conversion for SRE reaction over Co-MCM-41 at 500°C

As shown in Figure 6.13, ethanol conversion was 80% over Co-MCM-41 catalyst for steam reforming of ethanol reaction at 500°C for duration of nearly 3 hours.

The definition of hydrogen yield was given in the Eqn. 6.4. Hydrogen yield versus time for Co-MCM-41 catalyst at 500°C for steam reforming of ethanol reaction graph was plotted in Figure 6.14.

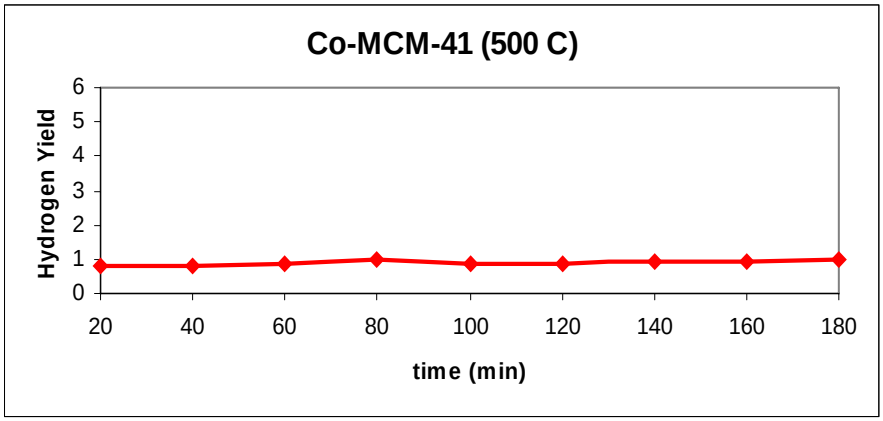

Figure 6.14: Hydrogen yield for SRE reaction over Co-MCM-41 at 500°C

As shown in Fig. 6.14, hydrogen yield values were very low, indicating formation of side reactions. Selectivity of CO, CH_4, CO_2, C_2H_4 and CH_2O were calculated with the definition given in Eqn. 6.5. The selectivity of side products with respect to time is given in Figure 6.15.

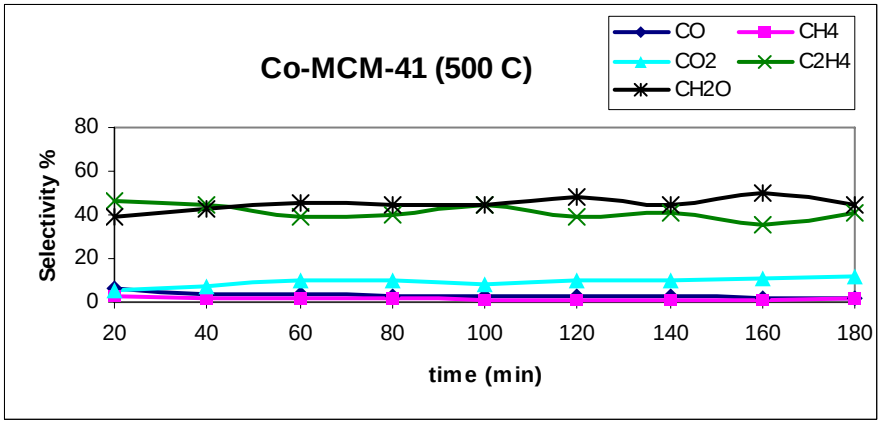

Figure 6.15: Side product selectivity for SRE reaction over Co-MCM-41 at 500°C

As shown in Figure 6.15, average % selectivity values of CO, CH_4, CO_2, C_2H_4 and CH_2O were 3.2, 1.5, 9.3, 41.2 and 44.8, respectively. Formation of side products with high selectivity is responsible for low hydrogen yield over Co-MCM-41 catalyst at 500°C. If only desired reaction (steam reforming of ethanol reaction) had occurred during the experiment, hydrogen yield would reach to 6.0; however, due to formation of CO, CH_4, C_2H_4 and CH_2O, hydrogen yield over Co-MCM-41 catalyst at 500°C was only 0.9. These results indicated that ethanol dehydration to ethylene and ethanol decomposition reactions are the main reactions which contribute to conversion of ethanol.

The percentage of products obtained at 500°C in the product stream is illustrated in Figure 6.16.

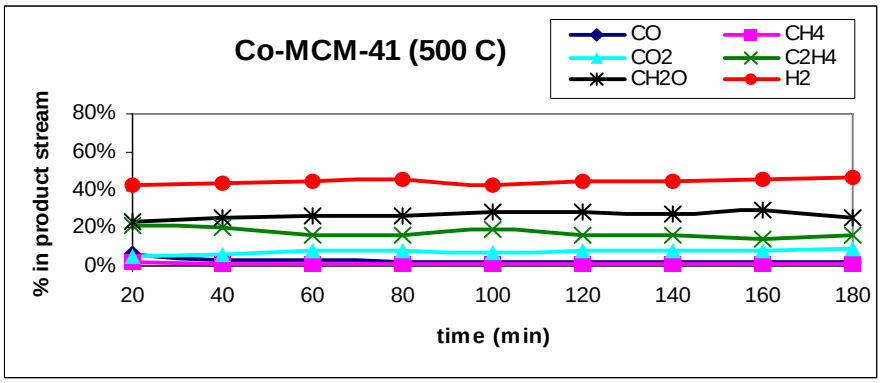

Figure 6.16: The percentage of products for SRE reaction over Co-MCM-41 at 500°C

6.2.1.i.b. Sorption Enhanced Steam Reforming of Ethanol Reaction (500°C)

Conversion of ethanol with respect to time for Co-MCM-41 catalyst at 500°C for sorption enhanced steam reforming of ethanol reaction is plotted in Figure 6.17.

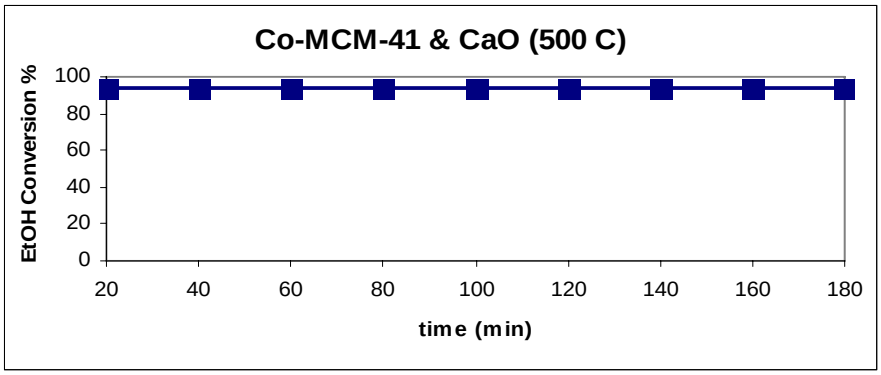

Figure 6.17: Ethanol conversion for SESRE reaction over Co-MCM-41 at 500^{o}C

As shown in Figure 6.17, ethanol conversion value increased to around 94% in sorption enhanced steam reforming of ethanol reaction at the same temperature. At the same conditions, ethanol conversion was 80% in the case of steam reforming reaction in the absence of CaO, which is lower than the conversion value of sorption enhanced process, indicating that in situ CO_2 capture enhanced the ethanol conversion at 500^{o}C.

Hydrogen yield versus time for Co-MCM-41 catalyst at 500^{o}C in sorption enhanced steam reforming of ethanol reaction graph is plotted in Figure 6.18.

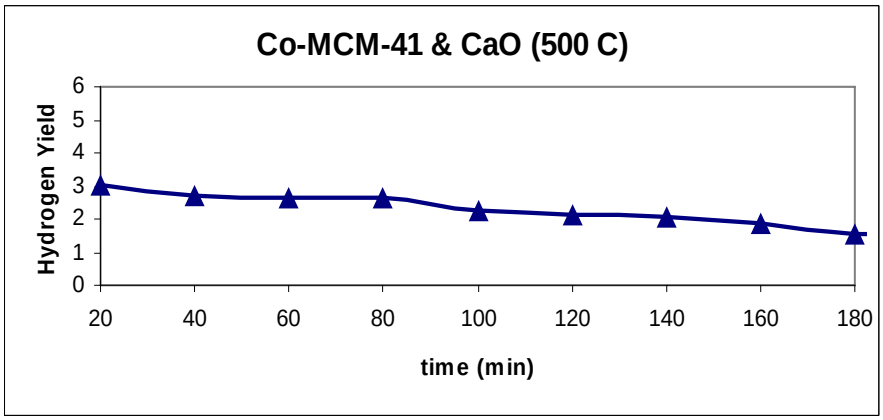

Figure 6.18: Hydrogen yield for SESRE reaction over Co-MCM-41 at 500^{o}C

As shown in Fig. 6.18, CO_2 capture enhanced the hydrogen yield. Hydrogen yield increased from 0.9 (Fig. 6.14) to 3.1 in the presence of CaO. Hydrogen yield decreased with time and at the end of 3 hours yield decreased from 3.1 to 1.57, probably due to saturation of CaO to form $CaCO_3$. Although sorption enhance

process helped to increase in hydrogen yield, it is still quite low and side reactions have still significant contribution to product distribution.

The selectivity of side products with respect to time in sorption enhanced steam reforming of ethanol performed at 500°C is given in Figure 6.19.

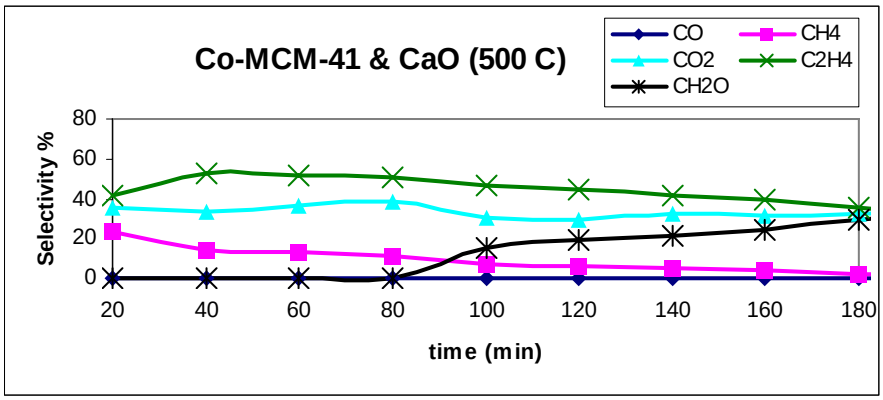

Figure 6.19: Selectivity of side products at 500°C with CO_2 capture

As shown in Figure 6.19, the selectivity of C_2H_4 was nearly 50% which is very high and indicated that the catalyst has acidic sites. CO_2 selectivity was evaluated considering CO_2 captured by CaO as well as CO_2 in the reactor exit stream (sample calculation is given in Appendix E2). Overall CO_2 selectivity via sorption enhanced process was higher than CO_2 selectivity in steam reforming reaction, which is a sign of that in situ CO_2 capture enhanced the reaction pathway towards the desired reaction.

The percentages of products in the reactor exit stream are given in Figure 6.20. When Figure 6.16 and Figure 6.20 are compared, it can be seen that sorption enhanced technology enhanced the production of hydrogen. While the product gas contained only 40% H_2 via steam reforming reaction, the product gas of sorption enhanced steam reforming of ethanol process contained nearly 80% H_2.

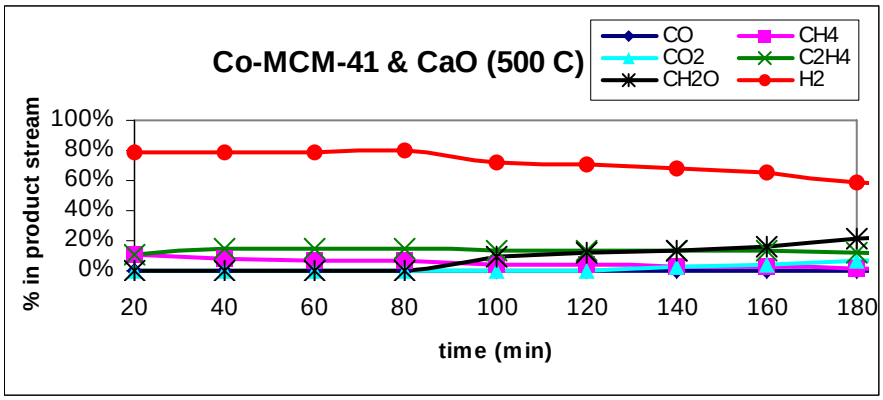

Figure 6.20: Percentage of products in the product stream at 500°C with CO_2 capture

As shown in Figure 6.20, CO_2 was not observed in the product stream until about 140 minutes, which meant that CaO adsorbed all CO_2 during this period. After this period, CO_2 began to emerge in the product stream, since most CaO turned to $CaCO_3$. It is interesting that during this period, no formaldehyde formation occurred, probably due to reaction between formaldehyde and CaO. From this reaction, an intermediate product $Ca(OOCH)_2$ (calcium formate) was produced **[60]**. Then at reaction conditions, calcium formate probably decomposed to $CaCO_3$, hydrogen and carbon monoxide.

6.2.1.i.c. Comparison of Steam Reforming and Sorption Enhanced Steam Reforming of Ethanol Reaction Results at 500°C

The ethanol conversion values obtained in steam reforming of ethanol reaction and sorption enhanced steam reforming of ethanol reaction at 500°C are compared in Figure 6.21.

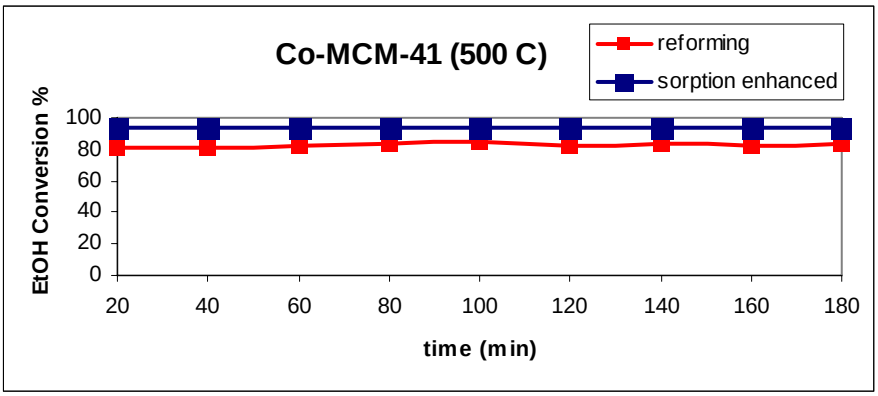

Figure 6.21: EtOH conversion for SRE and SESRE reactions over Co-MCM-41 at 500°C

As shown in Figure 6.21, ethanol conversion in sorption enhanced steam reforming of ethanol reaction at 500°C was higher than ethanol conversion in steam reforming of ethanol reaction.

Hydrogen yield data obtained in steam reforming reaction and sorption enhanced steam reforming of ethanol reactions over Co-MCM-41 catalyst at 500°C are compared in Figure 6.22.

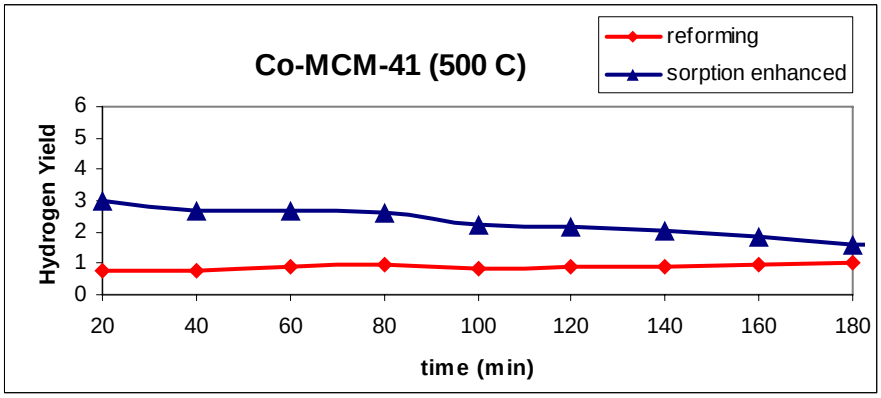

Figure 6.22: Hydrogen yield for SRE and SESRE reactions over Co-MCM-41 at 500°C

As shown in Figure 6.22, it is clear that in situ capture of CO_2 in steam reforming of ethanol process increased the hydrogen yield.

6.2.1.ii. 550°C Results with Co-MCM-41

Reactions mentioned in this section were performed at atmospheric pressure at 550°C. In section 6.2.1.ii.a, catalytic activity of Co-MCM-41 catalyst towards steam reforming of ethanol reaction at 550°C will be evaluated according to ethanol conversion, hydrogen yield and product selectivity values. In section 6.2.1.ii.b, catalytic activity of Co-MCM-41 catalyst towards sorption enhanced steam reforming of ethanol reaction will be evaluated. Finally in section 6.2.1.ii.c, steam reforming of ethanol and sorption enhanced steam reforming of ethanol reactions will be compared according to ethanol conversion and hydrogen yield values.

6.2.1.ii.a. Steam Reforming of Ethanol Reaction (550°C)

Ethanol conversion obtained with respect to time with Co-MCM-41 catalyst at 550°C for steam reforming of ethanol reaction is plotted in Figure 6.23.

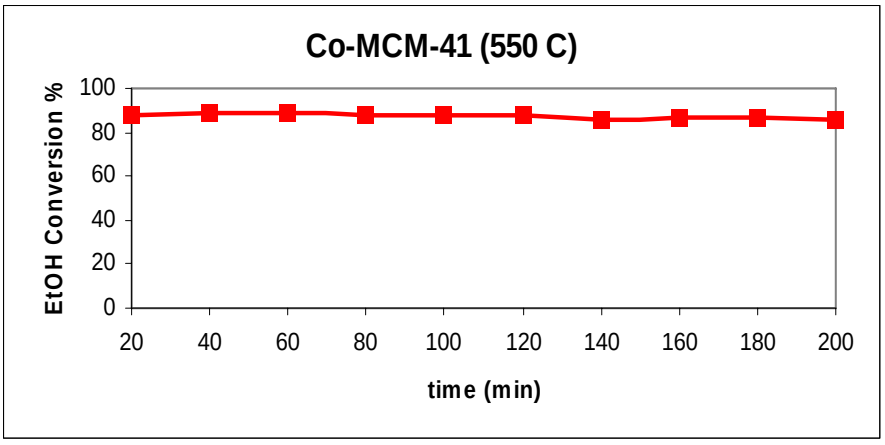

Figure 6.23: Ethanol conversion for SRE reaction over Co-MCM-41 at 550°C

As shown in Figure 6.23, ethanol conversion was about 88%, with the Co-MCM-41 catalyst in steam reforming of ethanol reaction at 550°C, for a period of nearly 3 hours.

Hydrogen yield versus time for Co-MCM-41 catalyst at 550°C in steam reforming of ethanol reaction graph is plotted in Figure 6.24. The average hydrogen yield was 1.62, during this reaction period, over Co-MCM-41 catalyst, at 550°C.

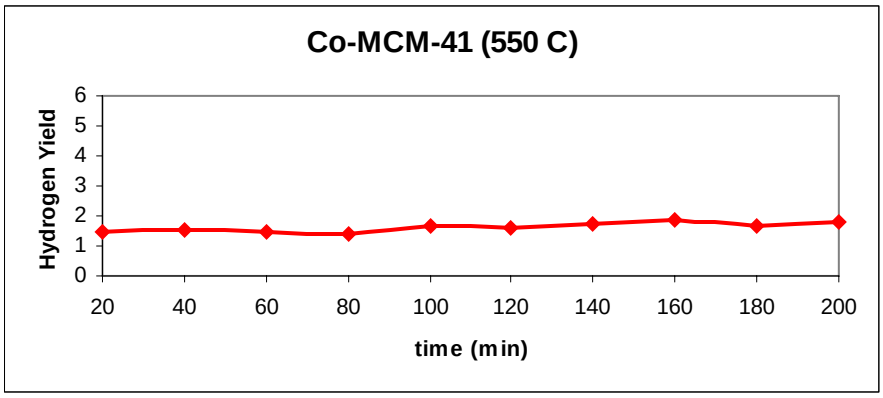

Figure 6.24: Hydrogen yield for SRE reaction over Co-MCM-41 at 550 ^{o}C

The variation of selectivity values of side products CO, CH_4, CO_2, C_2H_4 and CH_2O, with respect to time, is given in Figure 6.25.

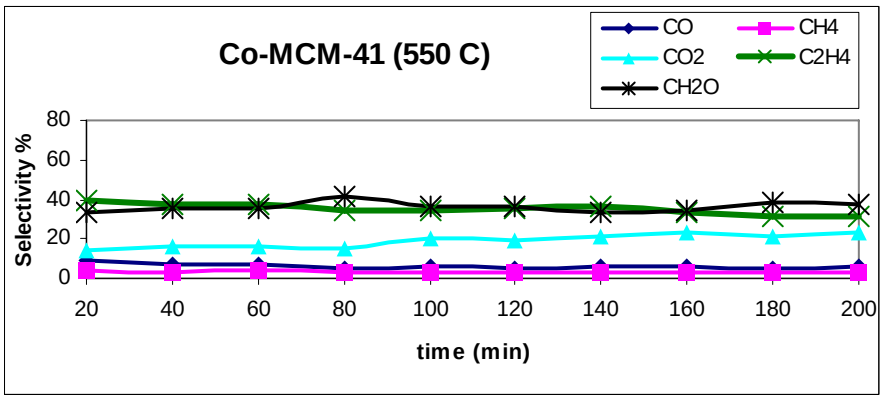

Figure 6.25: Selectivity of side products over Co-MCM-41 at 550^{o}C

As shown in Figure 6.25, average % selectivity of CO, CH_4, CO_2, C_2H_4 and CH_2O were 6.26, 3.34, 19.02, 35.22 and 36.16, respectively. The selectivity of side products C_2H_4 and CH_2O were again quite high but lower than the reaction results obtained at 500 ^{o}C. As a result, ethanol conversion and hydrogen yield were higher at higher temperature 550^{o}C than at 500^{o}C. However, hydrogen yield is still quite low.

The percentage of products in the product stream in steam reforming of ethanol reaction over Co-MCM-41 catalyst obtained at 550^{o}C is shown in Figure 6.26.

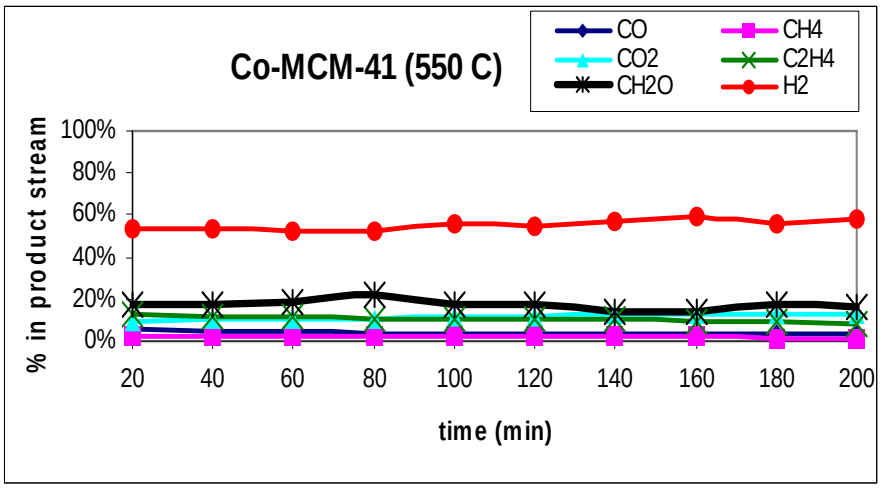

Figure 6.26: The percentage of product for SRE reaction over Co-MCM-41 at 550°C

6.2.1.ii.b. Sorption Enhanced Steam Reforming of Ethanol Reaction (550°C)

Complete conversion of ethanol was achieved with Co-MCM-41 catalyst at 550°C in sorption enhanced steam reforming of ethanol reaction, which was carried out in the presence of CaO.

Hydrogen yield versus time for Co-MCM-41 catalyst at 550°C in sorption enhanced steam reforming of ethanol reaction is plotted in Figure 6.27.

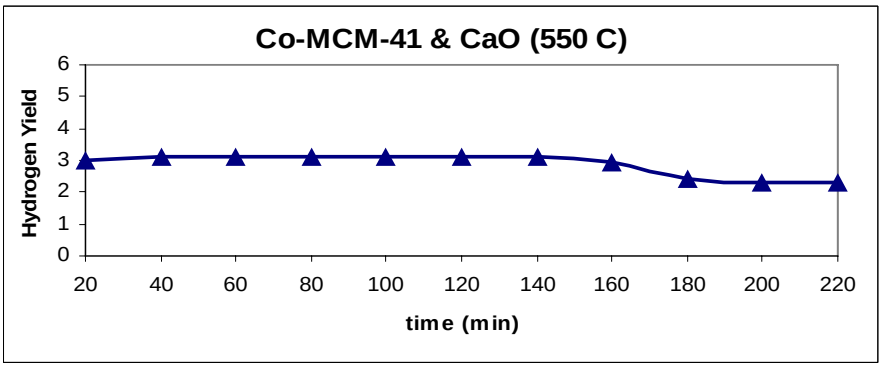

Figure 6.27: Hydrogen yield for SESRE reaction over Co-MCM-41 at 550°C

Hydrogen yield increased from 1.62 to 3.1, in the case of CO_2 captured by CaO during the reaction at 550°C. Hydrogen yield decreased with time and at the end of 3 hours yield decreased from 3.1 to 2.30, since most of CaO turned to $CaCO_3$.

The selectivity of side products with respect to time via sorption enhanced steam reforming of ethanol reaction over Co-MCM-41 catalyst at 550°C is given in Figure 6.28. In this figure, CO_2 selectivity corresponds to the summation of sorbed (by CaO) and gas phase CO_2.

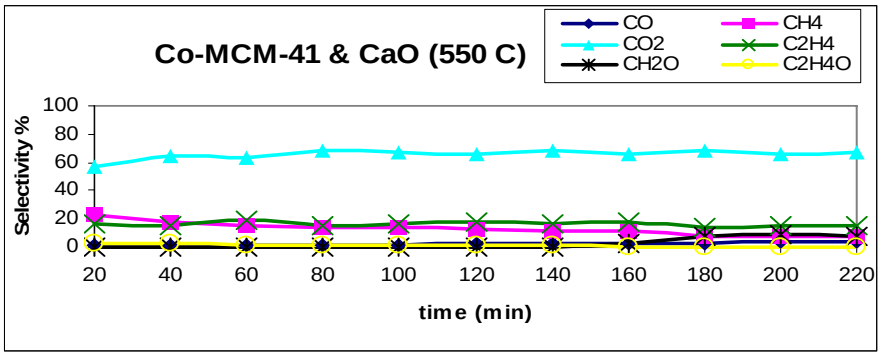

Figure 6.28: Product selectivity in SESRE reaction over Co-MCM-41 at 550°C

The percentage of products in the product stream for sorption enhanced steam reforming of ethanol reaction at 550°C is shown in Figure 6.29.

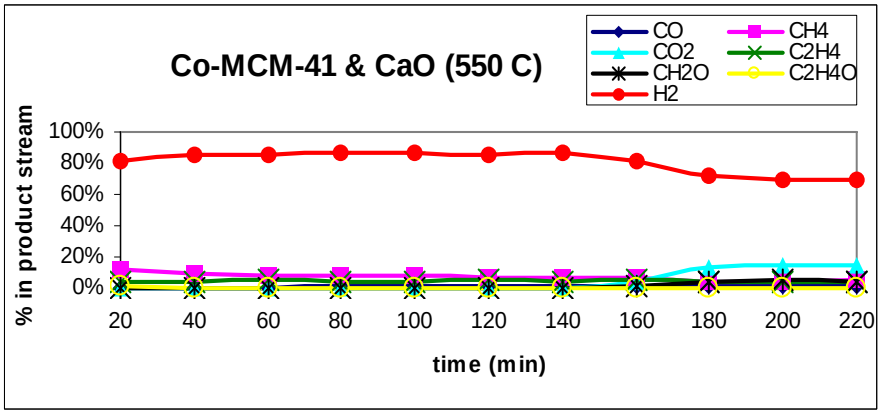

Figure 6.29: The percentage of products for SESRE reaction at 550 °C

6.2.1.ii.c. Comparison of Steam Reforming and Sorption Enhanced Steam Reforming of Ethanol Reaction Results at 550°C

The ethanol conversion values obtained in steam reforming of ethanol reaction and sorption enhanced steam reforming of ethanol reaction over Co-MCM-

41 catalyst at 550°C are compared in Figure 6.30. As shown in this figure, ethanol conversion increased to complete conversion at 550°C.

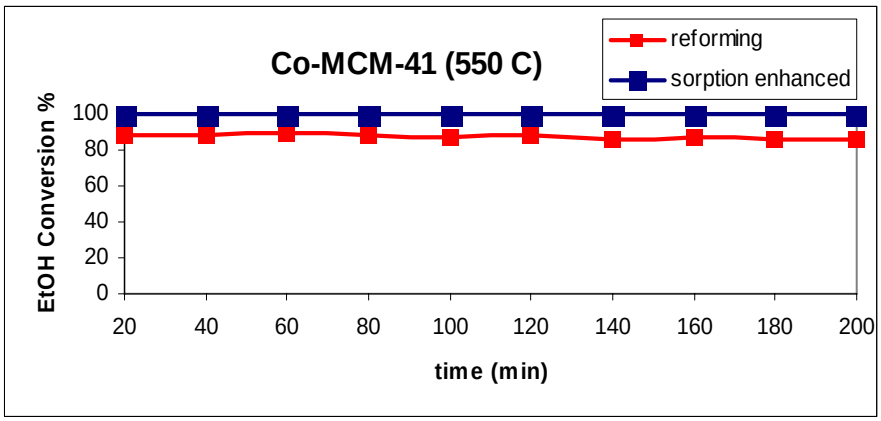

Figure 6.30: Ethanol conversion for SRE and SESRE reactions over Co-MCM-41 at 550°C

Hydrogen yield data obtained in steam reforming reaction and sorption enhanced steam reforming of ethanol reactions over Co-MCM-41 catalyst at 550 °C are compared in Figure 6.31. These data also indicated the positive effect of CO_2 capture by CaO on hydrogen yield.

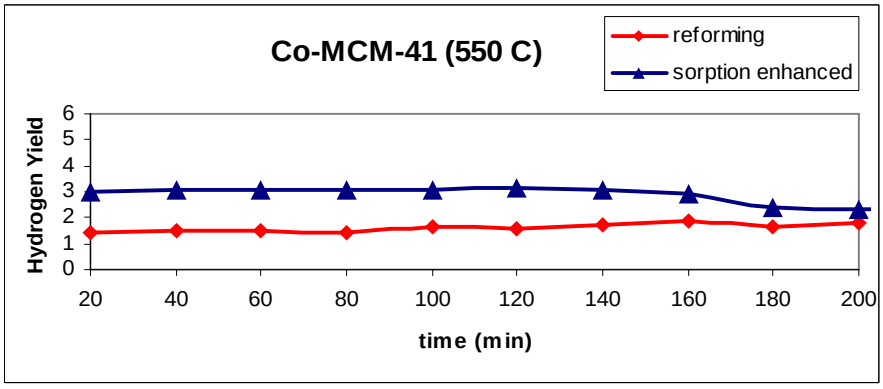

Figure 6.31: Hydrogen yield for SRE and SESRE reactions over Co-MCM-41 at 550°C

6.2.1.iii. 600°C Results with Co-MCM-41

6.2.1.iii.a. Steam Reforming of Ethanol Reaction (600°C)

Conversion of ethanol with respect to time for Co-MCM-41 catalyst at 600°C for steam reforming of ethanol reaction was plotted in Figure 6.32. Results obtained at this temperature are quite similar to the results obtained at 550°C.

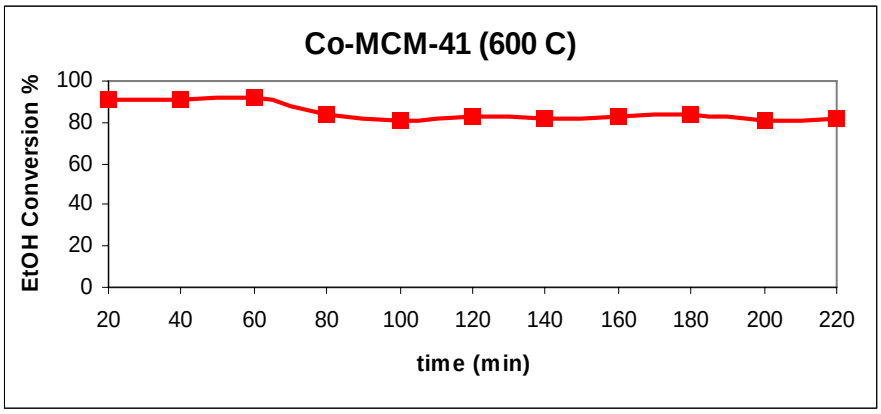

Figure 6.32: Ethanol conversion for SRE reaction over Co-MCM-41 at 600°C

Hydrogen yield versus time for Co-MCM-41 catalyst at 600°C for steam reforming of ethanol reaction graph was plotted in Figure 6.33. The average hydrogen yield was 1.50 during the steam reforming of ethanol reaction over Co-MCM-41 catalyst at 600°C.This is again quite low.

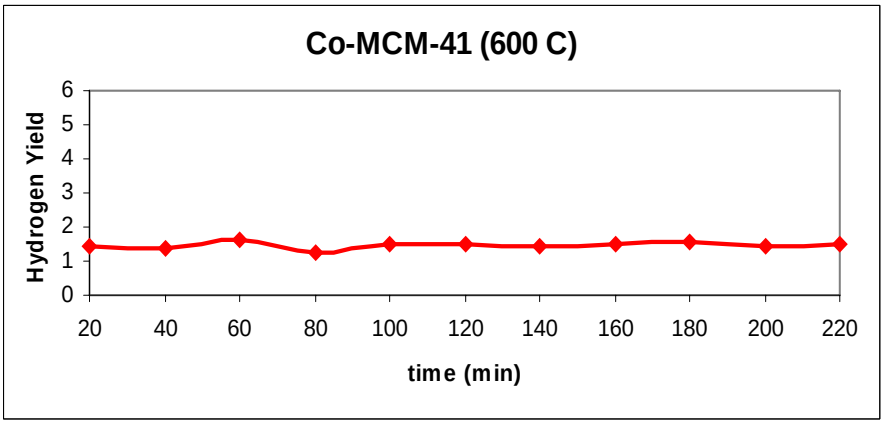

Figure 6.33: Hydrogen yield for SRE reaction over Co-MCM-41 at 600 °C

The selectivity of side products with respect to time in steam reforming of ethanol reaction over Co-MCM-41 catalyst, at 600°C, is given in Figure 6.34.

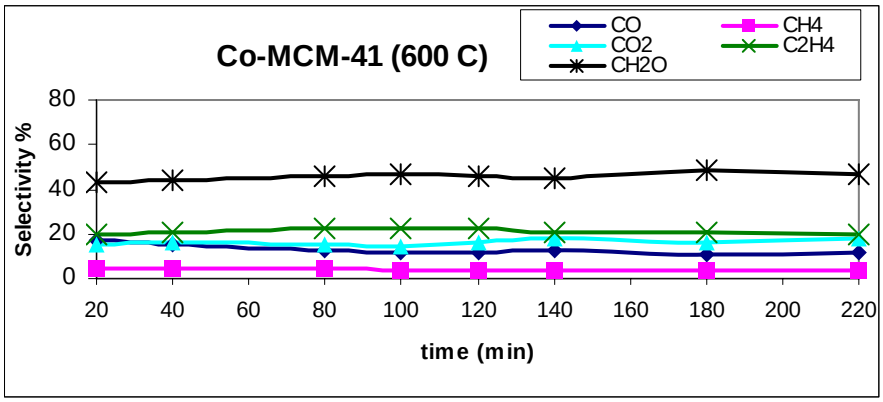

Figure 6.34: Selectivity of side products for SRE reaction over Co-MCM-41 at 600°C

The percentage of products in the product stream for steam reforming of ethanol reaction over Co-MCM-41at 600°C is shown in Figure 6.35. Increase of temperature from 500°C to 600°C caused some decrease in C_2H_4 formation. However, formation of CH_2O is still high. These results indicated the possibility of coke formation over this catalyst.

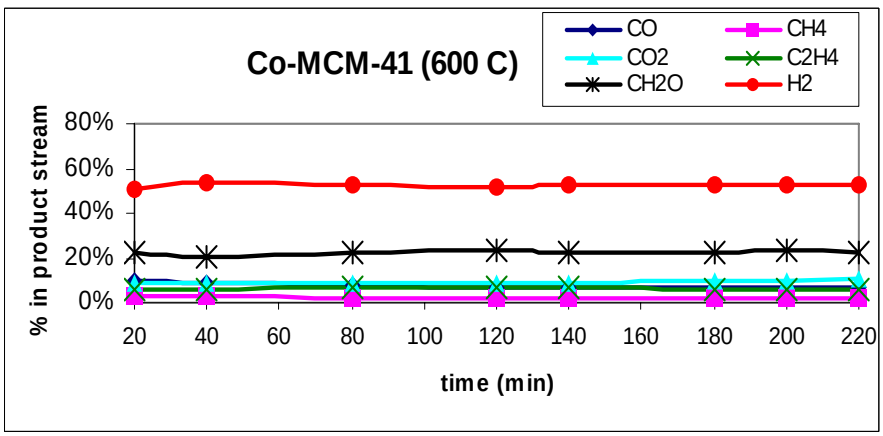

Figure 6.35: The percentage of products for SRE reaction over Co-MCM-41 at 600°C

6.2.1.iii.b. Sorption Enhanced Steam Reforming of Ethanol Reaction (600°C)

Complete conversion of ethanol was achieved in sorption enhanced steam reforming of ethanol reaction over Co-MCM-41 catalyst, at 600°C.

Hydrogen yield versus time for Co-MCM-41 catalyst at 600°C for sorption enhanced steam reforming of ethanol reaction graph is plotted in Figure 6.36.

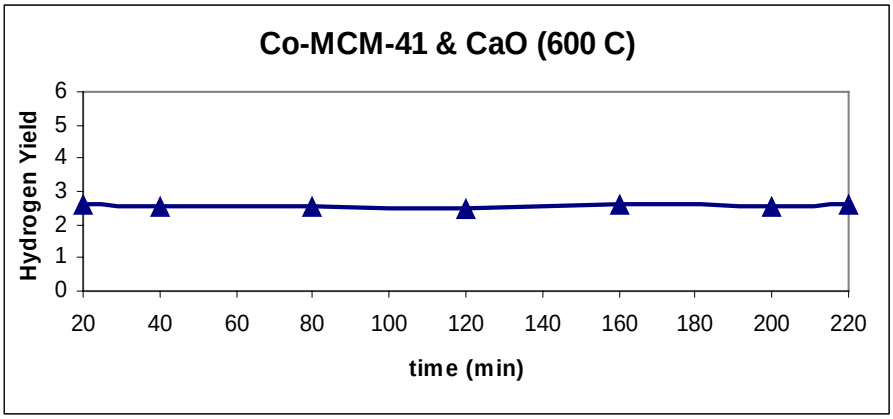

Figure 6.36: Hydrogen yield graph for SESRE reaction over Co-MCM-41 at 600°C

The selectivity of side products with respect to time in sorption enhanced steam reforming of ethanol reaction over Co-MCM-41 catalyst, at 600°C, is given in Figure 6.37. Results proved that total CO_2 (adsorbed and gas phase) significantly increased in the presence of CaO, due to its capture by calcium oxide. This also enhanced hydrogen yield.

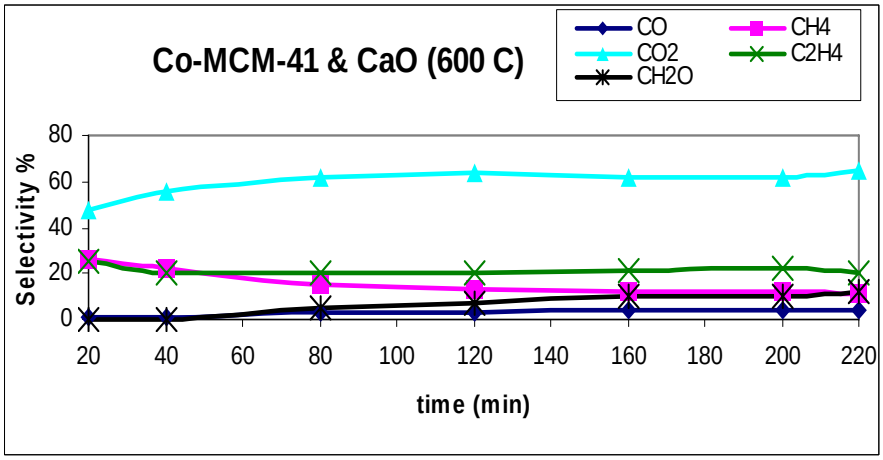

Figure 6.37: Product selectivity for SESRE reaction over Co-MCM-41 at 600°C

The percentage of products in the product stream in sorption enhanced steam reforming of ethanol reaction at 600°C, is shown in Figure 6.38.

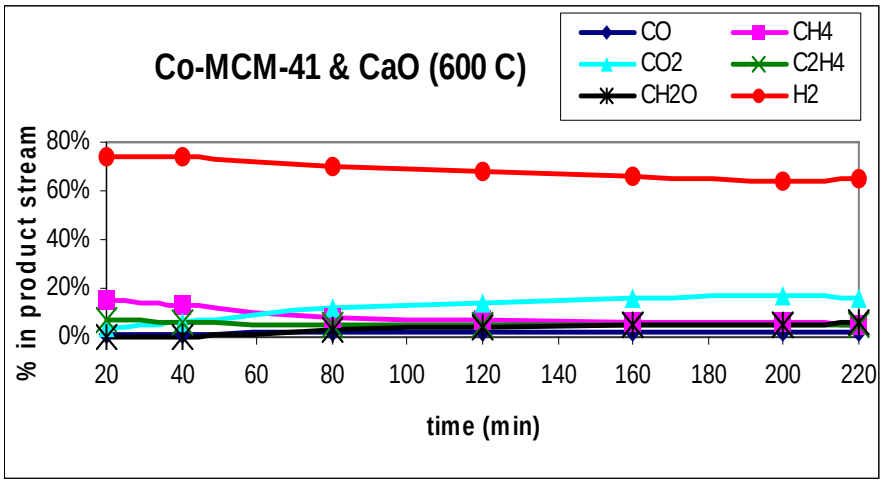

Figure 6.38: The percentage of products for SESRE reaction over Co-MCM-41 at 600°C

6.2.1.iii.c. Comparison of Steam Reforming and Sorption Enhanced Steam Reforming of Ethanol Reaction Results at 600°C

The ethanol conversion values obtained in steam reforming of ethanol reaction and sorption enhanced steam reforming of ethanol reaction at 600°C over Co-MCM-41 catalyst are compared in Figure 6.39.

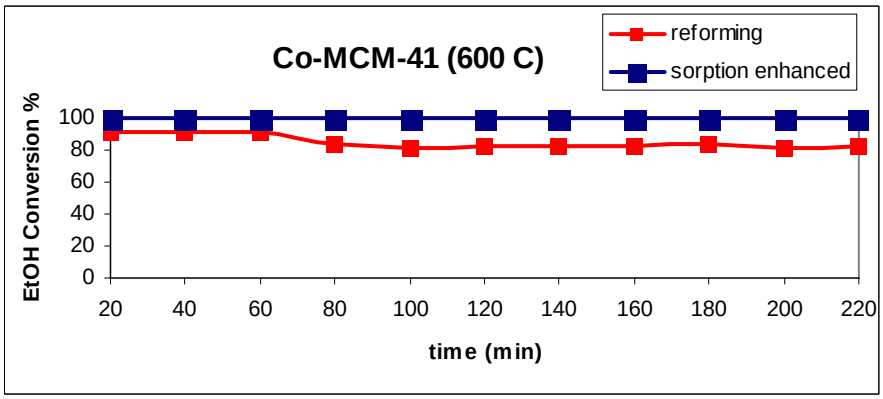

Figure 6.39: Ethanol conversion for SRE and SESRE reactions over Co-MCM-41 at 600°C

Hydrogen yield data obtained in steam reforming reaction and sorption enhanced steam reforming of ethanol reactions over Co-MCM-41 catalyst at 600°C are compared in Figure 6.40. This figure showed that some enhancement was achieved in hydrogen yield due to sorption of CO_2. However, hydrogen yield values are still not very high over this catalyst for practical application.

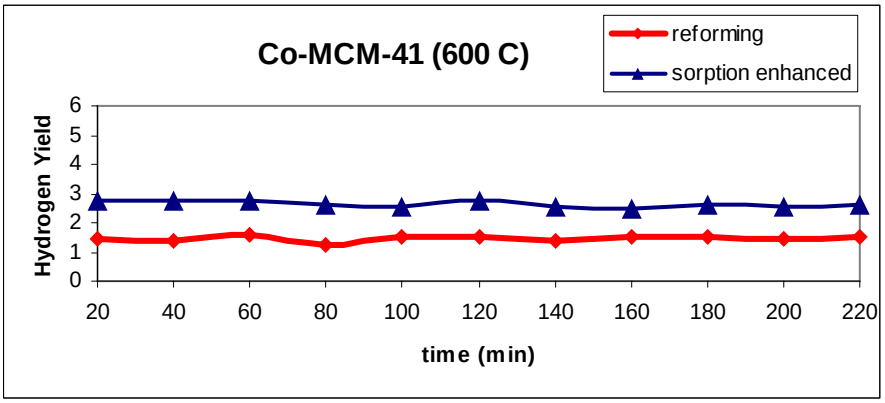

Figure 6.40: Hydrogen yield for SRE and SESRE reactions at 600 °C

6.2.2. Ni-MCM-41 Test Results

Three steam reforming of ethanol reaction experiments and three sorption enhanced steam reforming of ethanol reaction experiments were performed over Ni-MCM-41 catalyst at 500°C, 550°C and 600°C.

6.2.2.i. 500°C Reaction Results with Ni-MCM-41

Reactions mentioned in this section were performed at atmospheric pressure and at 500°C. In section 6.2.2.i.a, catalytic activity of Ni-MCM-41 catalyst towards steam reforming of ethanol reaction will be evaluated according to ethanol conversion, hydrogen yield and product selectivities. In section 6.2.2.i.b, catalytic activity of Ni-MCM-41 catalyst in sorption enhanced steam reforming reaction of ethanol will be evaluated and in section 6.2.2.i.c, ethanol conversion and hydrogen yield values obtained in steam reforming of ethanol and sorption enhanced steam reforming of ethanol will be compared.

6.2.2.i.a. Steam Reforming of Ethanol Reaction (500°C)

Conversion of ethanol with respect to time over Ni-MCM-41 catalyst at 500°C in steam reforming of ethanol reaction is plotted in Figure 6.41. As shown in this figure Ni-MCM-41 showed much higher activity than Co-MCM-41. Even at 500°C, ethanol conversion values were very close to 100%.

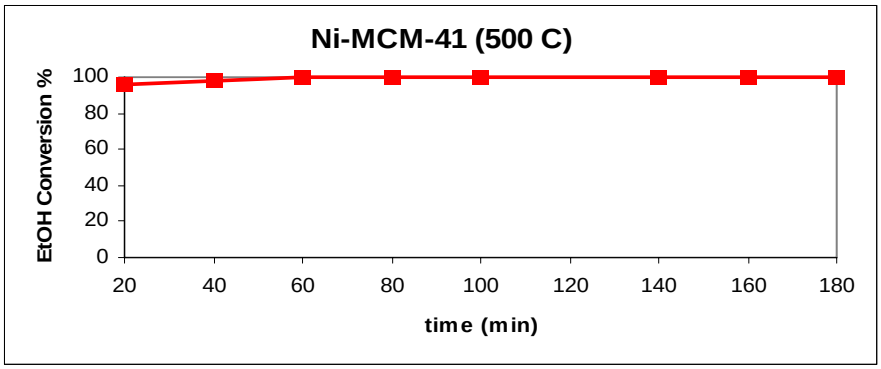

Figure 6.41: Ethanol conversion for SRE reaction over Ni-MCM-41 at 500°C

Hydrogen yield versus time in steam reforming of ethanol reaction over Ni-MCM-41 catalyst at 500°C is shown in Figure 6.42. The average hydrogen yield was about 3.0 during steam reforming of ethanol reaction over Ni-MCM-41 catalyst, at 500°C. This is higher than the corresponding value obtained with Co-MCM-41 at 500°C.

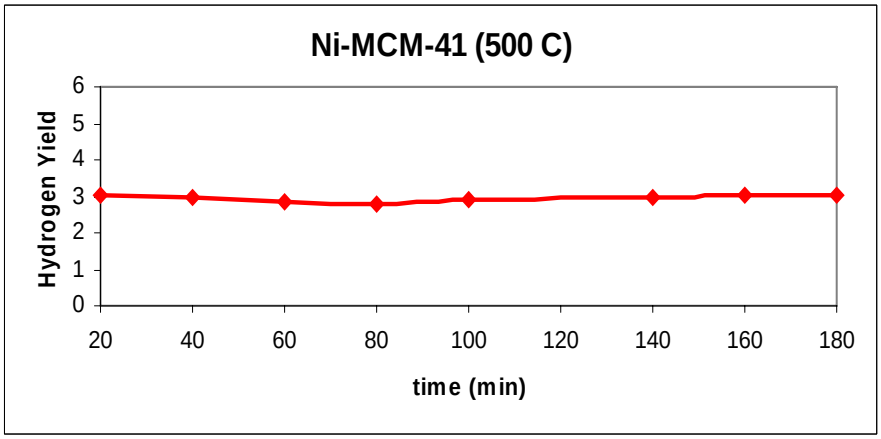

Figure 6.42: Hydrogen yield for SRE reaction over Ni-MCM-41 at 500°C

The selectivity values of side products in steam reforming of ethanol reaction over Ni-MCM-41 at 500°C is shown in Figure 6.43. As reported in this figure, CO_2 and CH_4 are the main carbon containing products observed with Ni-MCM-41 at this temperature. Absence of C_2H_4 proved the negligible contribution of ethanol dehydration over this catalyst.

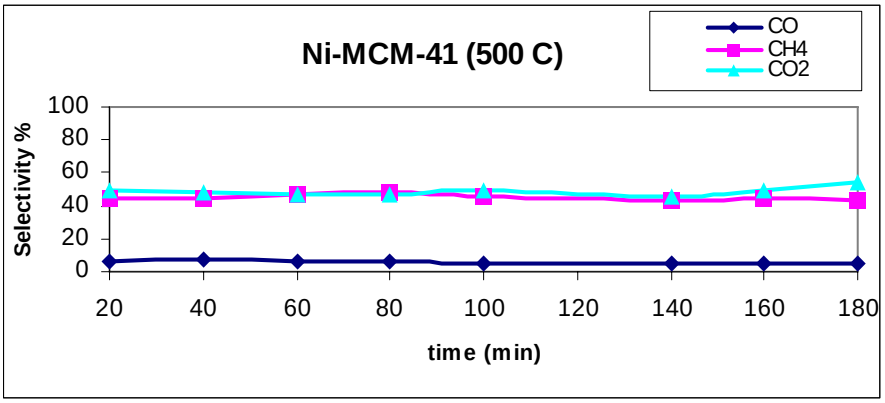

Figure 6.43: Selectivity of side products for SRE reaction over Ni-MCM-41 at 500°C

The percentage of products in the product stream in steam reforming of ethanol reaction at 500°C is shown in Figure 6.44.

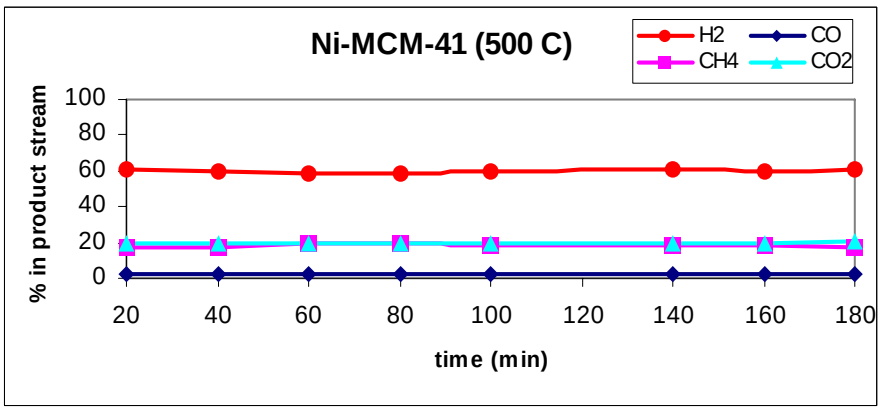

Figure 6.44: Percentage of products for SRE reaction over Ni-MCM-41 at 500°C

6.2.2.i.b. Sorption Enhanced Steam Reforming of Ethanol Reaction (500°C)

Complete conversion of ethanol was achieved in sorption enhanced steam reforming of ethanol at 500°C, over Ni-MCM-41 catalyst.

Hydrogen yield with respect to time in sorption enhanced steam reforming of ethanol reaction over Ni-MCM-41 catalyst at 500°C is plotted in Figure 6.45.

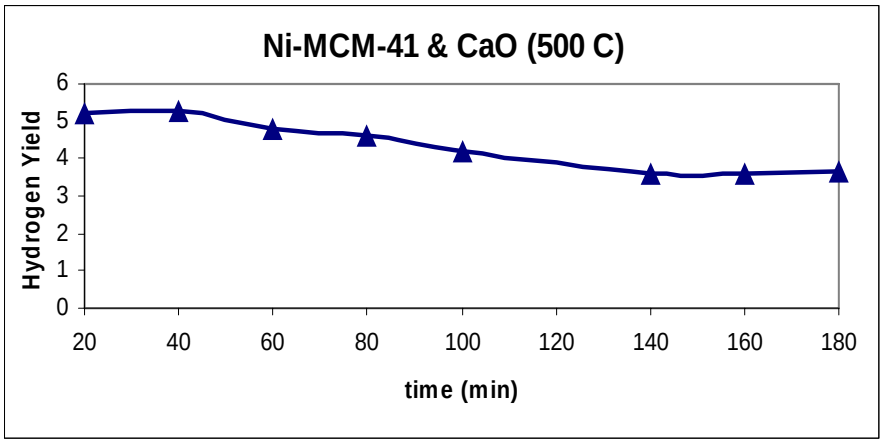

Figure 6.45: Hydrogen yield for SESRE reaction over Ni-MCM-41 at 500°C

As shown in Figure 6.45, during the in situ capture of CO_2, hydrogen yield was 5.0 during the first 50 minutes of reaction. This is quite a high value and over 80% of the maximum possible hydrogen yield of six. This result indicated that sorption enhanced process enhanced the hydrogen yield significantly over Ni-MCM-41 catalyst. Since sorbent CaO lost its adsorbent activity with time, hydrogen yield decreased with time and reached to a value of 3.6 over 140 min reaction time.

Selectivity values of side products in sorption enhanced steam reforming of ethanol reaction over Ni-MCM-41 catalyst at 500°C is shown in Figure 6.46.

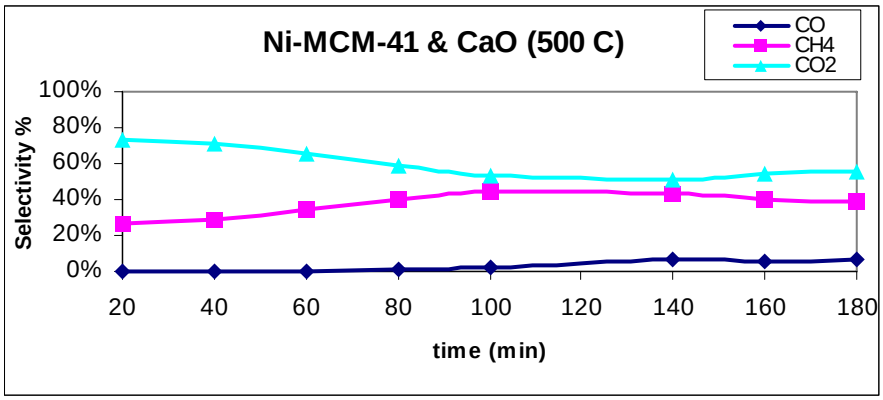

Figure 6.46: Selectivity of side products for SESRE reaction over Ni-MCM-41 at 500°C

The percentage of products in the product stream via sorption enhanced steam reforming of ethanol reaction over Ni-MCM-41 catalyst at 500°C is given in Figure 6.47. As shown in this figure, hydrogen mole fraction in the product stream was over 90% during the first hour of the reaction. CO_2 was not observed in the reactor exit stream during this period. However overall CO_2 selectivity, including captured CO_2 by CaO, was more than 70% (Fig. 6.46) in the same period. Results proved that CO_2 was captured by CaO and as a result the water gas shift reaction shifted to the product side, enhancing hydrogen yield. Appearance of CO_2 in the product gas after about 80 minutes is due to saturation of CaO.

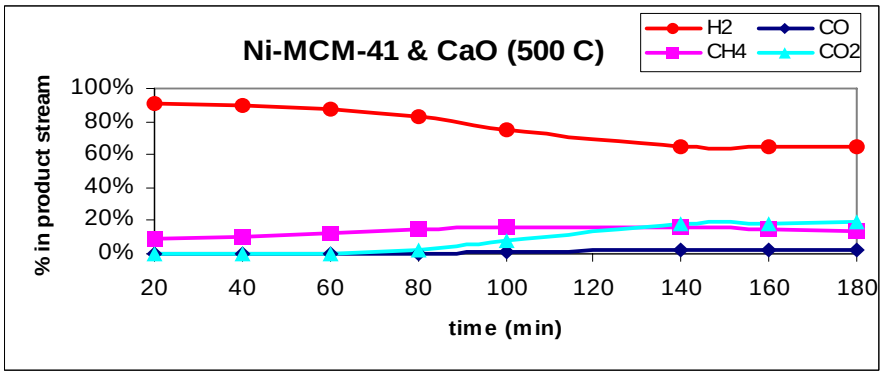

Figure 6.47: The percentage of products for SESRE reaction over Ni-MCM-41 at 500°C

6.2.2.i.c. Comparison of Steam Reforming and Sorption Enhanced Steam Reforming of Ethanol Reaction Results over Ni-MCM-41 at 500°C

Complete conversion of ethanol was achieved for both steam reforming and sorption enhanced steam reforming of ethanol reactions over Ni-MCM-41 catalyst at 500°C.

Hydrogen yield data obtained in steam reforming reaction and sorption enhanced steam reforming of ethanol reactions over Ni-MCM-41 catalyst at 500°C are compared in Figure 6.48. Significant hydrogen yield enhancement is apparent, especially during the first 80 minutes of reaction. At longer times, hydrogen yield values obtained in the presence and absence of CaO approached to each other, indicating saturation of CaO.

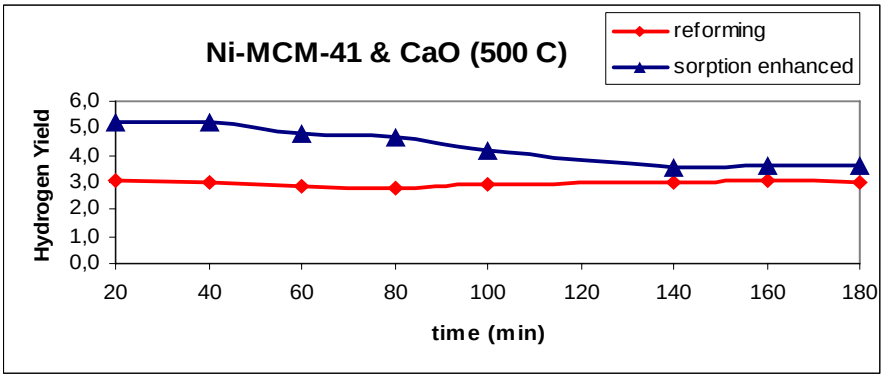

Figure 6.48: Hydrogen yield for SRE and SESRE reactions over Ni-MCM-41 at 500°C

6.2.2.ii.a. Steam Reforming of Ethanol Reaction over Ni-MCM-41 (550°C)

Complete conversion of ethanol was achieved in steam reforming of ethanol reaction over Ni-MCM-41 catalyst, at 550°C.

Hydrogen yield versus time in steam reforming of ethanol reaction over Ni-MCM-41 catalyst at 550°C is plotted in Figure 6.49. The average hydrogen yield was 4.00 during the steam reforming of ethanol reaction over Ni-MCM-41 catalyst at 550°C. This is higher than the value obtained at 500°C, with the same catalyst.

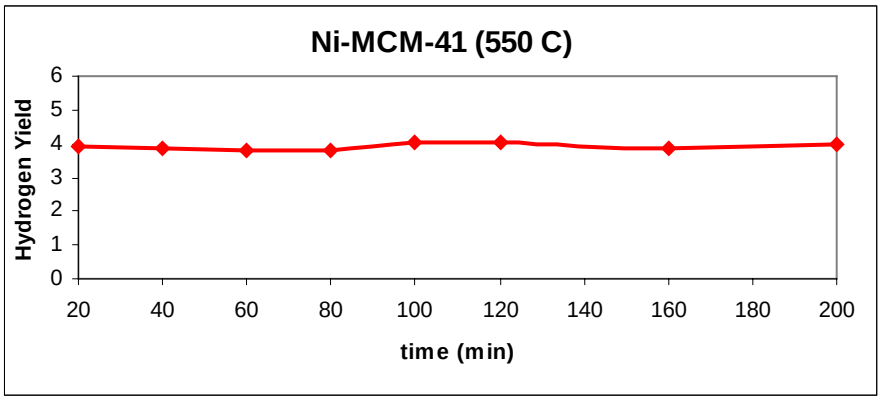

Figure 6.49: Hydrogen yield for SRE reaction over Ni-MCM-41 at 550°C

The selectivity values of side products in steam reforming of ethanol reaction over Ni-MCM-41 catalyst at 550°C is given in Figure 6.50.

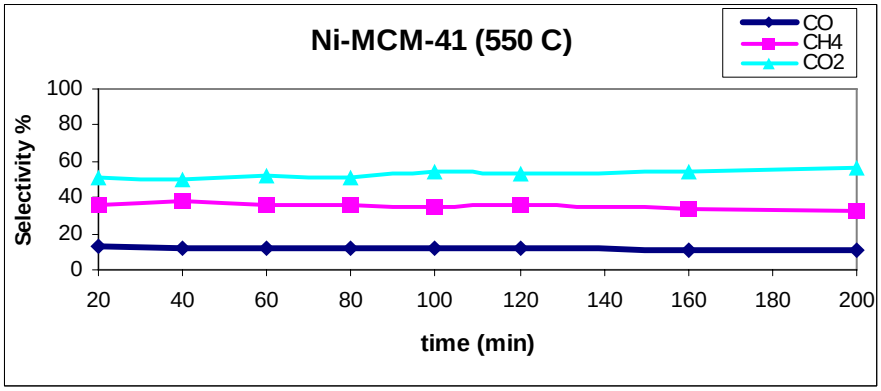

Figure 6.50: Selectivity of side products for SRE reaction over Ni-MCM-41 at 550°C

The percentage of products in the product stream in steam reforming of ethanol reaction over Ni-MCM-41 at 550°C is shown in Figure 6.51.

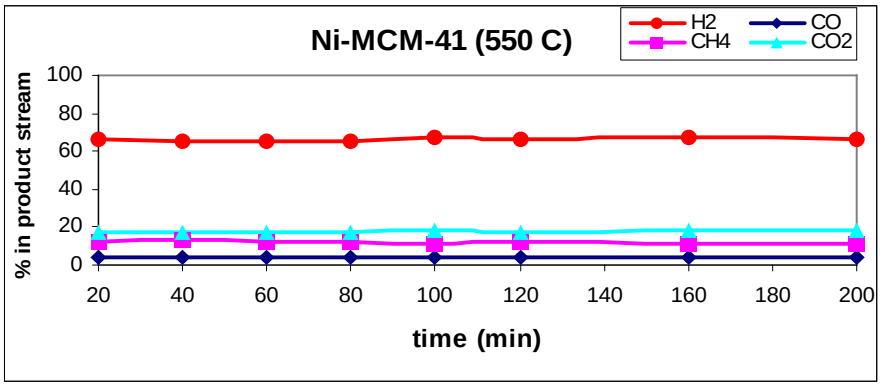

Figure 6.51: The percentage of products for SRE reaction over Ni-MCM-41 at 550°C

6.2.2.ii.b. Sorption Enhanced Steam Reforming of Ethanol Reaction (550°C)

Complete conversion of ethanol was achieved in sorption enhanced steam reforming of ethanol reaction over Ni-MCM-41 catalyst, at 550°C.

Hydrogen yield versus time graph via sorption enhanced steam reforming of ethanol reaction over Ni-MCM-41 catalyst at 550°C is shown in Figure 6.52. As shown in this figure, very high hydrogen yield values, close to 90% of the maximum possible value of six, were obtained during the first 80 minutes of reaction at this temperature.

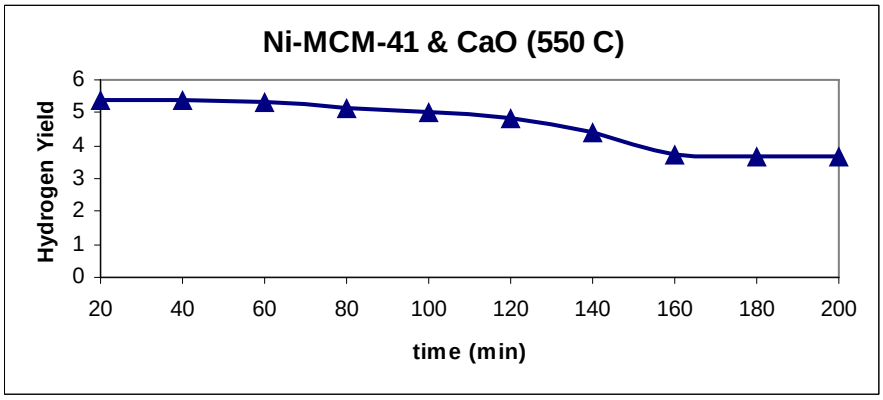

Figure 6.52: Hydrogen yield for SESRE reaction over Ni-MCM-41 at 550°C

The selectivity values of side products in sorption enhanced steam reforming of ethanol reaction over Ni-MCM-41 catalyst at 550°C are shown in Figure 6.53. As

indicated in this figure, the only side product which caused some decrease of hydrogen yield from the maximum possible value of six is methane during the first 80 minutes of reaction.

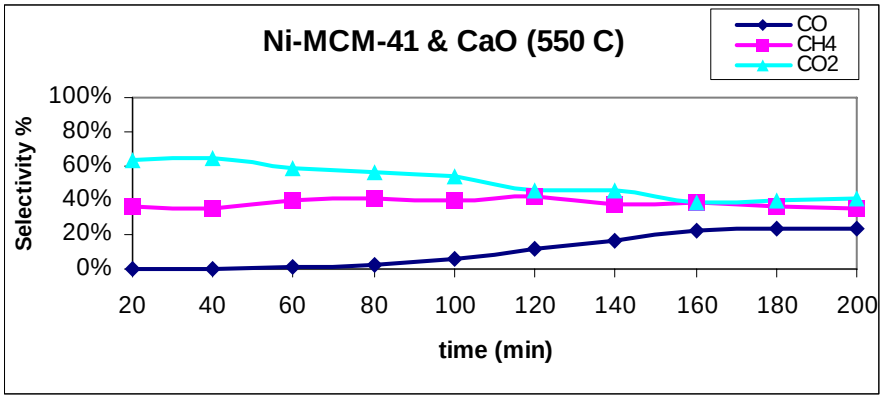

Figure 6.53: Selectivity of side products for SESRE reaction over Ni-MCM-41 at 550°C

The percentage of products in the product stream in sorption enhanced steam reforming of ethanol reaction over Ni-MCM-41 at 550°C is given in Figure 6.54.

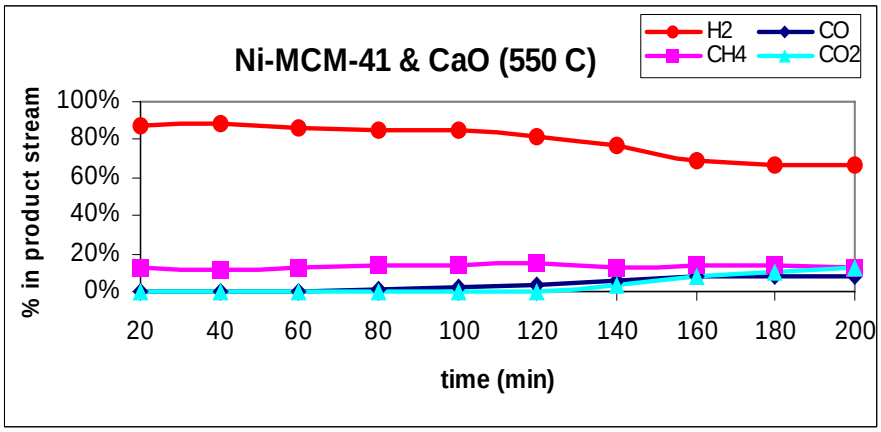

Figure 6.54: The percentage of products for SESRE reaction over Ni-MCM-41 at 550°C

6.2.2.ii.c. Comparison of Steam Reforming and Sorption Enhanced Steam Reforming of Ethanol Reaction Results over Ni-MCM-41 at 550°C

Complete conversion was achieved in both steam reforming and sorption enhanced steam reforming of ethanol reactions over Ni-MCM-41 catalyst, at 550°C.

Hydrogen yield data obtained in steam reforming reaction and sorption enhanced steam reforming of ethanol reaction over Ni-MCM-41 catalyst, at 550°C, are compared in Figure 6.55. Significant hydrogen yield enhancement is obvious during the first 80 minutes of reaction.

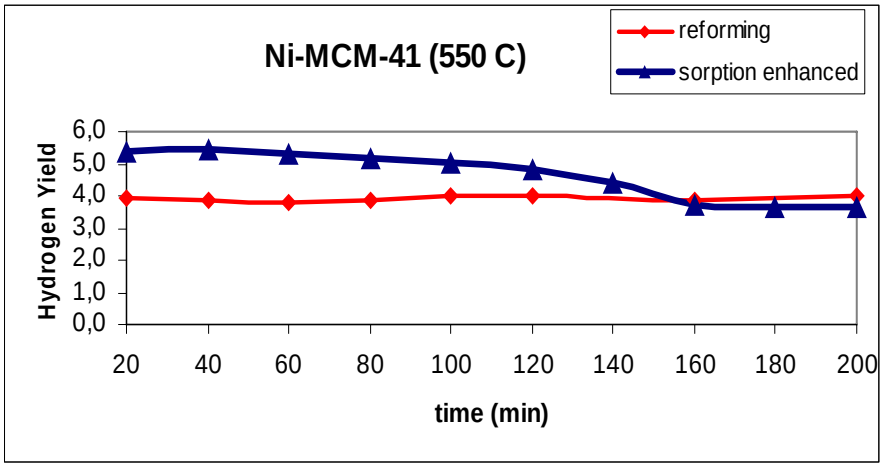

Figure 6.55: Hydrogen yield for SRE and SESRE reactions over Ni-MCM-41 at 550°C

6.2.2.iii.a. Steam Reforming of Ethanol Reaction over Ni-MCM-41 (600°C)

Complete conversion was achieved in steam reforming of ethanol reaction over Ni-MCM-41 catalyst at 600°C.

Hydrogen yield versus time in steam reforming of ethanol reaction over Ni-MCM-41 catalyst at 600°C graph is plotted in Figure 6.56. The average hydrogen yield was about 4.50 during the steam reforming of ethanol reaction over Ni-MCM-41 catalyst at 600°C. This value is quite high in the absence of CaO. In fact, this value is much higher than the corresponding value obtained with Co-MCM-41 at the

same temperature, showing that Ni-MCM-41 was a much better catalyst for steam reforming of ethanol.

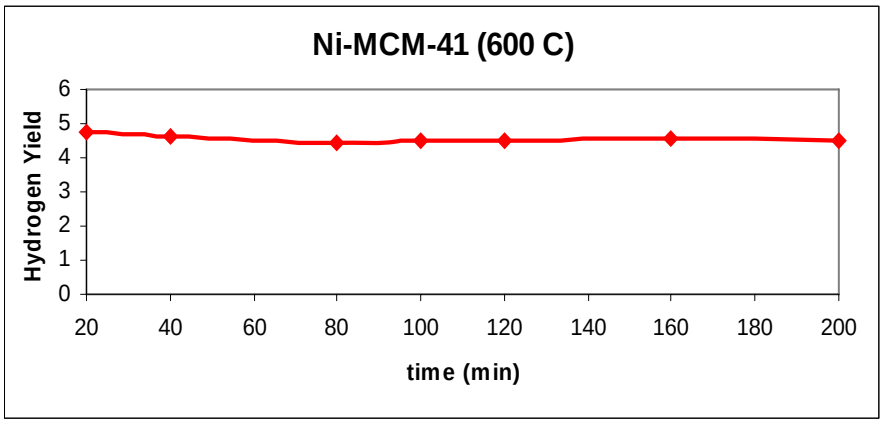

Figure 6.56: Hydrogen yield for SRE reaction over Ni-MCM-41 at 600°C

The selectivity of side products in steam reforming of ethanol reaction over Ni-MCM-41 catalyst at 600°C is given in Figure 6.57. As shown in this figure, the overall selectivity of CO_2 (including CO_2 captured by CaO) is about 60%. Formation of CO and CH_4 caused negative effects on hydrogen yield.

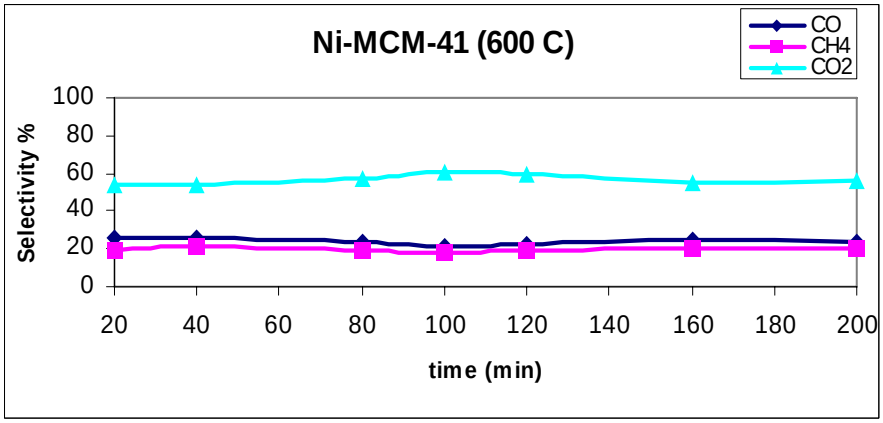

Figure 6.57: Selectivity of side products for SRE reaction over Ni-MCM-41 at 600°C

The percentage of products in the product stream in steam reforming of ethanol reaction over Ni-MCM-41, at 600°C is shown in Figure 6.58. Hydrogen mole

fraction in the product stream reached to about 70% at this temperature over Ni-MCM-41.

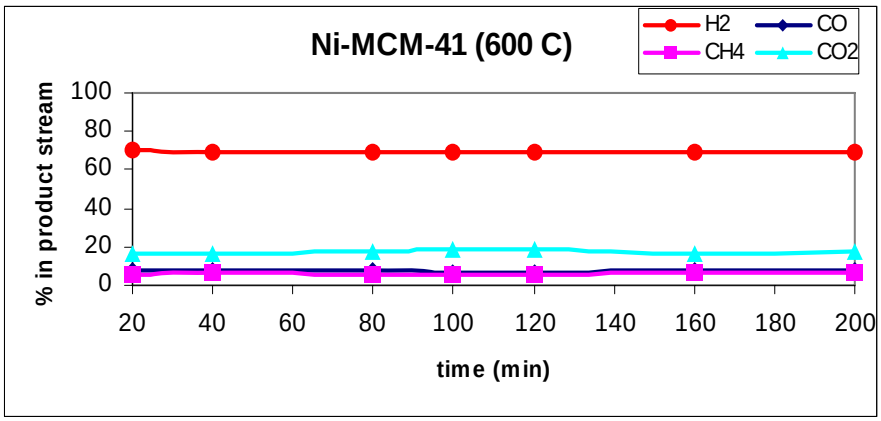

Figure 6.58: The percentage of products for SRE reaction over Ni-MCM-41 at 600°C

6.2.2.ii.b. Sorption Enhanced Steam Reforming of Ethanol Reaction over Ni-MCM-41 (600°C)

Complete conversion of ethanol was achieved for sorption enhanced steam reforming of ethanol reaction over Ni-MCM-41 catalyst at 600°C.

Hydrogen yield versus time graph via sorption enhanced steam reforming of ethanol reaction over Ni-MCM-41 catalyst at 600°C is shown in Figure 6.59.

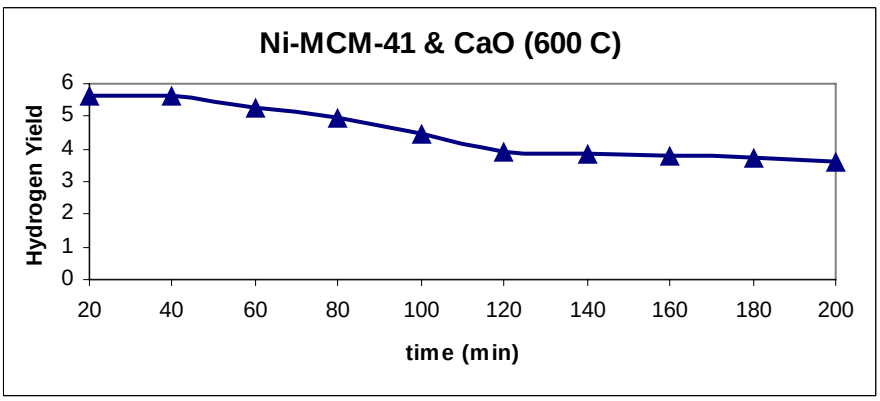

Figure 6.59: Hydrogen yield for SESRE reaction over Ni-MCM-41 at 600°C

As shown in Figure 6.59, initially hydrogen yield reached to 5.6 which is very close to the maximum value of six. This is about 94% of the maximum possible hydrogen yield. Hydrogen yield decreased with time and became almost constant at 3.9.

The selectivity of side products in sorption enhanced steam reforming of ethanol over Ni-MCM-41 catalyst, at 600°C, is shown in Figure 6.60. The only side product which cause some decrease in hydrogen yield is CH_4.

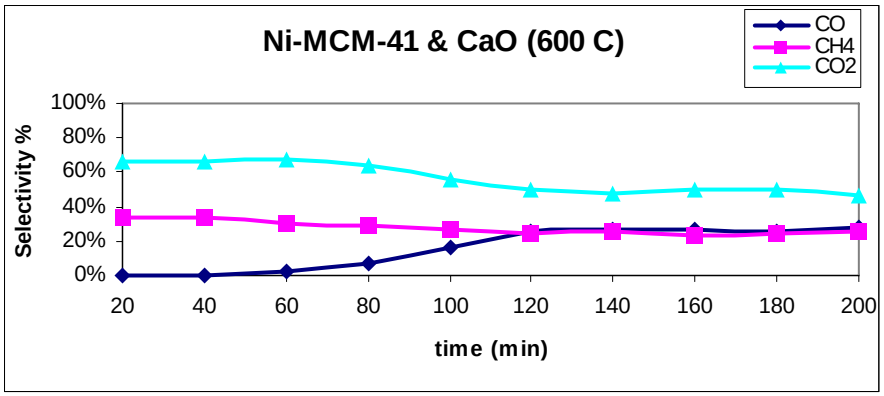

Figure 6.60: Selectivity of side products for SESRE reaction over Ni-MCM-41 at 600°C

The percentage of products in the product stream in sorption enhanced steam reforming of ethanol over Ni-MCM-41, at 600°C, is given in Figure 6.61.

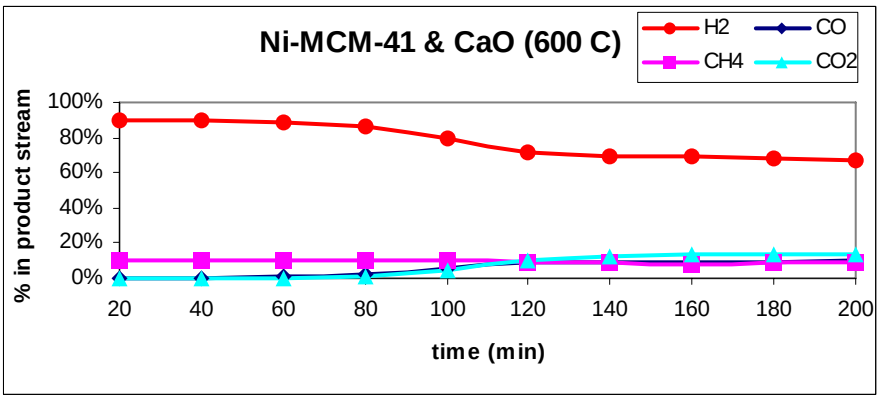

Figure 6.61: The percentage of products for SESRE reaction over Ni-MCM-41 at 600°C

6.2.2.ii.c. Comparison of Steam Reforming and Sorption Enhanced Steam Reforming of Ethanol Reaction Results over Ni-MCM-41 at 600°C

Complete conversion was achieved in both steam reforming and sorption enhanced steam reforming of ethanol over Ni-MCM-41 catalyst, at 600°C.

Hydrogen yield data obtained in steam reforming reaction and sorption enhanced steam reforming of ethanol reactions over Ni-MCM-41 catalyst at 600°C are compared in Figure 6.62. Hydrogen yield enhancement by CaO is clear during first 80 minutes. However, it was interesting that at times longer than 100 min lower hydrogen yield values were observed in sorption enhanced reactions.

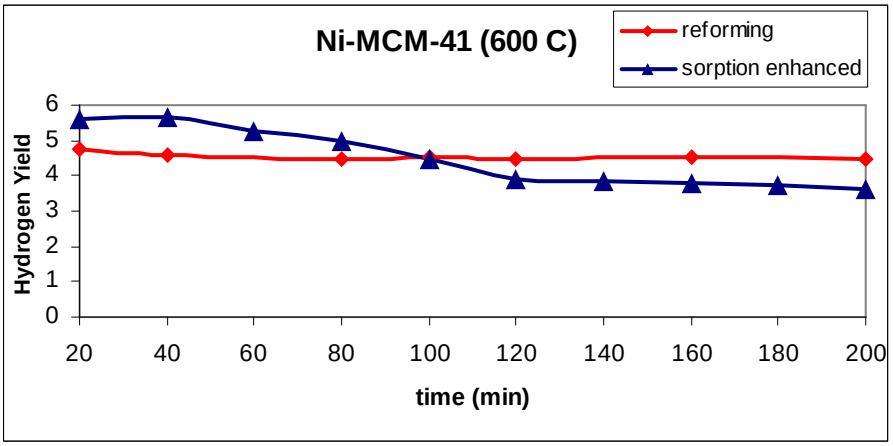

Figure 6.62: Hydrogen yield for SRE and SESRE reactions over Ni-MCM-41 at 600°C

6.3. Characterization Results of Spent Catalysts in the Reaction

In this section, characterization results of the used catalysts after the reaction will be given. To characterize the spent catalysts, XRD, BET, SEM and TGA techniques were performed.

6.3.1. Characterization Results of Spent Catalyst Co-MCM-41

6.3.1.i. XRD Results

The XRD pattern of Co-MCM-41 catalyst synthesized by impregnation method is given in Figure 6.5 in Section 6.1.2.i. The XRD patterns of Co-MCM-41 catalyst used in the steam reforming of ethanol reaction performed at 500°C, 550°C and 600°C compared with fresh Co-MCM-41 are shown in Figure 6.63, Figure 6.64 and Figure 6.65 respectively.

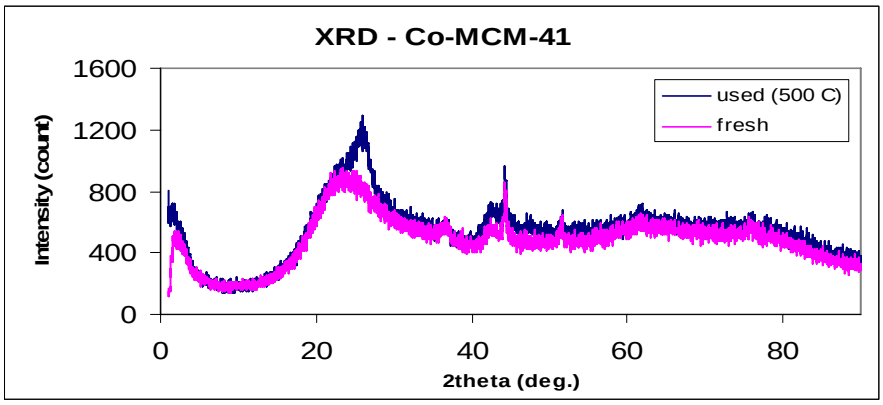

Figure 6.63: XRD pattern of fresh and used Co-MCM-41 in SRE reaction at 500°C

As it is seen from Figure 6.63, there is no obvious difference between the fresh and used Co-MCM-41 catalyst at 500°C indicating that catalyst structure was conserved during steam reforming of ethanol reaction performed at 500°C.

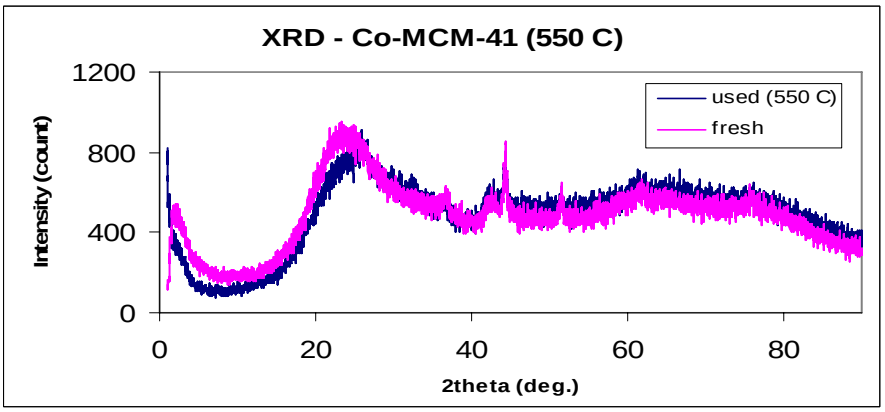

Figure 6.64: XRD pattern of fresh and used Co-MCM-41 in SRE reaction at 550°C

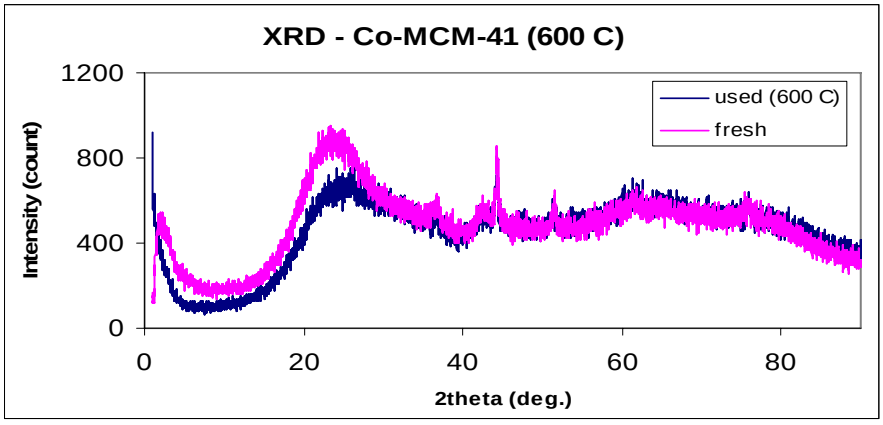

Figure 6.65: XRD pattern of fresh and used Co-MCM-41 in SRE reaction at 600^{o}

As it is seen from Figure 6.64 and Figure 6.65, XRD patterns of used Co-MCM-41 catalysts at 550^{o}Cand 600^{o}C are very similar to XRD pattern of fresh Co-MCM-41 which showed that the catalyst structure was conserved during reaction.

XRD patterns of used Co-MCM-41 catalysts and adsorbent (CaO) mixture are given in Appendix F1. In these patterns, $CaCO_3$ and CaO peaks are clearly seen indicating that CaO turned to $CaCO_3$ during sorption enhanced steam reforming of ethanol reaction but small portion of the adsorbent still remained as CaO.

.

6.3.1.ii. SEM Results

The SEM images of Co-MCM-41 catalyst used in the steam reforming of ethanol reaction at 500^{o}C are given in Figure 6.66.

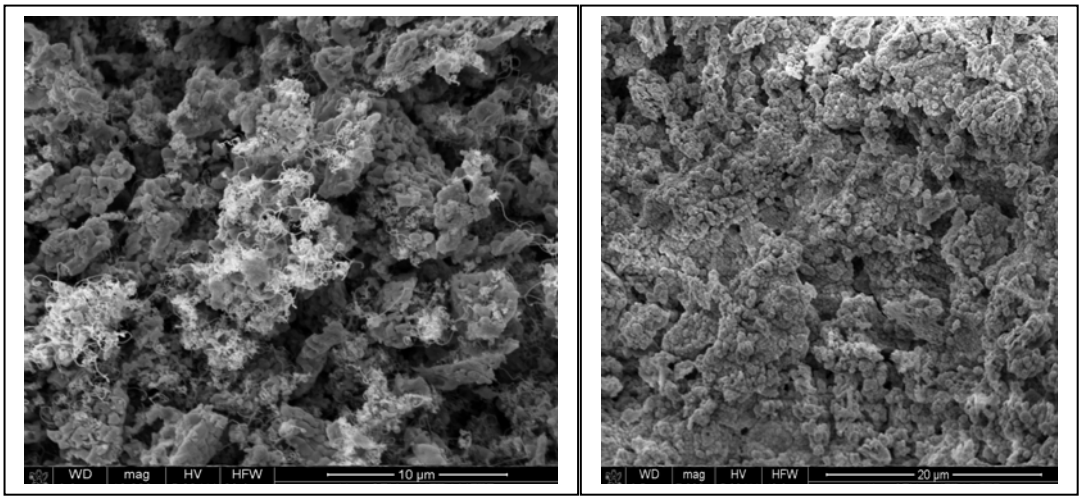

Figure 6.66: SEM images of Co-MCM-41 used in SRE reaction at 500^{o}C.

The difference between the SEM images of fresh Co-MCM-41 and used one is the filamentous carbon structure seen in SEM image of used Co-MCM-41.

6.3.1.iii. Nitrogen Physisorption (BET) Results

BET and BJH surface area values, pore size and pore volume data of fresh and used Co-MCM-41 catalysts are listed and compared in Table 6.8.

Table 6.8: Surface area, pore size and pore volume data of fresh and spent Co-MCM-41

Sample	Reaction Temperature (^oC)	BET Surface Area (m^2/g)	BJH Surface Area (m^2/g)	Pore Volume (cc/g)	Pore Diameter (nm)
Co-MCM-41 (fresh)	-	303.6	271.6	0.259	1.891
Co-MCM-41 (spent–500 ^oC)	500	193.1	179.7	0.334	1.640
Co-MCM-41 (spent-600 ^oC)	600	142.6	145.7	0.132	1.642

As shown in Table 6.8, BET surface areas of the used catalysts were lower than the surface area of fresh catalyst. In addition, surface areas of the spent catalysts decreased with the reaction temperature. This is probably due to the formation of coke on the catalyst surface during reaction. In fact, formation of significant amount of C_2H_4 and CH_2O over Co-MCM-41 was an indication of possibility of coke formation.

6.3.1.iv. TGA Results

TGA analyses of spent catalysts were done to investigate the carbon deposition on the catalyst during the reaction. It is known that thermograms can be divided into 3 different temperature intervals; region I at temperatures lower than 573 K represents the loss of water and volatile species such as reactants, products

and reaction intermediates, region II at temperatures between 573 K and 803 K ascribed to oxidation of coke deposits which originated directly from ethylene polymerization reaction given below **[61]**.

$$C_2H_4 \rightarrow polymerization \rightarrow coke$$

Region III located at temperatures above 803 K represents the oxidation of coke deposits with a different degree of graphitization originated from Boudouard reaction given below **[61]**.

$$2CO \rightarrow CO_2 + C_{(s)}$$

Figures 6.67 and 6.68 are the TGA results of Co-MCM-41 catalyst spent in the reforming reaction at 500°C and 600°C respectively. TGA results indicated weight loss due to coke combustion in the temperature range of 400-600°C. Total weight loss was about 7-10%. This result is also justified by the exothermic DTA peaks observed at 500 and 550°C. Results proved that most of the coke formed on the catalyst is due to polymerization of C_2H_4 over Co-MCM-41.

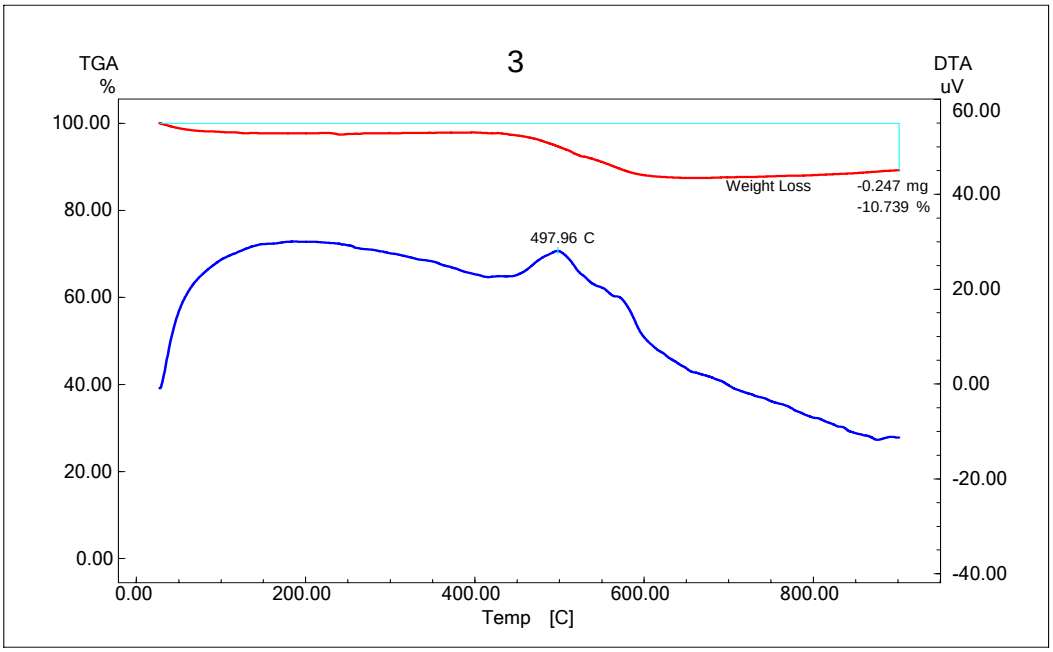

Figure 6.67: TGA result of spent Co-MCM-41 at 500°C

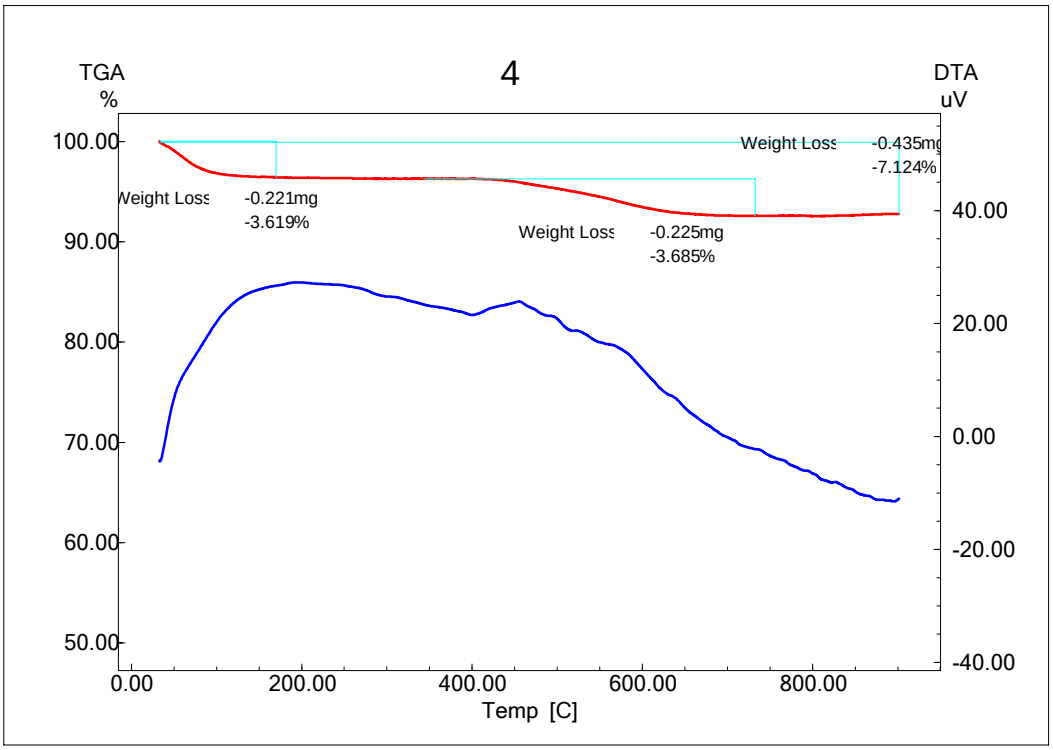

Figure 6.68: TGA result of spent Co-MCM-41 at 600^{o}C

6.3.2. Characterization Results of Spent Catalyst Ni-MCM-41

6.3.2.i. XRD Results

The XRD pattern of Ni-MCM-41 catalyst synthesized by impregnation method is given in Figure 6.9 in Section 6.1.3.i. The XRD patterns of Ni-MCM-41 catalyst used in the steam reforming of ethanol reaction performed at 500^{o}C, 550^{o}C and 600^{o}C are shown in Figure 6.69, Figure 6.70 and Figure 6.71 respectively.

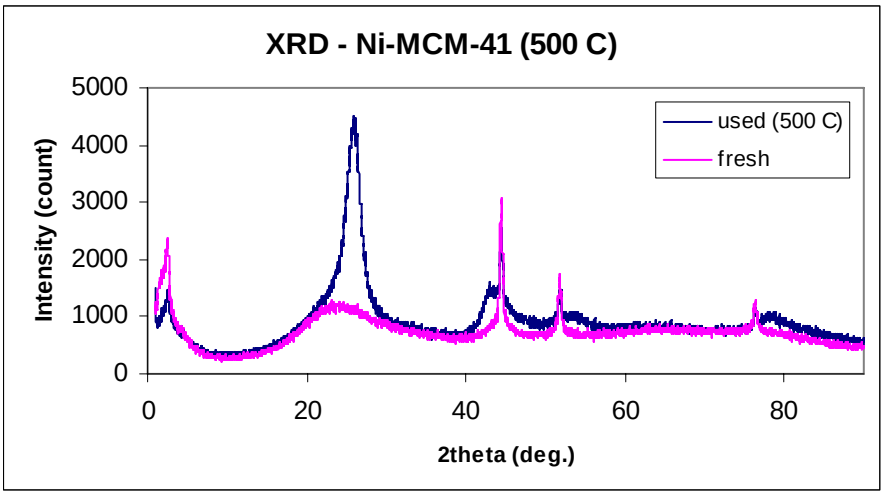

Figure 6.69: XRD pattern of fresh and used Ni-MCM-41 in SRE reaction at 500°C.

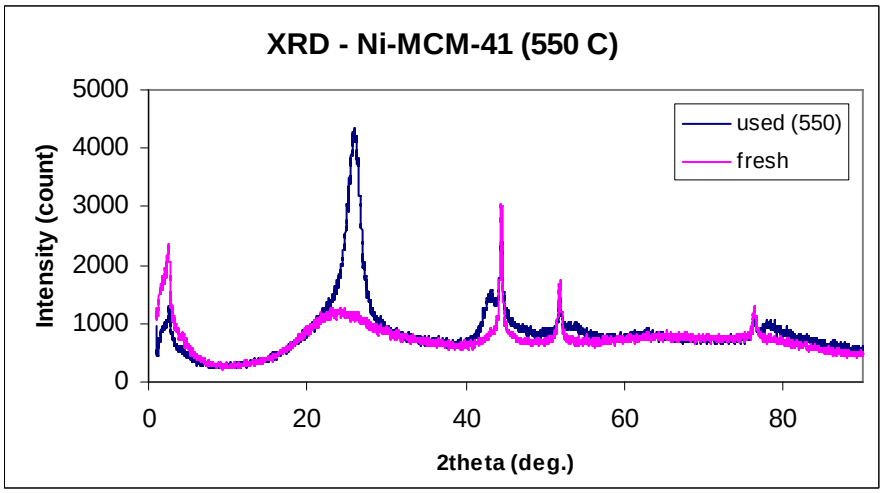

Figure 6.70: XRD pattern of fresh and used Ni-MCM-41 in SRE reaction at 550°C

As shown in Figure 6.69 and Figure 6.70, wide peak at 24.1° corresponding to amorphous silica can be clearly seen in XRD pattern of fresh Ni-MCM-41. Sharp peak at 26.4° in XRD pattern of used Co-MCM-41 corresponds to carbon indicating coke formation on catalyst during reaction.

XRD patterns of used Ni-MCM-41 catalyst and adsorbent (CaO) mixture is given in Appendix F1. $CaCO_3$ and CaO peaks can be clearly seen in these patterns.

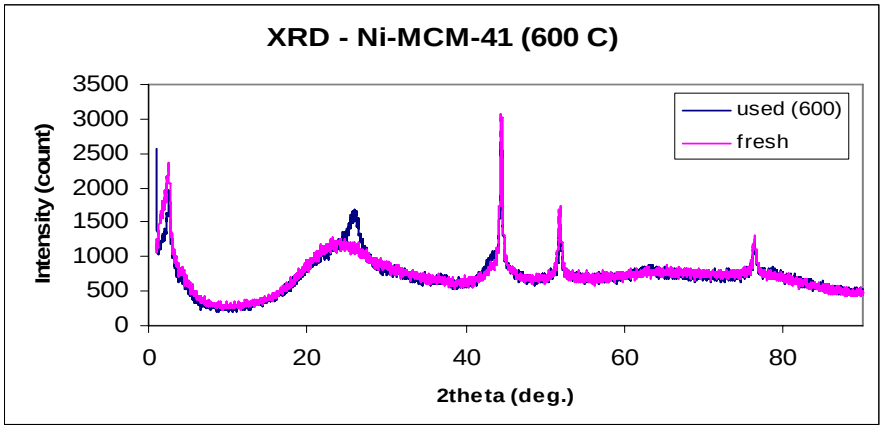

Figure 6.71: XRD pattern of Ni-MCM-41 used in SRE reaction at 600°C

6.3.1.ii. SEM Results of used Ni-MCM41.

The SEM images of Ni-MCM-41 catalyst used in the steam reforming of ethanol reaction at 600°C are given in Figure 6.72.

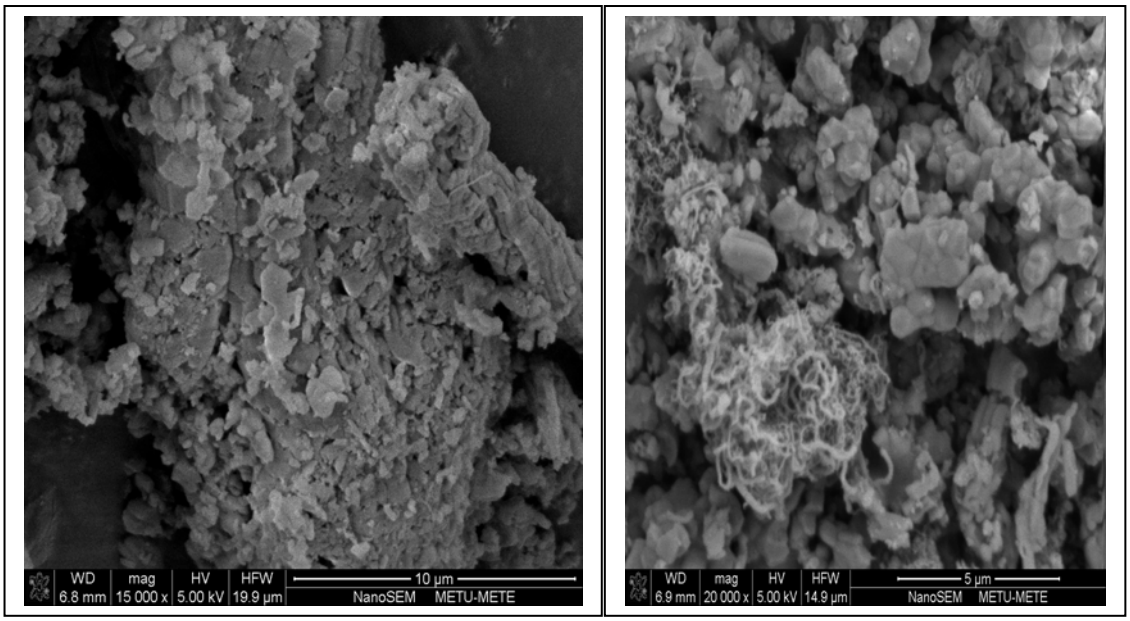

Figure 6.72: SEM images of Ni-MCM-41 used in SRE reaction at 600°C

Filamentous structure seen in the right side SEM image in Figure 6.72 belongs to the carbon deposited during the reaction which can be also proved with the TGA result of the spent Ni-MCM-41 catalyst.

6.3.2.iii. Nitrogen Physisorption (BET) Results

BET and BJH surface area values, pore size and pore volume data of fresh and spent Ni-MCM-41 catalysts are listed and compared in Table 6.9. As shown in this table, surface area values of the used catalysts were lower than the fresh catalyst, indicating closure of pore mouths of some of the pores by coke.

Table 6.9: Surface area, pore size and pore volume data of fresh and spent Ni-MCM-41

Sample	Reaction Temperature (^oC)	BET Surface Area (m^2/g)	BJH Surface Area (m^2/g)	Pore Volume (cc/g)	Pore Diameter (nm)
Ni-MCM-41 (fresh)	-	449.0	351.3	0.293	2.172
Ni-MCM-41 (spent–500 ^oC)	500	287.0	272.6	0.252	2.149
Ni-MCM-41 (spent-600 ^oC)	600	212.9	186.9	0.430	1.909

6.3.2.iv. TGA Results of Used Ni-MCM-41

Figures 6.73 and 6.74 are the TGA results of spent Ni-MCM-41 catalyst in the reforming reaction at 500^{o}C and 600^{o}C, respectively. Results showed sharp weight loss over 600^{o}C, indicating the formation of coke on the catalyst surface, most probably due to a graphitization following Boudouard reaction.

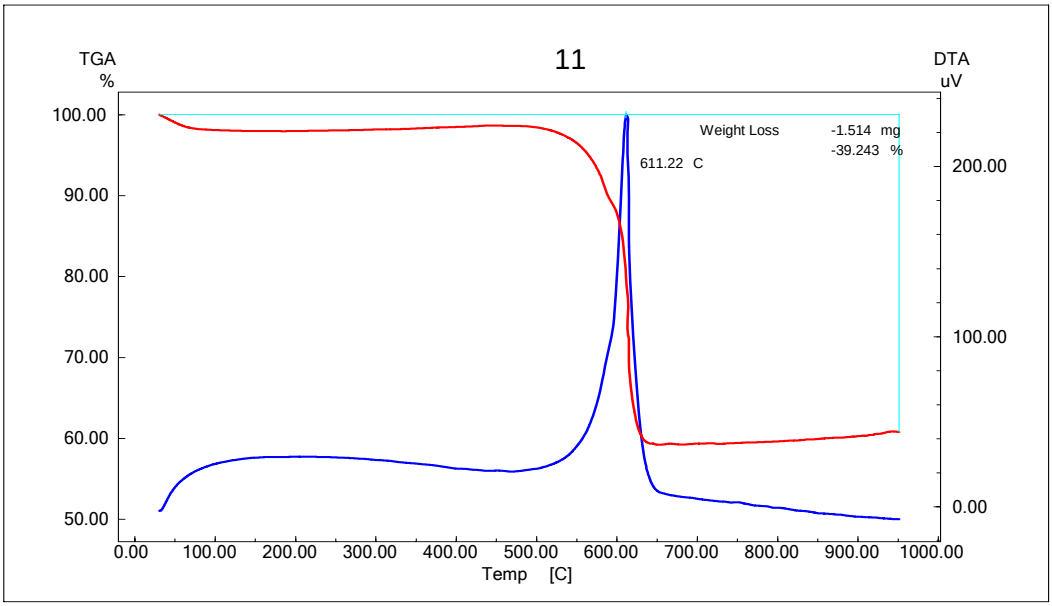

Figure 6.73: TGA result of spent Ni-MCM-41 catalyst at 500^{o}C

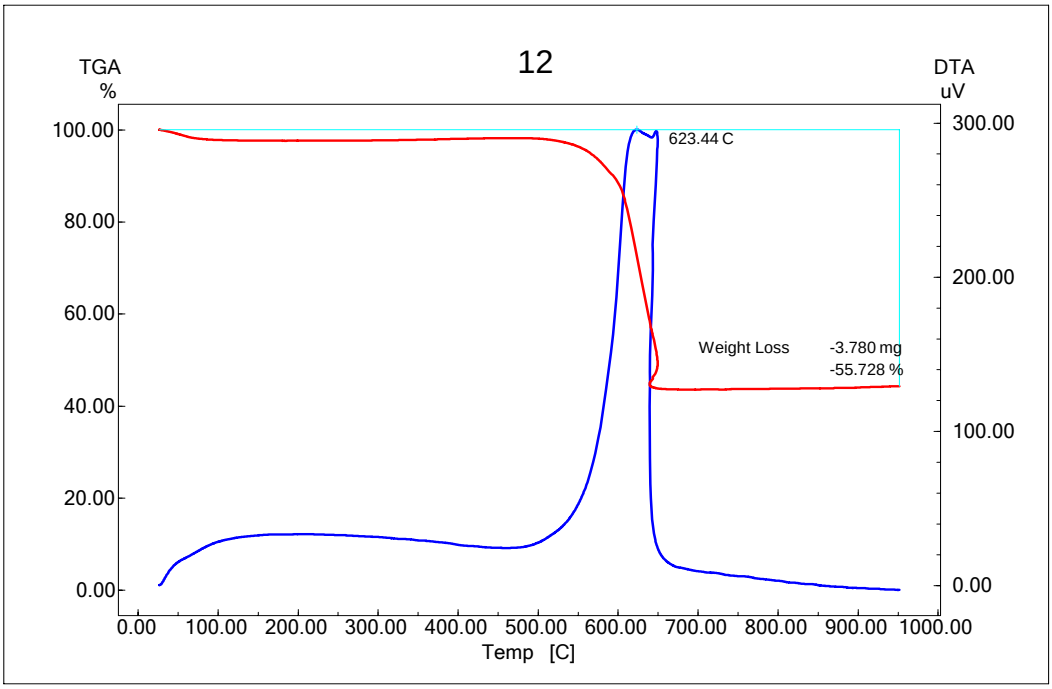

Figure 6.74: TGA result of spent Ni-MCM-41 catalyst at 600^{o}C

CHAPTER 7

CONCLUSIONS AND RECOMMENDATIONS

In this study, Co-MCM-41 and Ni-MCM-41 catalysts were synthesized by impregnation method and tested in both steam reforming of ethanol and sorption enhanced steam reforming of ethanol reactions at 500^{o}C, 550^{o}C and 600^{o}C, at atmospheric pressure. At the end of the study following conclusions were reached;

- Cobalt and nickel incorporated MCM-41 type catalysts were successfully synthesized without destroying the characteristic ordered pore structure of MCM-41, by using impregnation method.

- Synthesized Co-MCM-41 having Co/Si molar ratio of 0.1 had d_{100} and lattice parameter values of 4.75 nm and 5.48 nm, respectively. Surface area of Co-MCM-41 was sufficiently high (303.6 m^2/g) and pore diameter was 1.89 nm. Surface area result showed that smaller pores were choked by Co and CoO clusters due to impregnation. Co and CoO were very well distributed in the catalyst with average cluster sizes of 11.6 nm and 4.9 nm, respectively.

- Synthesized Ni-MCM-41 having Ni/Si molar ratio of 0.1 had d_{100} and lattice parameter values of 3.53 nm and 4.1 nm, respectively. Surface area of Ni-MCM-41 was 449 m^2/g and pore diameter was 2.2 nm. Results showed that smaller pores were choked by Ni and NiO clusters due to impregnation. Ni and NiO were found to be well dispersed within the catalyst with cluster sizes of 21.2 nm and 25.0 nm, respectively.

- Although Co-MCM-41 catalyst showed good activity on ethanol conversion, product distribution indicated that main reactions were ethanol dehydration to ethylene and ethanol decomposition, rather than reforming. Consequently,

obtained hydrogen yield values were quite low. As a result, it was concluded that this catalyst was not good for ethanol reforming to produce hydrogen.

- Co-MCM-41 catalyst was also tested in sorption enhanced steam reforming of ethanol reaction at 500^{o}C. Ethanol conversion increased from 80% to 94% and hydrogen yield increased from 0.9 to 3.1 in sorption enhanced steam reforming of ethanol reaction at 500^{o}C. Increasing ethanol conversion and hydrogen yield in the presence of CaO indicated that in situ CO_2 capture enhanced both the ethanol conversion and hydrogen yield. However, the hydrogen yield value is still much lower than the maximum possible hydrogen yield value of six. Side products observed in sorption enhanced steam reforming of ethanol reaction at 500^{o}C were CO, CH_4, CO_2, C_2H_4 and CH_2O. The selectivity of C_2H_4 was nearly 50% indicating that the dominant reaction was ethanol dehydration reaction, even in sorption enhanced steam reforming of ethanol over Co-MCM-41 at 500^{o}C.

- Co-MCM-41 catalyst was also tested in steam reforming of ethanol and sorption enhanced reforming at higher temperatures (550^{o} and 600^{o}C). Increase of temperature improved hydrogen yield, as well as ethanol conversion. However, hydrogen yield values were still not high, indicating unsatisfactory performance of Co-MCM-41 in ethanol reforming. Sorption of CO_2 by CaO during improved hydrogen yield, also at these temperatures. However, hydrogen yield values were not high enough for practical applications.

- Ni-MCM-41 catalyst having Ni/Si molar ratio of 0.1 was tested in both steam reforming of ethanol and sorption enhanced steam reforming of ethanol reactions at 500^{o}C, 550^{o}C and 600^{o}C as in the case of Co-MCM-41 catalyst. Catalytic performance of Ni-MCM-41 was much better than Co-MCM-41 in ethanol reforming.

- Ethanol conversion and hydrogen yield values obtained at 500^{o}C over Ni-MCM-41 catalyst were 100% and 3.0 respectively, which were higher than the corresponding values obtained with Co-MCM-41 catalyst at. CO and CH_4 were the main carbon containing side products observed with Ni-MCM-41 at 500^{o}C. Absence of C_2H_4 in product stream indicated absence of ethanol dehydration and led to increase in hydrogen yield.

  At the same temperature, sorption enhanced steam reforming of ethanol reaction was also performed with Ni-MCM-41. Complete conversion was achieved at 500^{o}C. During the first 50 minutes of the reaction, hydrogen yield was 5.0 which was over 80% of maximum possible hydrogen yield of 6, indicating that in situ capture of CO_2 had a significant effect on hydrogen yield at 500^{o}C over Ni-MCM-41 catalyst. Results were highly promising for practical applications.

- Ni-MCM-41 catalyst was also tested at 550^{o}C and 600^{o}C. Complete conversion was achieved with a hydrogen yield of 4.0 and 4.5, respectively at these temperatures. Results proved that increase of temperature improved hydrogen yield, by increasing the contributions of steam reforming and water gas shift reactions.

- Sorption enhanced steam reforming of ethanol reaction was performed over Ni-MCM-41 catalyst at 550^{o}C and 600^{o}C gave hydrogen yield values of 5.2 and 5.6, respectively. These values are very high, showing the enhancement of hydrogen production by in-situ sorption of CO_2 with CaO. This hydrogen yield enhancement decreased after about 80 minutes due to saturation of CaO.

- Chemical and physical analysis of the used catalyst showed coke formation on the catalyst surface during reaction. In the case of Ni-MCM-41, coke was in the form of filamentous form, which did not cause significant catalyst deactivation.

From all the conclusions listed above, it is recommended that in order to increase the catalyst stability, coke formation should be eliminated in the future studies. To see the effect of amount of metal loading on ethanol conversion and hydrogen yield, catalysts having different metal/Si molar ratios may be synthesized and tested in both steam reforming of ethanol and sorption enhanced steam reforming of ethanol reactions. In order to achieve higher temperatures with less energy, different reactors, such as microwave reactors, can be designed and used in the future studies. These recommendations may further improve ethanol conversion and hydrogen yield values and also enhance the process economy.

REFERENCES

[1] Subramani, V., Song, C., Advances in catalysis and process for hydrogen production from ethanol reforming, Catalysis, 2007, 20, 65-106.

[2] Song, C. S., Fuel processing for low-temperature and high-temperature fuel cells, challenges and opportunities for sustainable development in the 21st century, Catal. Today, 2002, 77, 17-50.

[3] Sarria, F., Vargas, J. C., Roger, A. C., Kiennemann, A., Hydrogen production by steam reforming of ethanol study of mixed oxide catalysts $Ce_2Zr_{1.5}Me_{0.5}O_8$: Comparison of Ni/Co and effect of Rh, Catalysis Today, 133-135, 149-153.

[4] Haryanto, A., Fernando, S., Murali, N., Adhikari, S., Current status of hydrogen production techniques by steam reforming of ethanol : A review, Energy & Fuels, 2005, 19, 2098-2106.

[5] Levin, D. B., Pitt, L., Love, M., Biohydrogen production: Prospects and limitations to practical application, Int. J. Hydrogen Energy, 2004, 29, 173-185.

[6] FY 2003 Progress Report on Hydrogen, Fuel Cells and Infrastructure Technologies, http://www.eere.energy.gov.hydrogenandfuelcells/pdfs/iic5_miller.pdf.

[7] Velu, S., Satoh, N., Gobinath, C. S., Suzuki, K., Oxidative reforming of bioethanol over CuNiZnAl mixed oxide catalysts for hydrogen production, Catal. Lett., 2002, 82, 145-152.

[8] Garcia, E. Y., Laborde, M. A., Hydrogen production by the steam reforming of ethanol: Thermodynamic analysis, Int. J. Hydrogen Energy, 1991, 16, 307-312.

[9] Vasudeva, K., Mitra, N., Umasankar, P., Dhingra, S. C., Steam reforming of ethanol for hydrogen production: thermodynamic analysis, Int. J. Hydrogen Energy, 1996, 21, 13-18.

[10] Fishtik, I., Alexander, A., Datta, R., Geana, D., A thermodynamic analysis of hydrogen production by steam reforming of ethanol via response reactions, Int. J. Hydrogen Energy, 2000, 25, 31-45.

[11] Wang, W., Wang, Y. Q., Thermodynamic analysis of steam reforming of ethanol for hydrogen generation, Int. J. Energy Res., 2008, 32, 1432-1443.

[12] Ionnides, T., Thermodynamic analysis of ethanol processors for fuel cell applications, Journal of Power Sources, 2001, 92, 17-25.

[13] Llorca, J., Piscina, P., Sales, J., Homs, N., Direct production of hydrogen from ethanolic aqueous solutions over oxide catalysts, Chem. Commun., 2001, 641-642.

[14] Haga, F., Nakajima, T., Miya, H., Mishima, S., Catalytic properties of supported cobalt catalysts for steam reforming of ethanol, Catalysis Letters, 1997, 48, 223-227.

[15] Comas, J., Marino, F., Laborde, M., Amadeo, N., Bio-ethanol steam reforming on Ni/Al_2O_3 catalyst, Chemical Engineering Journal, 2004, 98, 61-68.

[16] He, L., Berntsen, H., Chen, D., Approaching sustainable H_2 production: Sorption enhanced steam reforming of ethanol, J. Phys. Chem. A, 2010, 114, 3834-3844.

[17] Barelli, L., Bidini, G., Gallorini, F., Servili, S., Hydrogen production through sorption-enhanced steam methane reforming and membrane technology: A review, Energy, 2008, 33, 554-570.

[18] Batista, M. S., Assaf, E. M., Assaf, J. M., Ticianelli, E. A., Double bed reactor for the simultaneous steam reforming of ethanol and water gas shift reactions, Int. J. Hydrogen Energy, 2006, 31, 1204-1209.

[19] Wang, Y. N., Rodriguez, A. E., Hydrogen production from methane reforming coupled with in situ CO_2 capture: Conceptual parametric study, Fuel, 2005, 84, 1778-1789.

[20] Yi, K. B., Harrison, D. P., Low-pressure sorption-enhanced hydrogen production, Ind. Eng. Chem. Res., 2005, 44, 1665-1669.

[21] Wang, X., Wang, N., Wang, L., Hydrogen production by sorption enhanced steam reforming of propane: A thermodynamic investigation, Int. J. Hydrogen Energy, 2010, 1-7.

[22] Dupont, V., Dou, B., Rickett, G., Blakeman, N., Williams, P. T., Chen, H., Ding, Y., Ghadiri, M., Hydrogen production by sorption-enhanced steam reforming of glycerol, Bioresource Technology, 2009, 100, 3540-3547.

[23] Lysikov, A. I., Trukhan, S. N., Okunev, A. G., Sorption enhanced hydrocarbons reforming for fuel cell powered generators, Int. J. Hydrogen Energy, 2008, 33, 3061-3066.

[24] Iwasaki, Y., Suzuki, Y., Kitajima, T., Sakurai, M., Kameyama, H., Non-equilibrium hydrogen production from ethanol using CO_2 absorption ceramic and precious metal catalysts, J. Chem. Eng. Jpn., 2007, 40, 178-185.

[25] Essaki, K., Muramatsu, T., Kato, M., Effect of equilibrium-shift in the case of using lithium silicate pellets in ethanol steam reforming, Int. J. Hydrogen Energy, 2008, 33, 6612-6618.

[26] Guo, X., Lai, M., Kong, Y., Ding, W., Yan, Q., Novel coassembly route to Cu-SiO_2 MCM-41-like mesoporous materials, Langmuir, 2004, 20, 2879-2882.

[27] Oye, G., Sjöblom, J., Stöcker, M., Synthesis, characterization and potential applications of new materials in the mesoporous range, Advances in Colloid and Interface Science, 2001, 89-90, 439-466.

[28] Corma, A., From microporous to mesoporous molecular sieve materials and their use in catalysis, Chem. Rev., 1997, 97, 2373-2419.

[29] Vartuli, J. C., Roth, W. J., Degnan, T. F., Mesoporous materials (M41S): From discovery to application, Dekker Encyclopedia of Nanoscience and Nanotechnology, 2004.

[30] Zhai, Q. Z., Wang, P., Preparation, characterization and optical properties of lanthanum-(nanometer MCM-41) composite materials, J. Iran. Chem. Soc., 2008, 5, 268-273.

[31] Zhao, X. S., Lu, G. Q., Millar, G. J., Advances in mesoporous molecular sieve MCM-41, Ind. Eng. Chem. Res., 1996, 35, 2075-2090.

[32] Melo, R. A. A., Giotto, M. V., Rocha, J., Gonzalez, E. A., MCM-41 ordered mesoporous molecular sieves synthesis and characterization, Materials Research, 1999, 2, 173-179.

[33] Sener, C., Synthesis and characterization of Pd-MCM-Type mesoporous nanocomposite materials, Master Thesis, METU, 2007.

[34] Beck, J. S., Vartuli, J. C., Roth, W. J., Leonowicz, M. E., Kresge, C. T., Sheppard, E. W., McCullen, S. B., Higgins, J. B., Schlenker, J. L., A new family of mesoporous molecular sieves prepared with liquid crystal templates, J. Am. Chem. Soc., 1992, 114, 10834-10843.

[35] Stucky, G. D., MacDougall, J. E., Quantum confinement and host/guest chemistry: Probing a new dimension, Science, 1990, 247, 669-678.

[36] Gao, C., Formation mechanism of anionic-surfactant-templated mesoporous silica (AMS), Master Thesis, Stockholm University, 2009.

[37] Chen, C. Y., Li, H. Y., Davis, M. A., Studies on mesoporous materials II: Synthesis mechanism of MCM-41, Microporous Mater., 1993, 2, 27.

[38] Schumacher, K., Grün, M., Unger, K. K., Novel synthesis of spherical MCM-48, Microporous and Mesoporous Materials, 1999, 27, 201-206.

[39] Vartuli, J. C., Malek, A., Roth, W. J., Kresge C. T., McCullen, S. B., The sorption properties of as-synthesized and calcined MCM-41 and MCM-48, Microporous and Mesoporous Materials, 2001, 44-45, 691-695.

[40] Behrens, P., Glaue, A., Haggenmüller, C., Schechner, G., Structure-directed materials synthesis: Synthesis field diagrams for the preparation of mesostructured silicas, Solid State Ionics, 1997, 101-103, 255-260.

[41] Yao, N., Synthesis and characterization of Pt/Sn-MCM-41 petroleum reforming catalysts, PhD Thesis, Yale University, 2002.

[42] Sing, K., Physisorption of nitrogen by porous materials, Journal of Porous Materials, 1995, 2, 5-8.

[43] Wikipedia the Free Encyclopedia, http:// en.wikipedia.org / wiki / Energy_dispersive_X-ray_spectroscopy, Last access date: December, 2010.

[44] Wikipedia the Free Encyclopedia, http:// en.wikipedia.org / wiki / Scanning_electron_microscope, Last access date: December, 2010.

[45] Panpranot, J., Goodwin, J. G., Sayari, A., Synthesis and characteristics of MCM-41 supported CoRu catalysts, Catalysis Today, 2002, 77, 269-284.

[46] Haga, F., Nakajima, T., Miya, H., Mishima, S., Catalytic properties of supported cobalt catalysts for steam reforming of ethanol, Catalysis Letters, 1997, 48, 223-227.

[47] Llorca, J., Homs, N., Sales, J., Piscina, P., Efficient production of hydrogen over supported cobalt catalysts from ethanol steam reforming, Journal of Catalysis, 2002, 209, 306-317.

[48] Lin, S., Kim, D. H., Ha, S. Y., Hydrogen production from ethanol steam reforming over supported cobalt catalysts, Catall. Lett., 2008, 122, 295-301.

[49] Haga, F., Nakajima, T., Yamashita, K., Mishima, S., Effect of crystallite size on the catalysis of alumina-supported cobalt catalyst for steam reforming of ethanol, React. Kinet. Catal. Lett., 1998, 63, 253-259.

[50] Song, H., Mirkelamoglu, B., Ozkan, U., Effect of cobalt precursor on the performance of ceria-supported cobalt catalysts for ethanol steam reforming, Applied Catalysis A: General, 2010, 1-7.

[51] Lim, S., Ciuparu, D., Yang, Y., Du, G., **Haller, G. L**., Improved synthesis of highly ordered Co-MCM-41, Microporous and Mesoporous Materials, 2007, 101, 200-206.

[52] Liu, D., Cheo, W. N., Lim, Y. W., Borgna, A., Lau, R., **Yang, Y**., A comparative study on catalyst deactivation of nickel and cobalt incorporated MCM-41 catalysts modified by platinum in methane reforming with carbon dioxide, Catalysis Today, 2010, 1-8.

[53] Wosciejzak, R., Monteverdi, S., Mercy, M., Nowak, I., Ziolek, M., **Bettahar, M. M**., Nickel containing MCM-41 and AlMCM-41 mesoporous molecular sieves characteristics and activity in the hydrogenation of benzene, Applied Catalysis A: General, 2004, 268, 241-253.

[54] Du, G., Lim, S., Yang, Y., Wang, C., **Haller, G**., Methanation of carbon dioxide on Ni-incorporated MCM-41 catalysts: The influence of catalyst pretreatment and study of steady-state reaction, Journal of Catalysis, 2007, 249, 368-377.

[55] Liu, D., Quek, X. Y., Cheo, W. N., Lau, R., Borgna, A., **Yang, Y**., MCM-41 supported nickel-based bimetallic catalysts with superior stability during carbon dioxide reforming of methane: Effect of strong metal-support interaction, Journal of Catalysis, 2009, 266, 380-390.

[56] Fenelonov V. B., Romannikov, V. N., Derevyankin, A. Y., Mesopore size and surface area calculations for hexagonal mesophases (types MCM-41, FSM-16, etc) using low-angle XRD and adsorption data, Microporous and Mesoporous Materials, 1999, 28, 57-72.

[57] Patterson, A. L., The Scherrer formula for X-ray particle size determination, Physical Review, 1939, 56, 978-982.

[58] Doğu, T., Gözenekli kireç taşı ve kükürt dioksit arasındaki heterojen reaksiyon, Doçentlik Tezi, Mart 1979.

[59] Doğu, T., The importance of pore structure and diffusion in the kinetics of gas-solid non-catalytic reactions: Reaction of calcined limestone with SO_2, Chemical Engineering Journal, 1981, 21, 213-222.

[60] Werle, P., Trageser, M., Duderstadt, Ulrike, Process for the production of calcium formate, United States Patent, 1992.

[61] Cerritos, R. C., Ramirez, R. F., Alvarado, A. F. A., Rosales, J. M. M., Garcia, T. V., Esquivel, I. R. G., Steam reforming of ethanol over Ni/Al_2O_3-La_2O_3 catalysts synthesized by sol-gel, Ind. Eng. Chem. Res., A-I.

APPENDIX A

A1. PARTICLE SIZE CALCULATION

Particle sizes of metal or metal oxide clusters were calculated with Scherrer equation given below.

$$t_{particle} = \frac{C \times \lambda}{B \times \cos(\frac{2\theta}{2})} \quad \text{(A1)}$$

Co Particle Size Calculation:

C: crystal shape factor = 0.89

λ: Wavelength = 1.54 Å

B: Full Width at Half Max = 0.729^o

2θ = 44.32^o

$$B = 0.729^o \times \frac{\pi}{180} = 0.01272 \; radyans$$

$$t_{Co,particle} = \frac{(0.89) \times (1.54)}{(0.01272) \times \cos(\frac{44.32}{2})} = 116.35 \text{ A} = 11.6 \; nm$$

CoO Particle Size Calculation:

C: crystal shape factor = 0.89

λ: Wavelength = 1.54 Å

B: Full Width at Half Max = 1.718^o

2θ = 42.40^o

$$B = 1.718^o \times \frac{\pi}{180} = 0.02998 \; radyans$$

$$t_{CoO,particle} = \frac{(0.89)\times(1.54)}{(0.02998)\times\cos(\frac{42.40}{2})} = 49\ \text{A} = 4.9\ nm$$

Ni Particle Size Calculation:

C: crystal shape factor = 0.89

λ: Wavelength = 1.54 Å

B: Full Width at Half Max = 0.400°

2θ = 44.48°

$$B = 0.400^{o}\times\frac{\pi}{180} = 0.00698\ radyans$$

$$t_{Ni,particle} = \frac{(0.89)\times(1.54)}{(0.00698)\times\cos(\frac{44.48}{2})} = 212.14\ \text{A} = 21.2\ nm$$

NiO Particle Size Calculation:

C: crystal shape factor = 0.89

λ: Wavelength = 1.54 Å

B: Full Width at Half Max = 0.353°

2θ = 76.38°

$$B = 0.353^{o}\times\frac{\pi}{180} = 0.00616\ radyans$$

$$t_{NiO,particle} = \frac{(0.89)\times(1.54)}{(0.00616)\times\cos(\frac{76.38}{2})} = 248.83\ \text{A} = 25.0\ nm$$

APPENDIX B

B1. SEM IMAGES OF CATALYSTS

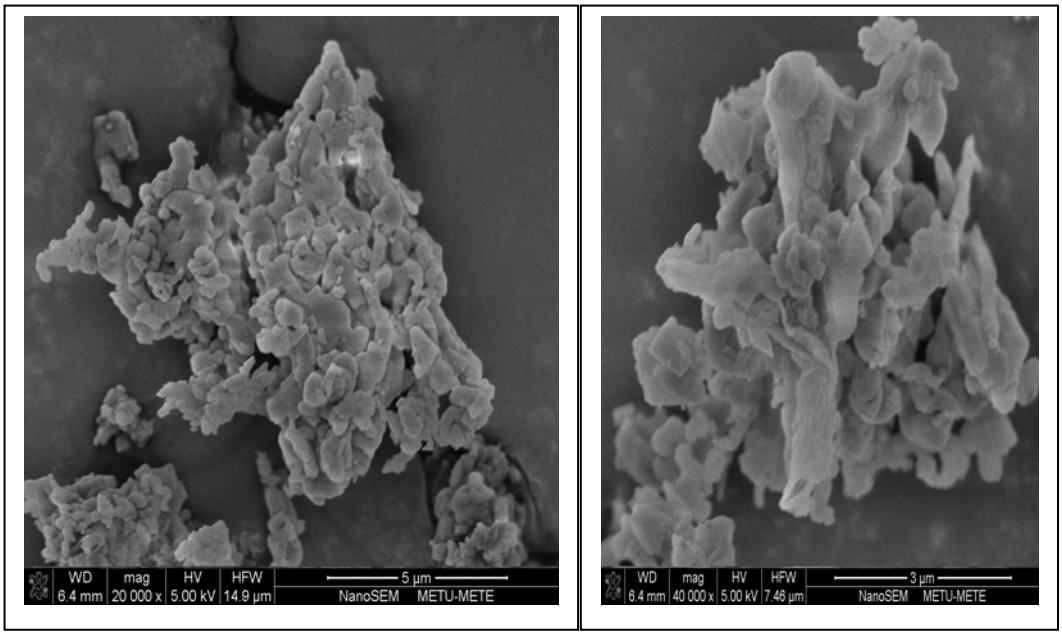

Figure B1: SEM image of Ni-MCM-41 (1) **Figure B2:** SEM image of Ni-MCM-41

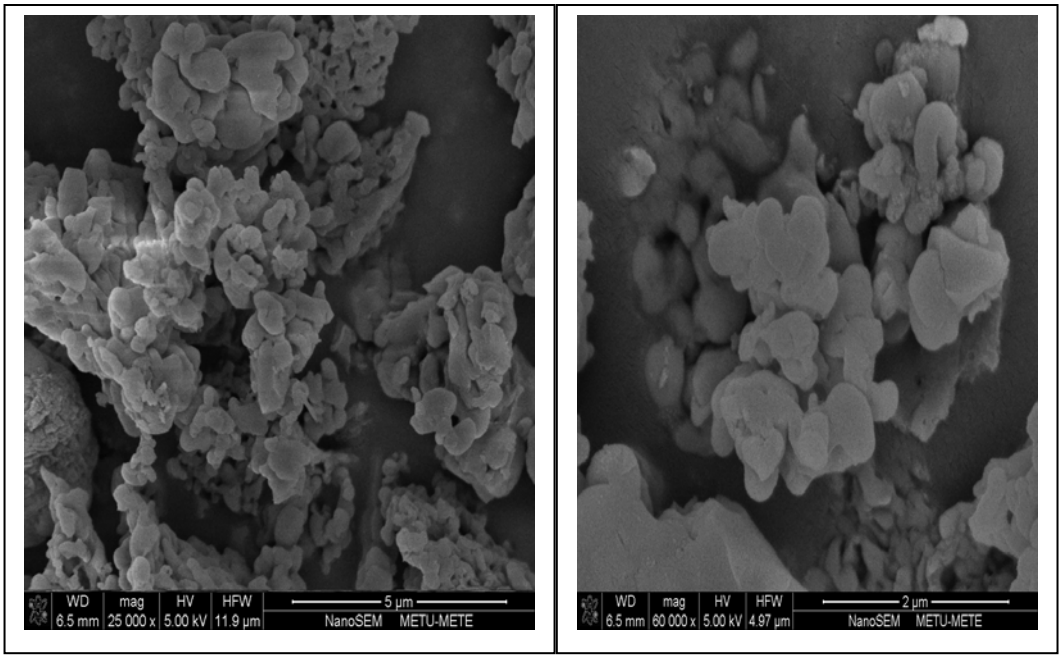

Figure B3: SEM image of Co-MCM-41 (1) **Figure B4:** SEM image of Co-MCM-41

APPENDIX C

C1. RAW SRE REACTION DATA

Table C1: Raw SRE data over Co-MCM-41 at 500^{o}C

SRE Reaction 1 **Catalyst: Co-MCM-41** **Temperature: 500^{o}C**		
RUN 1 (t=20 min)		
Element	**Area**	**Mole**
H_2	17460.9	6111.3
CO	190.3	837.32
CH_4	322.5	296.7
CO_2	223.9	738.87
C_2H_4	2413.6	2968.7
CH_2O	857.2	3257.4
C_2H_4O	0	0
C_2H_5OH	0	0
RUN 2 (t=40 min)		
H_2	17795.7	6228.5
CO	106.4	468.2
CH_4	216.5	199.2
CO_2	275	907.5
C_2H_4	2339	2877
CH_2O	965.8	3670
C_2H_4O	0	0
C_2H_5OH	0	0
RUN 3 (t=60 min)		
H_2	17733.6	6206.8
CO	95.2	418.9
CH_4	213.6	196.5
CO_2	353.4	1166.2
C_2H_4	1788.2	2199.5
CH_2O	957.1	3637
C_2H_4O	0	0
C_2H_5OH	0	0
RUN 4 (t=80 min)		
H_2	17876.6	6256.8
CO	71.1	312.8
CH_4	188.1	173.1
CO_2	342.2	1129.3
C_2H_4	1760.6	2165.5

Table C1 continued

CH_2O	948.2	3603.2
C_2H_4O	0	0
C_2H_5OH	0	0
RUN 5 (t=100 min)		
H_2	19379.4	6782.8
CO	72	316.8
CH_4	177.4	163.2
CO_2	324.7	1071.5
C_2H_4	2464.1	3030.8
CH_2O	1212.1	4606
C_2H_4O	0	0
C_2H_5OH	0	0
RUN 6 (t=120 min)		
H_2	19203.4	6721.2
CO	67.1	295.2
CH_4	169.2	155.7
CO_2	357.2	1178.8
C_2H_4	1936.9	2382.4
CH_2O	1120.1	4256.4
C_2H_4O	0	0
C_2H_5OH	0	0
RUN 7 (t=140 min)		
H_2	20554.2	7194
CO	77.5	341
CH_4	188	173
CO_2	407.8	1345.7
C_2H_4	2182.3	2684.2
CH_2O	1144.4	4348.7
C_2H_4O	0	0
C_2H_5OH	0	0
RUN 8 (t=160 min)		
H_2	19030.9	6660.8
CO	55	242
CH_4	166.6	153.3
CO_2	379.7	1253
C_2H_4	1672.7	2057.4
CH_2O	1128.7	4289.1
C_2H_4O	0	0
C_2H_5OH	0	0
RUN 9 (t=180 min)		
H_2	20702.2	7245.8
CO	59.8	263.1
CH_4	185.2	170.4
CO_2	419.3	1383.7

Table C1 continued

C_2H_4	1977.3	2432.1
CH_2O	1037.3	3941.7
C_2H_4O	0	0
C_2H_5OH	0	0

Table C2: Raw SRE data over Co-MCM-41 at 550^oC

SRE Reaction 2 Catalyst: Co-MCM-41 Temperature: 550^oC		
RUN 1 (t=20 min)		
Element	**Area**	**Mole**
H_2	22075.6	7726.5
CO	191	840.4
CH_4	430.9	396.4
CO_2	395	1303.5
C_2H_4	1507.1	1853.7
CH_2O	651.5	2475.7
C_2H_4O	0	0
C_2H_5OH	0	0
RUN 2 (t=40 min)		
H_2	26892.2	9412.3
CO	177.6	781.4
CH_4	411.4	378.5
CO_2	532.2	1756.3
C_2H_4	1670.3	2054.5
CH_2O	809	3074.2
C_2H_4O	0	0
C_2H_5OH	0	0
RUN 3 (t=60 min)		
H_2	23677.3	8287.1
CO	153.7	676.3
CH_4	396.6	364.9
CO_2	486.1	1604.1
C_2H_4	1497.5	1841.9
CH_2O	765.3	2908.1
C_2H_4O	0	0
C_2H_5OH	0	0
RUN 4 (t=80 min)		
H_2	24520.2	8582.1
CO	131.2	577.3
CH_4	350.3	322.3
CO_2	503.8	1662.5

Table C2 continued

C_2H_4	1488.5	1830.9
CH_2O	947.8	3601.6
C_2H_4O	0	0
C_2H_5OH	0	0
RUN 5 (t=100 min)		
H_2	28108.1	9837.8
CO	133.4	587
CH_4	366.4	337.1
CO_2	618.1	2039.7
C_2H_4	1441.1	1772.6
CH_2O	781.9	2971.2
C_2H_4O	0	0
C_2H_5OH	0	0
RUN 6 (t=120 min)		
H_2	28129.7	9845.4
CO	134	589.6
CH_4	361.2	332.3
CO_2	639	2108.7
C_2H_4	1552.2	1909.2
CH_2O	820.7	3118.7
C_2H_4O	0	0
C_2H_5OH	0	0
RUN 7 (t=140 min)		
H_2	28468.8	9964.1
CO	135.8	597.5
CH_4	374.4	344.4
CO_2	652.4	2152.9
C_2H_4	1462.6	1799
CH_2O	652	2477.6
C_2H_4O	0	0
C_2H_5OH	0	0
RUN 8 (t=160 min)		
H_2	27799.6	9729.9
CO	119.8	527.1
CH_4	345.5	317.9
CO_2	633.3	2089.9
C_2H_4	1228.7	1511.3
CH_2O	614.1	2333.6
C_2H_4O	0	0
C_2H_5OH	0	0
RUN 9 (t=180 min)		
H_2	29488.1	10320.8
CO	126.5	556.6
CH_4	306.9	282.3

Table C2 continued

CO_2	681.8	2250
C_2H_4	1367.9	1682.5
CH_2O	851.8	3236.8
C_2H_4O	0	0
C_2H_5OH	0	0
RUN 10 (t=200 min)		
H_2	29619.5	10366.8
CO	128.9	567.2
CH_4	322.8	297.9
CO_2	686.2	2264.5
C_2H_4	1232.6	1516.1
CH_2O	741	2815.8
C_2H_4O	0	0
C_2H_5OH	0	0

Table C3: Raw SRE data over Co-MCM-41 at 600^oC

SRE Reaction 3 Catalyst: Co-MCM-41 Temperature: 600^oC		
RUN 1 (t=20 min)		
Element	**Area**	**Mole**
H_2	25229.2	8830.2
CO	522.6	2299.4
CH_4	841.9	774.5
CO_2	286.3	944.8
C_2H_4	1067	1312.4
CH_2O	995.8	3784
C_2H_4O	0	0
C_2H_5OH	0	0
RUN 2 (t=40 min)		
H_2	27520.3	9632.1
CO	465.3	2047.3
CH_4	690.2	635
CO_2	349.8	1154.3
C_2H_4	1326.5	1631.6
CH_2O	1322	5023.6
C_2H_4O	0	0
C_2H_5OH	0	0
RUN 3 (t=60 min)		
H_2	28726.5	10054.3
CO	434.4	1911.4
CH_4	587.3	540.3
CO_2	540.6	1784
C_2H_4	938.6	1154.5

Table C3 continued

CH_2O	1146.5	4356.7
C_2H_4O	0	0
C_2H_5OH	0	0
RUN 4 (t=80 min)		
H_2	20529.7	7185.4
CO	388.9	1711.2
CH_4	562.5	517.5
CO_2	245.4	809.8
C_2H_4	892	1097.2
CH_2O	994.6	3778.5
C_2H_4O	0	0
C_2H_5OH	0	0
RUN 5 (t=100 min)		
H_2	28346.1	9921.1
CO	365.2	1606.9
CH_4	514.4	473.2
CO_2	513.4	1694.2
C_2H_4	873.4	1074.3
CH_2O	996.9	3788.2
C_2H_4O	0	0
C_2H_5OH	0	0
RUN 6 (t=120 min)		
H_2	29075.6	10176.5
CO	330.7	1455.1
CH_4	511.2	470.3
CO_2	517	1706.1
C_2H_4	1001.9	1232.3
CH_2O	1134.6	4311.5
C_2H_4O	0	0
C_2H_5OH	0	0
RUN 7 (t=140 min)		
H_2	28471.6	9965.1
CO	313.1	1377.6
CH_4	480.2	441.8
CO_2	508.2	1677.1
C_2H_4	1068.1	1313.8
CH_2O	1212.2	4606.4
C_2H_4O	0	0
C_2H_5OH	0	0
RUN 8 (t=160 min)		
H_2	28522.5	9982.9
CO	304.9	1341.6
CH_4	463.8	426.7
CO_2	530.5	1750.7

Table C3 continued

C_2H_4	1009.3	1241.4
CH_2O	1127.9	4286
C_2H_4O	0	0
C_2H_5OH	0	0
RUN 9 (t=180 min)		
H_2	29225.9	10229.1
CO	314.9	1385.6
CH_4	463.1	426.1
CO_2	604.6	1995.2
C_2H_4	927.5	1140.8
CH_2O	1135.8	4316
C_2H_4O	0	0
C_2H_5OH	0	0
RUN 10 (t=200 min)		
H_2	28467.8	9963.7
CO	279.1	1228
CH_4	456.3	419.8
CO_2	536.9	1771.8
C_2H_4	954.2	1173.7
CH_2O	1188.1	4514.8
C_2H_4O	0	0
C_2H_5OH	0	0
RUN 11 (t=220 min)		
H_2	29794.7	10428.1
CO	297.9	1310.8
CH_4	457.2	420.6
CO_2	635.6	2097.5
C_2H_4	921.4	1133.3
CH_2O	1175.3	4466.1
C_2H_4O	0	0
C_2H_5OH	0	0

Table C4: Raw SRE data over Ni-MCM-41 at 500^oC

SRE Reaction 4 Catalyst: Ni-MCM-41 Temperature: 500^oC		
RUN 1 (t=20 min)		
Element	**Area**	**Mole**
H_2	24865.5	8702.9
CO	73.6	323.8
CH_4	2644.6	2433
CO_2	819.4	2704
C_2H_4	0	0

Table C4 continued

CH_2O	0	0
C_2H_4O	0	0
C_2H_5OH	120.5	120.5
RUN 2 (t=40 min)		
H_2	25920.9	9072.3
CO	94	413.6
CH_4	2901.1	2669
CO_2	878.9	2900.4
C_2H_4	0	0
CH_2O	0	0
C_2H_4O	0	0
C_2H_5OH	63.2	63.2
RUN 3 (t=60 min)		
H_2	25863.6	9052.3
CO	86.6	381
CH_4	3182.6	2928
CO_2	902.9	2979.6
C_2H_4	0	0
CH_2O	0	0
C_2H_4O	0	0
C_2H_5OH	13.7	13.7
RUN 4 (t=80 min)		
H_2	26745.9	9361.1
CO	86.1	378.8
CH_4	3439	3163.9
CO_2	943.5	3113.6
C_2H_4	0	0
CH_2O	0	0
C_2H_4O	0	0
C_2H_5OH	15.1	15.1
RUN 5 (t=100 min)		
H_2	27447.4	9606.6
CO	78.5	345.4
CH_4	3267.5	3006.1
CO_2	972.4	3208.9
C_2H_4	0	0
CH_2O	0	0
C_2H_4O	0	0
C_2H_5OH	4.2	4.2
RUN 7 (t=140 min)		
H_2	27084.3	9479.5
CO	70.6	310.6
CH_4	3119.8	2870.2
CO_2	965.4	3185.8

Table C4 continued

C_2H_4	0	0
CH_2O	0	0
C_2H_4O	0	0
C_2H_5OH	0	0
RUN 8 (t=160 min)		
H_2	28300.6	9905.2
CO	66.6	293
CH_4	2999	2759.1
CO_2	1041.6	3437.3
C_2H_4	0	0
CH_2O	0	0
C_2H_4O	0	0
C_2H_5OH	0	0
RUN 9 (t=180 min)		
H_2	27332.5	9566.4
CO	60.8	267.5
CH_4	2993.8	2754.3
CO_2	1008.5	3328.1
C_2H_4	0	0
CH_2O	0	0
C_2H_4O	0	0
C_2H_5OH	0	0

Table C5: Raw SRE data over Ni-MCM-41 at 550^oC

SRE Reaction 5 Catalyst: Ni-MCM-41 Temperature: 550^oC		
RUN 1 (t=20 min)		
Element	**Area**	**Mole**
H_2	31602.5	11060.9
CO	163.8	720.7
CH_4	2197.2	2021.4
CO_2	874.1	2884.5
C_2H_4	0	0
CH_2O	0	0
C_2H_4O	0	0
C_2H_5OH	0	0
RUN 2 (t=40 min)		
H_2	30390.6	10636.7
CO	151.6	667
CH_4	2258	2077.4
CO_2	846.7	2794.1
C_2H_4	0	0

Table C5 continued

CH_2O	0	0
C_2H_4O	0	0
C_2H_5OH	0	0
RUN 3 (t=60 min)		
H_2	31039.5	10863.8
CO	154	677.6
CH_4	2234.3	2055.6
CO_2	893.7	2949.2
C_2H_4	0	0
CH_2O	0	0
C_2H_4O	0	0
C_2H_5OH	0	0
RUN 4 (t=80 min)		
H_2	32871.5	11505
CO	169.6	746.2
CH_4	2371	2181.3
CO_2	933.7	3081.2
C_2H_4	0	0
CH_2O	0	0
C_2H_4O	0	0
C_2H_5OH	0	0
RUN 5 (t=100 min)		
H_2	31857.7	11150.2
CO	143.7	632.3
CH_4	2072.7	1906.9
CO_2	906.7	2992.1
C_2H_4	0	0
CH_2O	0	0
C_2H_4O	0	0
C_2H_5OH	0	0
RUN 6 (t=120 min)		
H_2	31287.6	10950.7
CO	142.3	626.1
CH_4	2094.6	1927
CO_2	878.1	2897.7
C_2H_4	0	0
CH_2O	0	0
C_2H_4O	0	0
C_2H_5OH	0	0
RUN 8 (t=160 min)		
H_2	32822.6	11487.9
CO	149.9	659.6
CH_4	2185	2010.2
CO_2	983.8	3246.5

Table C5 continued

C_2H_4	0	0
CH_2O	0	0
C_2H_4O	0	0
C_2H_5OH	0	0
RUN 10 (t=200 min)		
H_2	31667.5	11083.6
CO	139.7	614.7
CH_4	1958.5	1801.8
CO_2	943.2	3112.6
C_2H_4	0	0
CH_2O	0	0
C_2H_4O	0	0
C_2H_5OH	0	0

Table C6: Raw SRE data over Ni-MCM-41 at 600^oC

SRE Reaction 6 Catalyst: Ni-MCM-41 Temperature: 600^oC		
RUN 1 (t=20 min)		
Element	**Area**	**Mole**
H_2	31807.6	11132.7
CO	281.1	1236.8
CH_4	976.9	898.7
CO_2	774.5	2555.9
C_2H_4	0	0
CH_2O	0	0
C_2H_4O	0	0
C_2H_5OH	0	0
RUN 2 (t=40 min)		
H_2	33684.9	11789.7
CO	295.3	1299.3
CH_4	1175.7	1081.6
CO_2	833.5	2750.6
C_2H_4	0	0
CH_2O	0	0
C_2H_4O	0	0
C_2H_5OH	0	0
RUN 4 (t=80 min)		
H_2	35746.6	12511.3
CO	299.9	1319.6
CH_4	1153.2	1060.9
CO_2	981.3	3238.3
C_2H_4	0	0

Table C6 continued

CH_2O	0	0
C_2H_4O	0	0
C_2H_5OH	0	0
RUN 5 (t=100 min)		
H_2	36187.6	12665.7
CO	273.9	1205.2
CH_4	1084.6	997.8
CO_2	1026.9	3388.8
C_2H_4	0	0
CH_2O	0	0
C_2H_4O	0	0
C_2H_5OH	0	0
RUN 6 (t=120 min)		
H_2	34418.4	12046.4
CO	269.4	1185.4
CH_4	1112.4	1023.4
CO_2	964.1	3181.5
C_2H_4	0	0
CH_2O	0	0
C_2H_4O	0	0
C_2H_5OH	0	0
RUN 8 (t=160 min)		
H_2	35031.5	12261
CO	298.7	1314.3
CH_4	1218.4	1120.9
CO_2	901.1	2973.6
C_2H_4	0	0
CH_2O	0	0
C_2H_4O	0	0
C_2H_5OH	0	0
RUN 10 (t=200 min)		
H_2	35384	12384.4
CO	295	1298
CH_4	1192.8	1097.4
CO_2	951.7	3140.6
C_2H_4	0	0
CH_2O	0	0
C_2H_4O	0	0
C_2H_5OH	0	0

APPENDIX C2. RAW SESRE REACTION DATA

Table C7: Raw SESRE data over Co-MCM-41 at 500^{o}C

SESRE Reaction 1 Catalyst: Co-MCM-41+CaO Temperature: 500^{o}C		
RUN 1 (t=20 min)		
Element	**Area**	**Mole**
H_2	3970.4	1389.6
CO	0	0
CH_4	215.5	198.3
CO_2	0	0
C_2H_4	146.8	180.5
CH_2O	0	0
C_2H_4O	0	0
C_2H_5OH	0	0
RUN 2 (t=40 min)		
H_2	25661.4	8981.5
CO	0	0
CH_4	947.3	871.5
CO_2	0	0
C_2H_4	1341.7	1650.3
CH_2O	0	0
C_2H_4O	0	0
C_2H_5OH	0	0
RUN 3 (t=60 min)		
H_2	24290.8	8501.8
CO	0	0
CH_4	834.1	767.4
CO_2	0	0
C_2H_4	1246.8	1533.6
CH_2O	0	0
C_2H_4O	0	0
C_2H_5OH	0	0
RUN 4 (t=80 min)		
H_2	22562.6	7896.9
CO	0	0
CH_4	653.4	601.1
CO_2	0	0
C_2H_4	1161.9	1429.1
CH_2O	0	0
C_2H_4O	0	0
C_2H_5OH	0	0

Table C7 continued

RUN 5 (t=100 min)		
H_2	25192	8817.2
CO	0	0
CH_4	593.2	545.7
CO_2	0	0
C_2H_4	1383.5	1701.7
CH_2O	297.2	1129.4
C_2H_4O	0	0
C_2H_5OH	0	0
RUN 6 (t=120 min)		
H_2	21207.2	7422.5
CO	0	0
CH_4	445.8	410.1
CO_2	0	0
C_2H_4	1182.6	1454.6
CH_2O	329.1	1250.6
C_2H_4O	0	0
C_2H_5OH	0	0
RUN 7 (t=140 min)		
H_2	20141.9	7049.7
CO	0	0
CH_4	369.9	337.5
CO_2	90.1	297.3
C_2H_4	1080.4	1328.9
CH_2O	358	1360.4
C_2H_4O	0	0
C_2H_5OH	0	0
RUN 8 (t=160 min)		
H_2	19328.5	6765
CO	0	0
CH_4	290.2	267
CO_2	131.5	433.9
C_2H_4	1096.9	1349.2
CH_2O	431.1	1638.2
C_2H_4O	0	0
C_2H_5OH	0	0
RUN 9 (t=180 min)		
H_2	16573.6	5800.8
CO	5.8	25.5
CH_4	168.7	155.2
CO_2	192.4	634.9
C_2H_4	986.9	1213.9
CH_2O	538.4	2045.9
C_2H_4O	0	0

Table C7 continued

C_2H_5OH	0	0
RUN 10 (t=200 min)		
H_2	16004.6	5601.6
CO	5.2	22.9
CH_4	155.6	143.2
CO_2	229.9	758.7
C_2H_4	857.8	1055.1
CH_2O	572.1	2174
C_2H_4O	0	0
C_2H_5OH	0	0

Table C8: Raw SESRE data over Co-MCM-41 at 550^oC

SESRE Reaction 2 Catalyst: Co-MCM-41+CaO Temperature: 550^oC		
RUN 1 (t=20 min)		
Element	**Area**	**Mole**
H_2	25017.3	8756.1
CO	10.9	48
CH_4	1424.8	1310.8
CO_2	11.4	37.6
C_2H_4	389.9	479.6
CH_2O	0	0
C_2H_4O	46.2	77.6
C_2H_5OH	0	0
RUN 2 (t=40 min)		
H_2	24958.3	8735.4
CO	12.8	56.3
CH_4	1055.8	971.3
CO_2	12.1	39.9
C_2H_4	347.9	427.9
CH_2O	0	0
C_2H_4O	32.7	54.9
C_2H_5OH	0	0
RUN 3 (t=60 min)		
H_2	27203	9521.1
CO	14.3	62.9
CH_4	1019.2	937.7
CO_2	12.6	41.6
C_2H_4	459.8	565.6
CH_2O	0	0
C_2H_4O	27.4	46.3
C_2H_5OH	0	0

Table C8 continued

RUN 4 (t=80 min)		
H_2	27202.9	9521
CO	19.1	84
CH_4	968.5	891
CO_2	14	46.2
C_2H_4	385.8	474.5
CH_2O	0	0
C_2H_4O	16.8	28.2
C_2H_5OH	0	0
RUN 5 (t=100 min)		
H_2	25839.7	9043.9
CO	23.6	103.8
CH_4	871.1	801.4
CO_2	14.2	46.9
C_2H_4	385.7	474.4
CH_2O	0	0
C_2H_4O	16.2	27.2
C_2H_5OH	0	0
RUN 6 (t=120 min)		
H_2	25916.4	9070.7
CO	29.2	128.5
CH_4	830.4	764
CO_2	14.8	48.8
C_2H_4	415.6	511.2
CH_2O	0	0
C_2H_4O	17.7	29.7
C_2H_5OH	0	0
RUN 7 (t=140 min)		
H_2	25889	9061.2
CO	35.8	157.5
CH_4	732.8	674.2
CO_2	17.4	57.4
C_2H_4	394.2	484.9
CH_2O	0	0
C_2H_4O	16.7	28.1
C_2H_5OH	0	0
RUN 8 (t=160 min)		
H_2	27191.5	9517
CO	43.9	193.2
CH_4	788.8	725.7
CO_2	152	501.6
C_2H_4	456.1	561
CH_2O	45.3	172.1
C_2H_4O	0	0

Table C8 continued

C_2H_5OH	0	0
RUN 9 (t=180 min)		
H_2	25404.6	8891.6
CO	44.5	195.8
CH_4	612.9	563.9
CO_2	482.9	1593.6
C_2H_4	406.9	500.5
CH_2O	138.3	525.5
C_2H_4O	0	0
C_2H_5OH	0	0
RUN 10 (t=200 min)		
H_2	25352.5	8873.4
CO	55.2	242.9
CH_4	622.1	572.3
CO_2	546.6	1803.8
C_2H_4	464.3	571.1
CH_2O	167.1	635
C_2H_4O	0	0
C_2H_5OH	0	0

Table C9: Raw SESRE data over Co-MCM-41 at 600^oC

SESRE Reaction 3 Catalyst: Co-MCM-41+CaO Temperature: 600^oC		
RUN 1 (t=20 min)		
Element	**Area**	**Mole**
H_2	37008.7	12953.1
CO	22.9	100.8
CH_4	2791.4	2568.1
CO_2	203.4	671.2
C_2H_4	990.6	1218.4
CH_2O	0	0
C_2H_4O	0	0
C_2H_5OH	0	0
RUN 2 (t=40 min)		
H_2	33602.6	11760.9
CO	29.5	129.8
CH_4	2227.8	2049.6
CO_2	307.1	1013.4
C_2H_4	769.4	946.4
CH_2O	0	0
C_2H_4O	0	0
C_2H_5OH	0	0
RUN 4 (t=80 min)		

Table C9 continued

H_2	33317.4	11661.1
CO	57.8	254.3
CH_4	1527.3	1405.1
CO_2	579.7	1913
C_2H_4	741.8	912.4
CH_2O	121.8	462.8
C_2H_4O	0	0
C_2H_5OH	0	0
RUN 6 (t=120 min)		
H_2	33856.9	11849.9
CO	71.6	315
CH_4	1310.4	1205.6
CO_2	756.8	2497.4
C_2H_4	756.8	930.9
CH_2O	187.2	711.4
C_2H_4O	0	0
C_2H_5OH	0	0
RUN 8 (t=160 min)		
H_2	33490.6	11721.7
CO	86.8	381.9
CH_4	1199.3	1103.4
CO_2	858.7	2833.7
C_2H_4	768.7	945.5
CH_2O	227.6	864.9
C_2H_4O	0	0
C_2H_5OH	0	0
RUN 10 (t=200 min)		
H_2	27405.6	9592
CO	73.6	323.8
CH_4	986.4	907.5
CO_2	762.3	2515.6
C_2H_4	668.5	822.3
CH_2O	209.1	794.6
C_2H_4O	0	0
C_2H_5OH	0	0
RUN 11 (t=220 min)		
H_2	32460.7	11361.3
CO	86.9	382.4
CH_4	1026.3	944.2
CO_2	872.6	2879.6
C_2H_4	720.8	886.6
CH_2O	270.9	1029.4
C_2H_4O	0	0
C_2H_5OH	0	0

Table C10: Raw SESRE data over Ni-MCM-41 at 500^{o}C

SESRE Reaction 4 Catalyst: Ni-MCM-41+CaO Temperature: 500^{o}C		
RUN 1 (t=20 min)		
Element	**Area**	**Mole**
H_2	39779.1	13922.7
CO	0	0
CH_4	1527.5	1405.3
CO_2	0	0
C_2H_4	0	0
CH_2O	0	0
C_2H_4O	0	0
C_2H_5OH	0	0
RUN 2 (t=40 min)		
H_2	39140.1	13699
CO	0	0
CH_4	1644.3	1512.8
CO_2	0	0
C_2H_4	0	0
CH_2O	0	0
C_2H_4O	0	0
C_2H_5OH	0	0
RUN 3 (t=60 min)		
H_2	39240.8	13734.3
CO	0	0
CH_4	2160.5	1987.7
CO_2	0	0
C_2H_4	0	0
CH_2O	0	0
C_2H_4O	0	0
C_2H_5OH	0	0
RUN 4 (t=80 min)		
H_2	35960.4	12586.1
CO	7.6	33.4
CH_4	2383.8	2193.1
CO_2	109.9	362.7
C_2H_4	0	0
CH_2O	0	0
C_2H_4O	0	0
C_2H_5OH	0	0
RUN 5 (t=100 min)		
H_2	32985.4	11544.9
CO	22.3	98.1
CH_4	2656	2443.5

Table C10 continued

CO_2	368	1214.4
C_2H_4	0	0
CH_2O	0	0
C_2H_4O	0	0
C_2H_5OH	0	0
RUN 7 (t=140 min)		
H_2	30204.4	10571.5
CO	82.5	363
CH_4	2765.2	2544
CO_2	899	2963.4
C_2H_4	0	0
CH_2O	0	0
C_2H_4O	0	0
C_2H_5OH	0	0
RUN 8 (t=160 min)		
H_2	29245.4	10235.9
CO	75.2	330.9
CH_4	2457.1	2260.5
CO_2	893.4	2948.2
C_2H_4	0	0
CH_2O	0	0
C_2H_4O	0	0
C_2H_5OH	0	0
RUN 9 (t=180 min)		
H_2	29984.7	10494.7
CO	81.5	358.6
CH_4	2401.5	2209.4
CO_2	940.6	3104
C_2H_4	0	0
CH_2O	0	0
C_2H_4O	0	0
C_2H_5OH	0	0

Table C11: Raw SESRE data over Ni-MCM-41 at 550^oC

SESRE Reaction 5 **Catalyst: Ni-MCM-41+CaO** **Temperature: 550^{o}C**		
RUN 1 (t=20 min)		
Element	**Area**	**Mole**
H_2	37657	13180
CO	0	0
CH_4	1974.7	1816.7
CO_2	0	0

Table C11 continued

C_2H_4	0	0
CH_2O	0	0
C_2H_4O	0	0
C_2H_5OH	0	0
RUN 2 (t=40 min)		
H_2	41786.9	14625.4
CO	0	0
CH_4	2080.7	1914.2
CO_2	0	0
C_2H_4	0	0
CH_2O	0	0
C_2H_4O	0	0
C_2H_5OH	0	0
RUN 3 (t=60 min)		
H_2	40112.8	14039.5
CO	8.4	37
CH_4	2314.4	2129.2
CO_2	0	0
C_2H_4	0	0
CH_2O	0	0
C_2H_4O	0	0
C_2H_5OH	0	0
RUN 4 (t=80 min)		
H_2	35428.5	12400
CO	24.9	109.6
CH_4	2162.1	1989.1
CO_2	0	0
C_2H_4	0	0
CH_2O	0	0
C_2H_4O	0	0
C_2H_5OH	0	0
RUN 5 (t=100 min)		
H_2	35277.3	12347.1
CO	66.4	292.2
CH_4	2121.8	1952.1
CO_2	6.6	21.8
C_2H_4	0	0
CH_2O	0	0
C_2H_4O	0	0
C_2H_5OH	0	0
RUN 6 (t=120 min)		
H_2	34809.3	12183.3
CO	129.8	571.1
CH_4	2340.9	2153.6

Table C11 continued

CO_2	7.4	24.4
C_2H_4	0	0
CH_2O	0	0
C_2H_4O	0	0
C_2H_5OH	0	0
RUN 7 (t=140 min)		
H_2	31860.4	11151.1
CO	186.1	818.8
CH_4	2056.1	1891.6
CO_2	173	570.9
C_2H_4	0	0
CH_2O	0	0
C_2H_4O	0	0
C_2H_5OH	0	0
RUN 8 (t=160 min)		
H_2	30755.2	10764.3
CO	292.9	1288.8
CH_4	2407.1	2214.5
CO_2	392.2	1294.3
C_2H_4	0	0
CH_2O	0	0
C_2H_4O	0	0
C_2H_5OH	0	0
RUN 9 (t=180 min)		
H_2	31257.9	10940.3
CO	318	1399.2
CH_4	2391	2199.7
CO_2	533.5	1760.6
C_2H_4	0	0
CH_2O	0	0
C_2H_4O	0	0
C_2H_5OH	0	0
RUN 10 (t=200 min)		
H_2	32512.2	11379.3
CO	326.4	1436.2
CH_4	2368.5	2179
CO_2	630.9	2082
C_2H_4	0	0
CH_2O	0	0
C_2H_4O	0	0
C_2H_5OH	0	0

Table C12: Raw SESRE data over Ni-MCM-41 at 600^{o}C

SESRE Reaction 6 Catalyst: Ni-MCM-41+CaO Temperature: 600^{o}C		
RUN 1 (t=20 min)		
Element	**Area**	**Mole**
H_2	44777.2	15672
CO	0	0
CH_4	2013.4	1852.3
CO_2	0	0
C_2H_4	0	0
CH_2O	0	0
C_2H_4O	0	0
C_2H_5OH	0	0
RUN 2 (t=40 min)		
H_2	41779.1	14622.7
CO	0	0
CH_4	1874.8	1724.8
CO_2	0	0
C_2H_4	0	0
CH_2O	0	0
C_2H_4O	0	0
C_2H_5OH	0	0
RUN 3 (t=60 min)		
H_2	38629.1	13520.2
CO	31.9	140.4
CH_4	1691.5	1556.2
CO_2	8.1	26.7
C_2H_4	0	0
CH_2O	0	0
C_2H_4O	0	0
C_2H_5OH	0	0
RUN 4 (t=80 min)		
H_2	38305.4	13406.9
CO	87.3	384.1
CH_4	1709.4	1572.6
CO_2	55.5	183.2
C_2H_4	0	0
CH_2O	0	0
C_2H_4O	0	0
C_2H_5OH	0	0
RUN 5 (t=100 min)		
H_2	35440.6	12404.2
CO	209.2	920.5
CH_4	1641.6	1510.3

Table C12 continued

CO_2	204.9	676.2
C_2H_4	0	0
CH_2O	0	0
C_2H_4O	0	0
C_2H_5OH	0	0
RUN 6 (t=120 min)		
H_2	33821.6	11837.6
CO	359.7	1582.7
CH_4	1588.3	1461.2
CO_2	527.8	1741.7
C_2H_4	0	0
CH_2O	0	0
C_2H_4O	0	0
C_2H_5OH	0	0
RUN 7 (t=140 min)		
H_2	31798.4	11129.4
CO	350	1540
CH_4	1572.9	1447.1
CO_2	605.5	1998.2
C_2H_4	0	0
CH_2O	0	0
C_2H_4O	0	0
C_2H_5OH	0	0
RUN 8 (t=160 min)		
H_2	31351.8	10973.1
CO	344.8	1517.1
CH_4	1475.7	1357.6
CO_2	639.8	2111.3
C_2H_4	0	0
CH_2O	0	0
C_2H_4O	0	0
C_2H_5OH	0	0
RUN 9 (t=180 min)		
H_2	32250.5	11287.7
CO	348.8	1534.7
CH_4	1623.1	1493.3
CO_2	685.9	2263.5
C_2H_4	0	0
CH_2O	0	0
C_2H_4O	0	0
C_2H_5OH	0	0
RUN 10 (t=200 min)		
H_2	33277	11647
CO	403.4	1775

Table C12 continued

CH_4	1776.3	1634.2
CO_2	714.8	2358.8
C_2H_4	0	0
CH_2O	0	0
C_2H_4O	0	0
C_2H_5OH	0	0

APPENDIX D

D.1. CALIBRATION FACTORS (β) FOR ELEMENTS

Calibration factor of ethanol ($\beta_{C_2H_5OH}$) is taken as 1. Calibration factors of other elements are calculated by using Equation D1.

$$\frac{n_A}{n_{C_2H_5OH}} = \frac{Area_A \times \beta_A}{Area_{C_2H_5OH} \times \beta_{C_2H_5OH}} \quad \text{(D1)}$$

Calculated calibration factors for the elements are tabulated in Table D1.

Table D1: Calculated calibration factors

Element	Location of peak	Calibration factor β
H_2	1.03	0.35
CO	1.27	4.4
CH_4	1.77	0.92
CO_2	3.9-4.0	3.3
C_2H_4	5.1-5.2	1.23
H_2O	8.2-8.3	0.96
CH_2O	8.7-8.8	3.8
C_2H_4O	10.37	1.68
C_2H_5OH	12.2	1.0

APPENDIX E

E1. SAMPLE CALCULATION FOR SRE REACTION

Raw data of vapor product obtained from gas chromatograph (GC) during steam reforming of ethanol (SRE) reaction with Co-MCM-41 catalyst at 600^{o}C taken at 40th minutes is given in Table E1. Liquid product obtained from condenser was analyzed after the reaction and the raw data is given in Table E3.

Table E1: Raw data of reactor exit vapor stream in SRE reaction with Co-MCM-41 at 600^{o}C at 40th minutes

Element	Area	Location
H_2	27520.3	1.03
CO	465.3	1.27
CH_4	690.2	1.77
CO_2	349.8	3.91
C_2H_4	1326.5	5.12
CH_2O	1322	8.73
C_2H_4O	0	10.38
C_2H_5OH	0	12.20

Moles of product species are calculated by Equation E1 given below.

$$Mole\ of\ \ A = (Area_A) \times \beta_A \qquad \text{(E1)}$$

$Mole\ of\ H_2\ (n_{H_2(out)}) = 27520.3 \times 0.35 = 9632.1\ moles$

$Mole\ of\ CO\ (n_{CO(out)}) = 465.3 \times 4.4 = 2047.3\ moles$

$Mole\ of\ CH_4\ (n_{CH_4(out)}) = 690.2 \times 0.92 = 635\ moles$

$Mole\ of\ CO_2\ (n_{CO_2(out)}) = 349.8 \times 3.3 = 1154.3\ moles$

$Mole\ of\ C_2H_4\ (n_{C_2H_4(out)}) = 1326.5 \times 1.23 = 1631.6\ moles$

$Mole\ of\ CH_2O\ (n_{CH_2O(out)}) = 1322 \times 3.8 = 5023.6\ moles$

$Mole\ of\ C_2H_4O\ (n_{C_2H_4O(out)}) = 0 \times 1.68 = 0\ moles$

$Mole\ of\ C_2H_5OH\ (n_{C_2H_5OH(out)}) = 0 \times 1 = 0\ moles$

Calculated moles of product species for steam reforming of ethanol (SRE) reaction with Co-MCM-41 catalyst at 600°C at 40 minutes is tabulated in Table E2.

Table E2: Calculated moles of species in SRE reaction with Co-MCM-41 at 600°C at 40th minutes

Element	Area	Mole
H_2	27520.3	9632.1
CO	465.3	2047.3
CH_4	690.2	635
CO_2	349.8	1154.3
C_2H_4	1326.5	1631.6
CH_2O	1322	5023.6
C_2H_4O	0	0
C_2H_5OH	0	0

Fraction of species in product gas stream was calculated with Equation E2 given below.

$$x_A = \frac{n_A}{n_{total\ (products)}} \qquad \text{(E2)}$$

$$x_{H_2} = \frac{9632.1}{(9632.1 + 2047.3 + 635 + 1154.3 + 1631.6 + 5023.6)} = 0.48$$

$$x_{CO} = \frac{2047.3}{(9632.1 + 2047.3 + 635 + 1154.3 + 1631.6 + 5023.6)} = 0.10$$

$$x_{CH_4} = \frac{635}{(9632.1 + 2047.3 + 635 + 1154.3 + 1631.6 + 5023.6)} = 0.03$$

$$x_{CO_2} = \frac{1154.3}{(9632.1 + 2047.3 + 635 + 1154.3 + 1631.6 + 5023.6)} = 0.06$$

$$x_{C_2H_4} = \frac{1631.6}{(9632.1 + 2047.3 + 635 + 1154.3 + 1631.6 + 5023.6)} = 0.08$$

$$x_{CH_2O} = \frac{5023.6}{(9632.1 + 2047.3 + 635 + 1154.3 + 1631.6 + 5023.6)} = 0.25$$

Volumetric flow rate of product gas stream was obtained by soap bubble flow meter. Volumetric flow rate of product gas stream at 40th minutes was 46.5 ml/min.

$Q_{out} = 46.5\ ml/\min$

$Q_{Ar} = 30\ ml/\min$

Volumetric flow rates of each species were calculated with Equation E3 given below.

$$Q_A = (Q_{out} - Q_{Ar}) \times x_A \qquad \text{(E3)}$$

$Q_{H_2} = (46.5 - 30) \times 0.48 = 7.92\ ml/\min$

$Q_{CO} = (46.5 - 30) \times 0.10 = 1.65\ ml/\min$

$Q_{CH_4} = (46.5 - 30) \times 0.03 = 0.50\ ml/\min$

$Q_{CO_2} = (46.5 - 30) \times 0.06 = 0.99\ ml/\min$

$Q_{C_2H_4} = (46.5 - 30) \times 0.08 = 1.32\ ml/\min$

$Q_{CH_2O} = (46.5 - 30) \times 0.25 = 4.13\ ml/\min$

Density of species at room temperature (20^{o}C) was calculated with Equation E4 given below.

$$\rho_A = \frac{P_{atm} \times M_A}{R \times T_{room}} \qquad \text{(E4)}$$

$$\rho_{H_2} = \frac{(1\ atm) \times (2\ g/mol)}{(82.05) \times (293\ K)} = 0.0000818\ g/ml$$

$$\rho_{CO} = \frac{(1\ atm) \times (28\ g/mol)}{(82.05) \times (293\ K)} = 0.00115\ g/ml$$

$$\rho_{CH_4} = \frac{(1\ atm) \times (16\ g/mol)}{(82.05) \times (293\ K)} = 0.000654\ g/ml$$

$$\rho_{CO_2} = \frac{(1\ atm) \times (44\ g/mol)}{(82.05) \times (293\ K)} = 0.0018\ g/ml$$

$$\rho_{C_2H_4} = \frac{(1\ atm) \times (28\ g/mol)}{(82.05) \times (293\ K)} = 0.00115\ g/ml$$

$$\rho_{CH_2O} = \frac{(1\ atm) \times (30\ g/mol)}{(82.05) \times (293\ K)} = 0.00123\ g/ml$$

Molar flow rates of each species were calculated with Equation E5 given below.

$$F_A = Q_A \times \frac{\rho_A}{M_A} \qquad \text{(E5)}$$

$$F_{H_2} = 7.92 \times \frac{0.0000818}{2} = 0.000324\ mol/\min$$

$$F_{CO} = 1.65 \times \frac{0.00115}{28} = 0.000068\ mol/\min$$

$$F_{CH_4} = 0.50 \times \frac{0.000654}{16} = 0.00002\ mol/\min$$

$$F_{CO_2} = 0.99 \times \frac{0.0018}{44} = 0.000041\ mol/\min$$

$$F_{C_2H_4} = 1.32 \times \frac{0.00115}{28} = 0.000054\ mol/\min$$

$$F_{CH_2O} = 4.13 \times \frac{0.00123}{30} = 0.00017\ mol/\min$$

Liquid product obtained from condenser at 40th minutes was analyzed in GC and data is given in Table E3.

Table E3: Liquid product in SRE reaction with Co-MCM-41 at 600^{o}C at 40th minutes

Element	Area	Mole
H_2O	174081.7	167118.4
CH_2O	1519.1	5772.6
C_2H_5OH	5634.3	5634.3

Fractions of species in liquid product were calculated as;

$$x_{H_2O_{liquid}} = \frac{167118.4}{(167118.4 + 5772.6 + 5634.3)} = 0.936$$

$$x_{CH_2O_{liquid}} = \frac{5772.6}{(167118.4 + 5772.6 + 5634.3)} = 0.032$$

$$x_{C_2H_5OH_{liquid}} = \frac{5634.3}{(167118.4 + 5772.6 + 5634.3)} = 0.032$$

Weight of liquid obtained from condenser outlet at 40th minutes was 0.52 g. Then mass flow rate of liquid product was calculated as 0.52/40 = 0.013 g/min.

Molar flow rates of liquid products obtained from condenser at 40th minutes were calculated with Equation E6.

$$F_{A_{liquid}} = x_{A_{liquid}} \frac{m^*_{liquid}}{(M_{H_2O} \times x_{H_2O_{liquid}}) + (M_{C_2H_5OH} \times x_{C_2H_5OH_{liquid}}) + (M_{CH_2O} \times x_{CH_2O_{liquid}}) + (M_{C_2H_4O} \times x_{C_2H_4O_{liquid}})} \quad \text{(E6)}$$

$$F_{C_2H_5OH_{liquid}} = 0.032 \times \frac{0.013\ g/\min}{(18 \times 0.936) + (46 \times 0.032) + (30 \times 0.032)} = 0.000021\ mol/\min$$

$$F_{CH_2O_{liquid}} = 0.032 \times \frac{0.013\ g/\min}{(18 \times 0.936) \times (46 \times 0.032) + (30 \times 0.032)} = 0.000021\ mol/\min$$

Carbon balance was done to calculate the molar flow rate of ethanol fed to the reactor ($F^o_{C_2H_5OH}$).

$$F^o_{C_2H_5OH} = \frac{F_{CO}}{2} + \frac{F_{CH_4}}{2} + \frac{F_{CO_2}}{2} + F_{C_2H_4} + \frac{F_{CH_2O}}{2} + F_{C_2H_5OH_{liquid}} + \frac{F_{CH_2O_{liquid}}}{2}$$

$$F^o_{C_2H_5OH} = \frac{0.000068}{2} + \frac{0.00002}{2} + \frac{0.000041}{2} + 0.000054 + \frac{0.00017}{2} + 0.000021 + \frac{0.000021}{2}$$

$$F^o_{C_2H_5OH} = 0.000236 mol/\min$$

Ethanol conversion was calculated with Equation E7 given below.

$$X_{EtOH} = \frac{(F^o_{C_2H_5OH}) - (F_{C_2H_5OH}) - (F_{C_2H_5OH_{liquid}})}{F^o_{C_2H_5OH}} \times 100 \quad \text{(E7)}$$

$$X_{EtOH} = \frac{(0.000236) - (0) - (0.000021)}{0.000236} \times 100 = 91\,\%$$

Hydrogen yield was calculated with Equation E8 given below.

$$Y_{H_2} = \frac{F_{H_2}}{F^{o}_{C_2H_5OH}} \tag{E8}$$

$$Y_{H_2} = \frac{0.000324}{0.000236} = 1.37$$

Selectivity of C-containing products was calculated with Equation E9 given below.

$$S_A = \frac{(\#\,of\ C\ atoms\ in\ product\ A) \times (F_A + F_{A_{liquid}})}{2 \times (F^{o}_{C_2H_5OH} - F_{C_2H_5OH} - F_{C_2H_5OH_{liquid}})} \times 100 \tag{E9}$$

$$S_{CO} = \frac{(1) \times (0.000068)}{(2) \times (0.000236 - 0.000021)} \times 100 = 15.81$$

$$S_{CH_4} = \frac{(1) \times (0.00002)}{(2) \times (0.000236 - 0.000021)} \times 100 = 4.65$$

$$S_{CO_2} = \frac{(1) \times (0.000041)}{(2) \times (0.000236 - 0.000021)} \times 100 = 9.53$$

$$S_{C_2H_4} = \frac{(2) \times (0.000054)}{(2) \times (0.000236 - 0.000021)} \times 100 = 25.12$$

$$S_{CH_2O} = \frac{(1) \times (0.00017 + 0.000021)}{(2) \times (0.000236 - 0.000021)} \times 100 = 44.42$$

APPENDIX E2. SAMPLE CALCULATION FOR SESRE REACTION

Raw data of vapor product obtained from gas chromatograph (GC) during sorption enhanced steam reforming of ethanol (SESRE) reaction with Co-MCM-41 catalyst at 500^{o}C taken at 40th minutes is given in Table E4. Liquid product obtained from condenser was analyzed after the reaction and raw data is given in Table E5.

Table E4: Raw data of reactor exit vapor stream in SESRE reaction with Co-MCM-41 at 500^{o}C at 40th minutes

Element	Area	Mole
H_2	25661.4	8981.5
CO	0	0
CH_4	947.3	871.5
CO_2	0	0
C_2H_4	1341.7	1650.3
CH_2O	0	0
C_2H_4O	0	0
C_2H_5OH	0	0

Fraction of species in product gas stream was calculated with Equation E2.

$$x_{H_2} = \frac{8981.5}{8981.5+0+871.5+0+1650.3+0+0} = 0.78$$
$$x_{CO} = \frac{0}{8981.5+0+871.5+0+1650.3+0+0} = 0$$
$$x_{CH_4} = \frac{871.5}{8981.5+0+871.5+0+1650.3+0+0} = 0.08$$
$$x_{CO_2} = \frac{0}{8981.5+0+871.5+0+1650.3+0+0} = 0$$
$$x_{C_2H_4} = \frac{1650.3}{8981.5+0+871.5+0+1650.3+0+0} = 0.14$$
$$x_{CH_2O} = \frac{0}{8981.5+0+871.5+0+1650.3+0+0} = 0$$
$$x_{C_2H_4O} = \frac{0}{8981.5+0+871.5+0+1650.3+0+0} = 0$$

Volumetric flow rate of product gas stream at 40th minutes was 46.5 ml/min.

$Q_{out} = 46.05\ ml/\min$

$Q_{Ar} = 30\ ml/\min$

Volumetric flow rates of each species were calculated with Equation E3 given below.

$$Q_A = (Q_{out} - Q_{Ar}) \times x_A \qquad \text{(E3)}$$

$Q_{H_2} = (46.05-30)\times 0.78 = 12.52\ ml/\min$
$Q_{CO} = (46.05-30)\times 0 = 0\ ml/\min$
$Q_{CH_4} = (46.05-30)\times 0.08 = 1.28\ ml/\min$
$Q_{CO_2} = (46.05-30)\times 0 = 0\ ml/\min$
$Q_{C_2H_4} = (46.05-30)\times 0.14 = 2.25\ ml/\min$
$Q_{CH_2O} = (46.05-30)\times 0 = 0\ ml/\min$
$Q_{C_2H_4O} = (46.05-30)\times 0 = 0\ ml/\min$

Density of species at room temperature (20^{o}C) was calculated with Equation E4.

$$\rho_{H_2} = \frac{(1\ atm)\times(2\ g/mol)}{(82.05)\times(293\ K)} = 0.0000818\ g/ml$$

$$\rho_{CO} = \frac{(1\ atm)\times(28\ g/mol)}{(82.05)\times(293\ K)} = 0.00115\ g/ml$$

$$\rho_{CH_4} = \frac{(1\ atm)\times(16\ g/mol)}{(82.05)\times(293\ K)} = 0.000654\ g/ml$$

$$\rho_{CO_2} = \frac{(1\ atm)\times(44\ g/mol)}{(82.05)\times(293\ K)} = 0.0018\ g/ml$$

$$\rho_{C_2H_4} = \frac{(1\ atm)\times(28\ g/mol)}{(82.05)\times(293\ K)} = 0.00115\ g/ml$$

$$\rho_{CH_2O} = \frac{(1\ atm)\times(30\ g/mol)}{(82.05)\times(293\ K)} = 0.00123\ g/ml$$

$$\rho_{C_2H_5OH} = \frac{(1\ atm)\times(46g/mol)}{(82.05)\times(293\ K)} = 0.00185\ g/ml$$

Molar flow rates of each species were calculated with Equation E5.

$$F_{H_2} = 12.52\times\frac{0.0000818}{2} = 0.000512\ mol/\min$$

$$F_{CO} = 0\times\frac{0.00115}{28} = 0\ mol/\min$$

$$F_{CH_4} = 1.28\times\frac{0.000654}{16} = 0.0000523\ mol/\min$$

$$F_{CO_2} = 0\times\frac{0.0018}{44} = 0\ mol/\min$$

$$F_{C_2H_4} = 2.25\times\frac{0.00115}{28} = 0.0000924\ mol/\min$$

$$F_{CH_2O} = 0\times\frac{0.00123}{30} = 0\ mol/\min$$

Liquid product obtained from condenser at 40th minutes was analyzed in GC and data is given in Table E5.

Table E5: Liquid product in SESRE reaction with Co-MCM-41 at 600°C at 40th minutes

Element	Area	Mole
H_2O	245733.1	235903.8
CH_2O	0	0
C_2H_5OH	3803.5	3803.5

Fractions of species in liquid product were calculated as;

$$x_{H_2O_{liquid}} = \frac{235903.8}{235903.8 + 0 + 3803.5} = 0.98$$

$$x_{CH_2O_{liquid}} = \frac{0}{235903.8 + 0 + 3803.5} = 0$$

$$x_{C_2H_5OH_{liquid}} = \frac{3803.5}{235903.8 + 0 + 3803.5} = 0.02$$

Weight of liquid obtained from condenser outlet at 40th minutes was 0.53 g. Then mass flow rate of liquid product was calculated as 0.53/40 = 0.013 g/min.

Molar flow rates of liquid products obtained from condenser at 40th minutes were calculated with Equation E6.

$$F_{C_2H_5OH_{liquid}} = 0.02 \times \frac{0.013\ g/\min}{(18 \times 0.98) + (46 \times 0.02) + (30 \times 0)} = 0.000014\ mol/\min$$

$$F_{CH_2O_{liquid}} = 0 \times \frac{0.013\ g/\min}{(18 \times 0.98) \times (46 \times 0.02) + (30 \times 0)} = 0\ mol/\min$$

Volumetric flow rate of reactant H_2O+C_2H_5OH mixture was adjusted to 20 ml/min. H_2O/C_2H_5OH molar ratio was 3.2. Therefore, volumetric flow rate of ethanol fed to the reactor was 4.76 ml/min.

Molar flow rate of ethanol fed to the reactor was calculated with Equation E5.

$$F^{o}_{C_2H_5OH} = 4.76\ ml/\min \times \frac{0.00185\ g/ml}{46\ g/mol} = 0.000191\ mol/\min$$

Ethanol conversion was calculated with Equation E7.

$$X_{EtOH} = \frac{(0.000191) - (0) - (0.000014)}{0.000191} \times 100 = 93\ \%$$

Hydrogen yield was calculated with Equation E8.

$$Y_{H_2} = \frac{0.000512}{0.000191} = 2.68$$

Carbon balance equation is illustrated in Equation E10 given below.

$$F^{o}_{C_2H_5OH} = \frac{F_{CO}}{2} + \frac{F_{CH_4}}{2} + \frac{F_{CO_2}}{2} + F_{C_2H_4} + \frac{F_{CH_2O}}{2} + F_{C_2H_4O} + \frac{F_{CH_2O_{liquid}}}{2} + F_{C_2H_5OH_{liquid}} + \frac{F_{CO_2(captured\ by\ CaO)}}{2} \quad \text{(E10)}$$

$$F_{CO_2(captured\ by\ CaO)} = (2 \times 0.000191) - 0.0000523 - (2 \times 0.0000924) - (2 \times 0.000014)$$
$$F_{CO_2(captured\ by\ CaO)} = 0.00012\ mol/\min$$

Selectivity of C-containing products was calculated with Equation E9.

$$S_{CH_4} = \frac{(1) \times (0.0000523)}{(2) \times (0.000191 - 0.000014)} \times 100 = 14.7$$
$$S_{CO_2} = \frac{(1) \times (0.00012)}{(2) \times (0.000191 - 0.000014)} \times 100 = 34.9$$
$$S_{C_2H_4} = \frac{(2) \times (0.0000924)}{(2) \times (0.000191 - 0.000014)} \times 100 = 52.2$$

APPENDIX F

F1. XRD PATTERN OF USED CATALYSTS IN SESRE REACTION

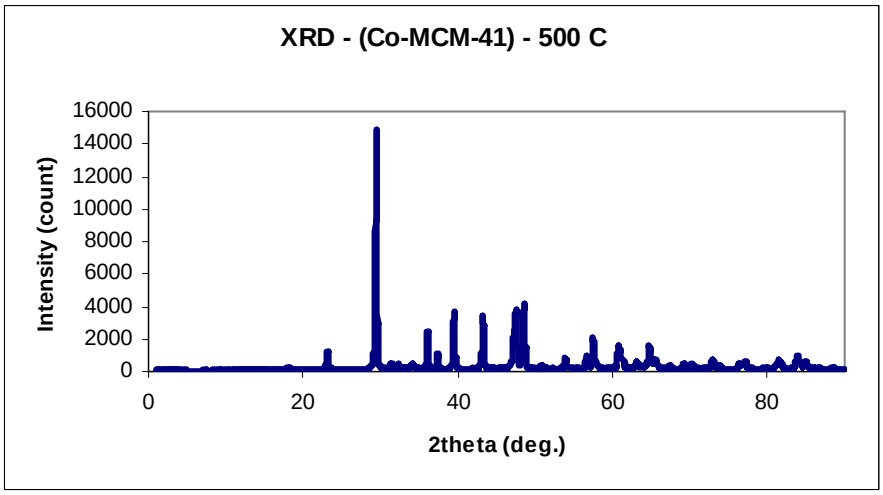

Figure F1: XRD pattern of used Co-MCM-41+CaO in SESRE reaction at 500^{o}C

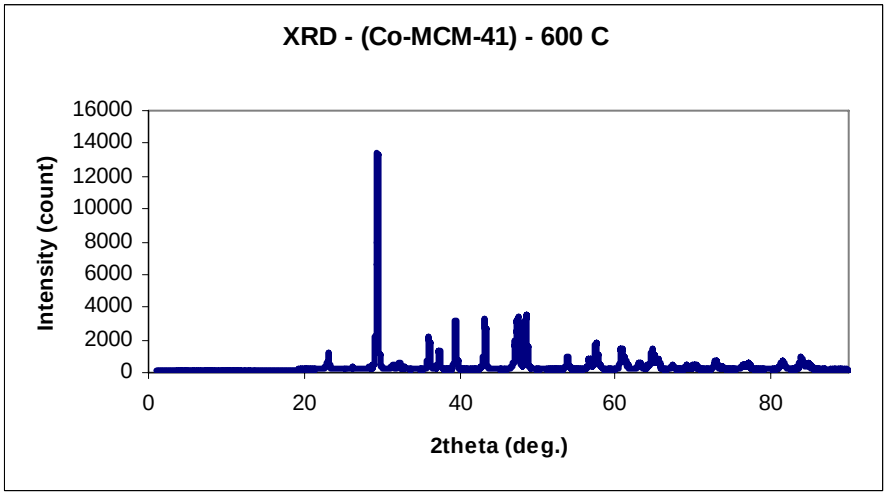

Figure F2: XRD pattern of used Co-MCM-41+CaO in SESRE reaction at 600^{o}C

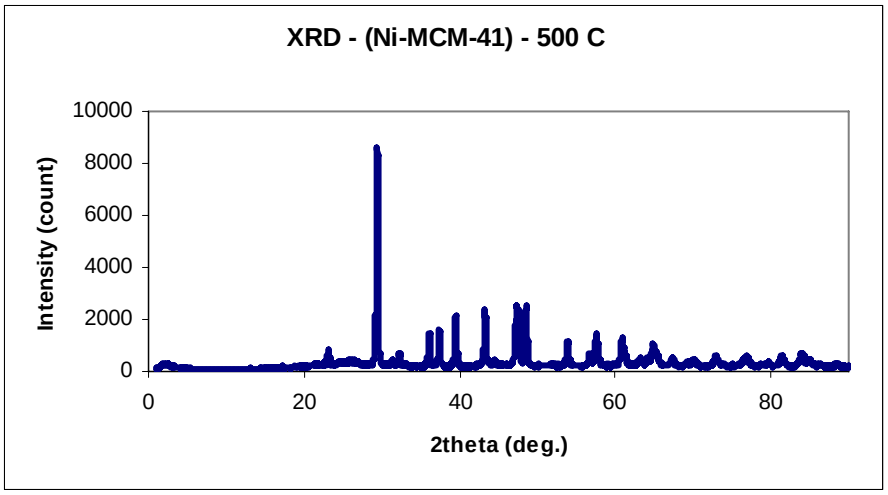

Figure F3: XRD pattern of used Ni-MCM-41+CaO in SESRE reaction at 500^{o}C

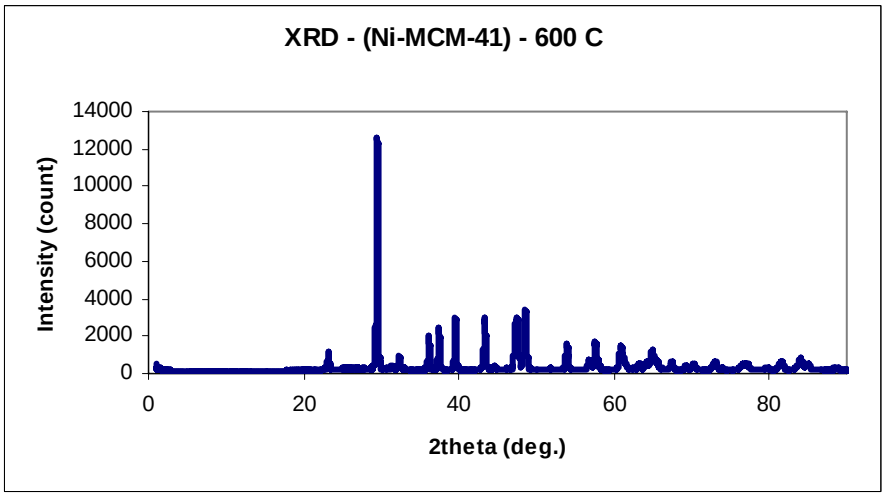

Figure F4: XRD pattern of used Ni-MCM-41+CaO in SESRE reaction at 600^{o}C

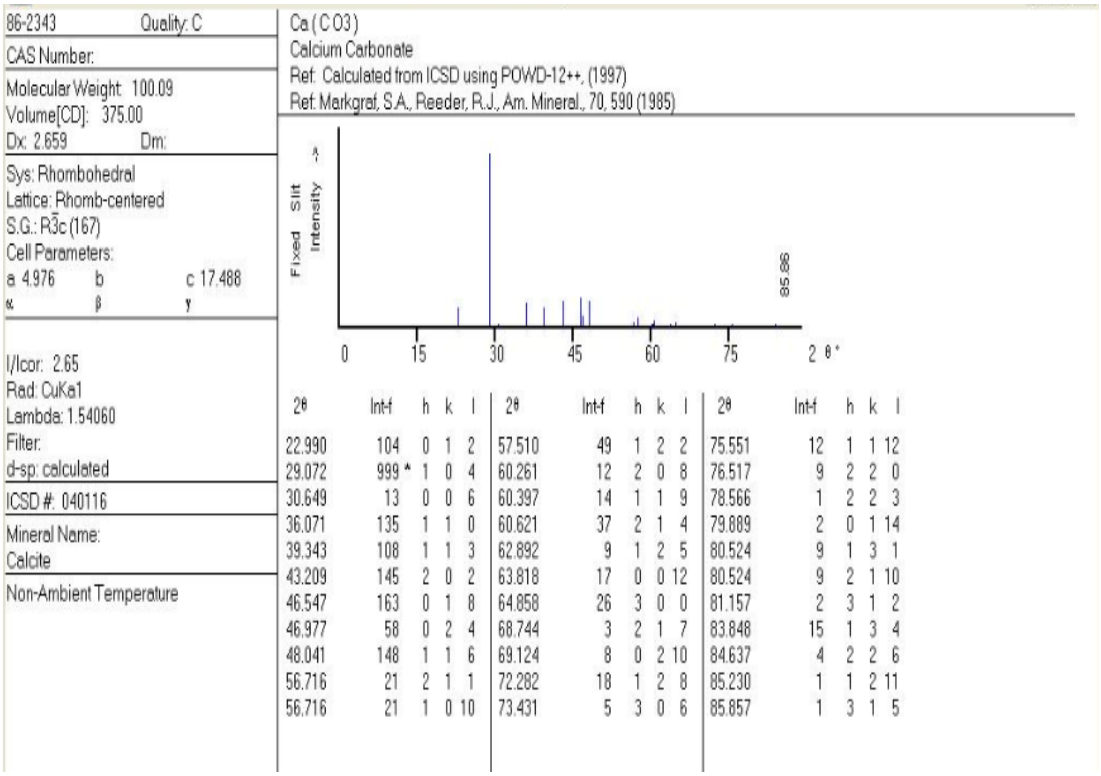

Figure F5: XRD pattern of pure $CaCO_3$

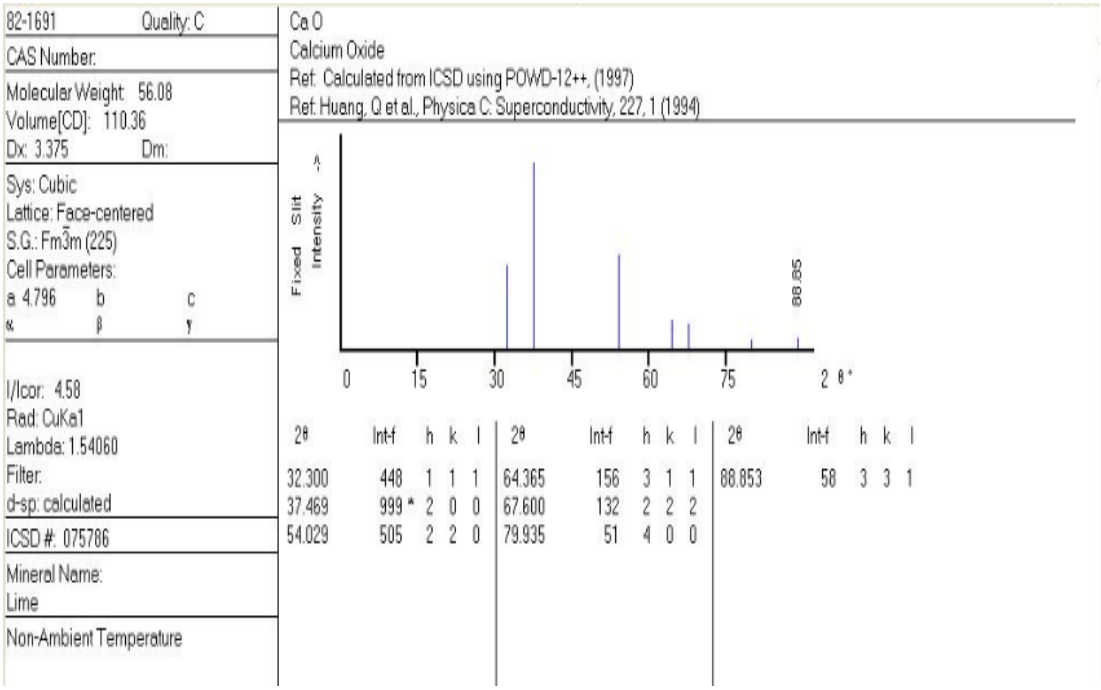

Figure F6: XRD pattern of pure CaO